ANALYSIS OF ELECTRON-ION MIXING IN ION ENGINES

FINAL REPORT

by

R. P. Wadhwa and D. F. Brauch

prepared for

NATIONAL AERONAUTICS AND SPACE ADMINISTRATION

CONTRACT NAS 3-5757

RESEARCH
LABORATORY

LITTON
INDUSTRIES

ELECTRON
TUBE
DIVISION

SAN CARLOS
CALIFORNIA

FINAL REPORT

ANALYSIS OF ELECTRON-ION MIXING IN ION ENGINES

by

R. P. Wadhwa and D. F. Brauch

prepared for

NATIONAL AERONAUTICS AND SPACE ADMINISTRATION

July 20, 1965

CONTRACT NAS 3-5757

Technical Management
NASA Lewis Research Center
Cleveland, Ohio
Space Craft Technology Division
S. Jones

RESEARCH LABORATORY
LITTON INDUSTRIES
ELECTRON TUBE DIVISION
960 INDUSTRIAL ROAD
SAN CARLOS, CALIFORNIA

FOREWORD

This is a summary report on the work performed under the subject study program from April 30, 1964 to June 30, 1965. Professor O. Buneman acted as a consultant throughout the program and made several significant contributions. Miss P. A. Vartanian contributed towards programming of the subroutine for plotting the equipotentials. This work was completed under the supervision of Dr. S. P. Yu, who also made several helpful suggestions.

OBJECTIVE

The objective of the work to be performed under this contract is the study of the transient and oscillatory phenomena in an ion beam into which electrons are injected for the purpose of neutralization. The studies are aimed at obtaining a more complete understanding of the ion-electron mixing process as it applies to ion-beam engines, with specific attention being given to factors which might affect the performance of such an ion engine.

ABSTRACT

The two-dimensional computer program for analyzing electron-ion mixing in ion engines has been extended to new geometrical configurations. A brief summary of the procedure for solving Poisson's equation is given. The program consists of injection of ions and electrons from appropriate locations as in an ion engine. The initial velocity distribution of the ions injected across the injection plane and the voltage variation along this plane are appropriately simulated. The injection plane is arbitrarily fixed according to convenience; on the left side of this plane lie the ion source and the other focusing electrodes while on the right side of this plane lies the electron emitter, which emits electrons according to Maxwellian distribution. Interplay between the plasma formation and ion injection has not been considered as yet.

Two sets of ion-beam configurations are analyzed; one corresponds to high voltage and the other to low voltage. Several values of ion-to-electron-mass-ratio are considered and a comparison is made between the withdrawn and immersed electron emitters. Different values of primary electron emission are simulated.

Macroscopic charge neutrality is achieved within about 200 time steps (less than 1 μsec). However, the plasma is not stabilized (at least within the time intervals investigated) due to the fact that electrons are still oscillating back and forth. Their average drift velocity is, however, about the same as that of the ions. These oscillations occur at the electron-plasma frequency and are also indicated in the ship potential variations. These fluctuations show up also in the equivalent temperature of electrons, which increases downstream near the electron emitter and is reduced further downstream. Ion temperature increases downstream because of the low-mass ions used in these calculations. There is a tendency to reach a state of thermodynamical equilibrium indicating a good electron-ion mixing mechanism.

TABLE OF CONTENTS

TABLE OF CONTENTS (Cont.)

LIST OF FIGURES

LIST OF FIGURES (Cont.)

ANALYSIS OF ELECTRON-ION MIXING IN ION ENGINES

1.0 INTRODUCTION

The objective of the work to be performed under this contract is the study of the transient and oscillatory phenomena in an ion engine into which electrons are injected for the purpose of neutralization. The computer program for solving Poisson's equation by using Fourier analysis and the "marching method" was developed under Contract No. NAS3-2503, and the details of the mathematical formulation and the results have been described in the final report for that contract[1]. In that program both one- and two-dimensional models were investigated. For the two-dimensional model, two configurations were analyzed. In the first configuration, the decel plane was assumed to be ideal, so that there was no potential variation along this plane; in the second configuration the potential at the isolated electron emitter, was simulated such that the potential along the decel plane could vary depending upon the size of the aperture and the space-charge distribution. In both cases electrons were emitted only from finite portions of the decel plane.

The work to be performed under this contract consisted of simulation of the accel aperture and of different shapes of the decel system. The simulation of the accel aperture requires a consideration of the appropriate potential distribution and both x- and y-components of the velocity distribution along the accel plane.

Basically the neutralization mechanism was investigated for two types of ion beams -- high voltage and low voltage*. Both withdrawn and immersed electron emitters were simulated for the case of high voltage ion beams while only the immersed emitter was simulated for the low-voltage ion beam. A considerable amount of experimental data for the low-voltage ion (cesium) beam has been obtained by Sellen[2] and the computer results were compared with Sellen's results wherever possible within limitations of computer simulation.

---

* Two different ion engines using different ion-voltage beams were simulated.

1

For the high-voltage ion beam the input data were obtained from Jones[3]; this data referred to an ion gun design without taking into account the effect of electrons emitted downstream for neutralization purposes. These input data -- namely, the potential distribution and velocity distribution of the ion beam -- were used as a boundary condition along the injection plane in the computer simulation. It may be necessary to mention here that this injection plane is not the same as the accel plane as identified in the previous work[1]. Studies were made for three values of ion mass and extrapolation was made for the actual ion mass.

For the low-voltage ion beam or Sellen's configuration, the input data were not readily available and efforts were made to simulate Sellen's configuration on the Litton Precision Resistance Network Analogue in order to obtain the potential distribution along the injection plane. These results were not very accurate because of lack of resolution on the Network as this required simulation of a one-inch diameter ion beam in a relatively very large tank. In the second phase the potential distribution beyond the accel grid along the injection plane in the x-y configuration was varied in order to obtain the potential distribution in space closer to that in the actual r-z configuration. This resulted in faster charge neutrality. However, plasma potential was not stabilized in both cases -- at least during the period of investigation. Wherever permissible comparison with different values of electron emission and electron emitter temperature was investigated.

Trajectories were plotted for several runs; plots for the variation of ship potential, thrust, and excess charge as a function of time were also make. Temperature calculations were made both for electrons and ions at different regions along the beam for all production runs. Equipotential plots were made corresponding to the charge distribution at different time steps and the results were correlated with other available data.

Section 2.0 gives briefly the mathematical formulation of the problem. The procedure for solving Poisson's equation has been discussed in detail in the earlier final report[1] and is included here for convenience of the reader. This section also discusses the electron interception tests and the evaluation of thrust using Maxwell's stress tensor. The simulation of the high-voltage ion beam and the results obtained from this simulation are discussed in Section 3.0 while Section 4.0 discusses the simulation of the low-voltage ion beam and the results obtained. Section 5.0 discusses the conclusions and suggestions for future work. The listings and explanations of the various computer programs developed under this contract are found in Sections 6.0 through 9.0 in the second volume.

2.0 MATHEMATICAL FORMULATION

2.1 DESCRIPTION OF THE COMPUTER MODEL

The coordinate configuration, along with the physical model of an ion engine is shown in Fig. 2-1. This is essentially the same model as studied under the previous contract (Contract NAS 3-2503). The system is assumed to be periodic in the transverse direction, and because of symmetry, only a half-period is analyzed. The half-period is divided into 24 meshes in the transverse or y-direction, 200 meshes in the longitudinal or x-direction. Figure 2-2 shows the grid mesh defined over the half-period. The potential distribution is calculated from the charge distribution using Fourier analysis and the so-called marching method discussed in detail in the final report[1] for Contract NAS3-2503.

Computer experiments made during the previous contract assumed an ideal injection (accel) plane; the assumption implies that there is no potential variation along the accel plane, and that the ions are injected across this plane with uniform x-directed velocity. The simulation of the injection plane made under the previous contract was not sufficiently realistic; thus, it was desirable to simulate this plane so that both the potential and velocity distributions along the aperture could be accounted for. In order to avoid any duplication of effort, it was considered appropriate not to extend the simulation into the gun region (between the ion source and the accel plane). The exit conditions in the gun region, obtained from programs developed by NASA, are used as the boundary conditions in our problem of investigation of space charge neutralization. The potential and velocity distributions at the injection (accel) plane do not take into account any space-charge neutralization. Moreover, it is not

clear how the space-charge neutralization would affect these potential and velocity distributions. This raises the question as to which potential distribution should be simulated along the injection plane.

The experiments made during the initial period of Contract NAS3-2503 assumed an ideal decel plane, i.e., constant potential, although electrons were emitted from a narrow strip, as shown in Fig. 2-1. Later under the same contract, an isolated strip emitter was simulated using a capacitance matrix[1]. Under Contract NAS3-5757 various shapes and sizes of isolated electron emitters with various positions in our system have been simulated using essentially the same method to maintain the boundary conditions on the emitter. Figure 2-2 illustrates a cylindrical electron emitter, one which was used extensively under the present contract. The shaded mesh squares are those in which potentials were used to define the emitter potential. The calculated potential at the mesh center (unshaded mesh) was very close (within about 0.001 normalized volts) to that corresponding to the shaded meshes.

This simulation can consider as many as 2200 ion rods and 2200 electron rods within the system at a particular time step, each rod representing as many as 10^7 actual ions or electrons. In the remainder of this report, the reference to ions and electrons will imply ion rods and electron rods, respectively. The particle positions are updated each time step, based on their velocities and the electric fields which they are experiencing.
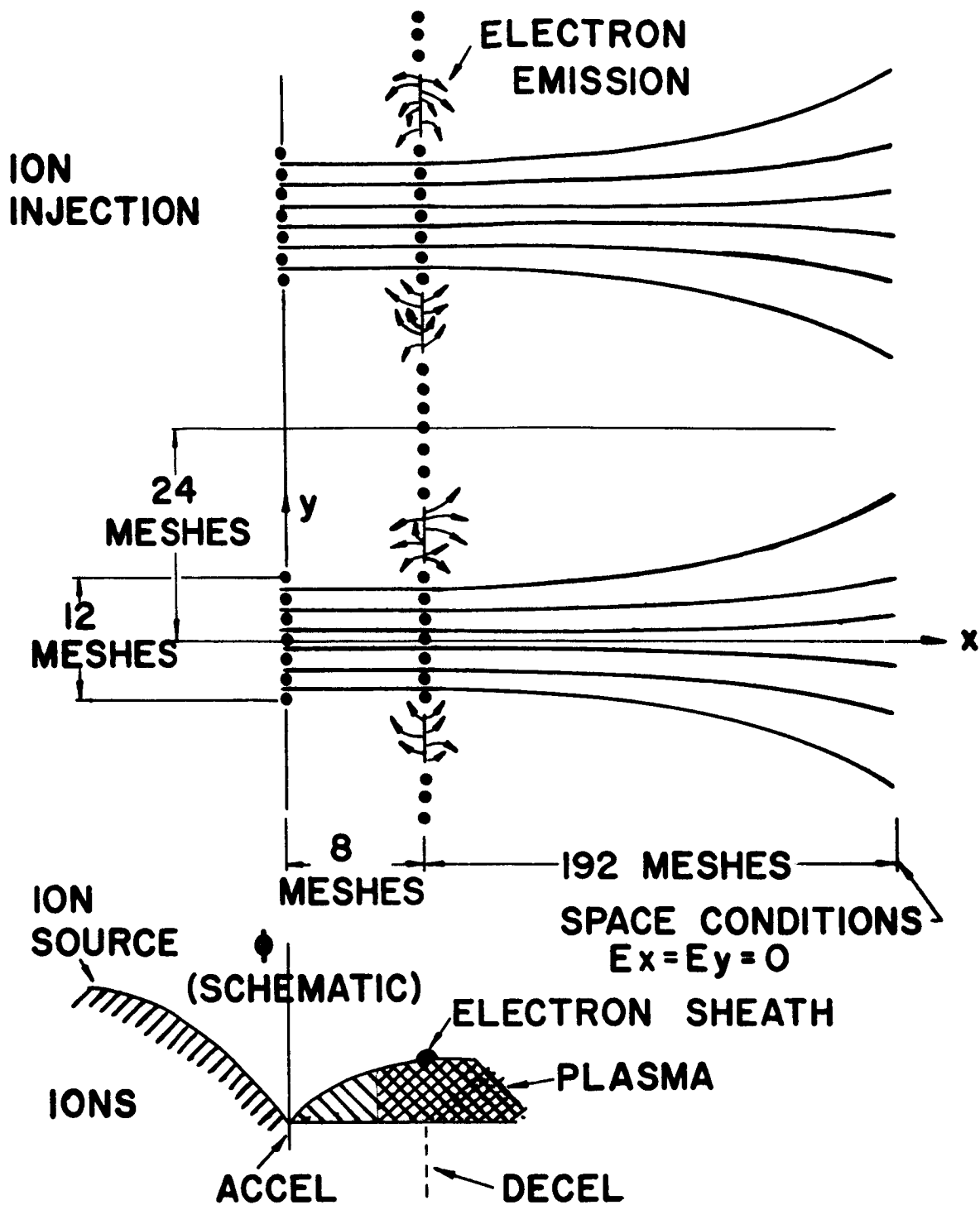
A SCHEMATIC OF THE ACCEL-DECEL SYSTEM WITH IDEAL POTENTIAL PROFILE

Fig. 2-1
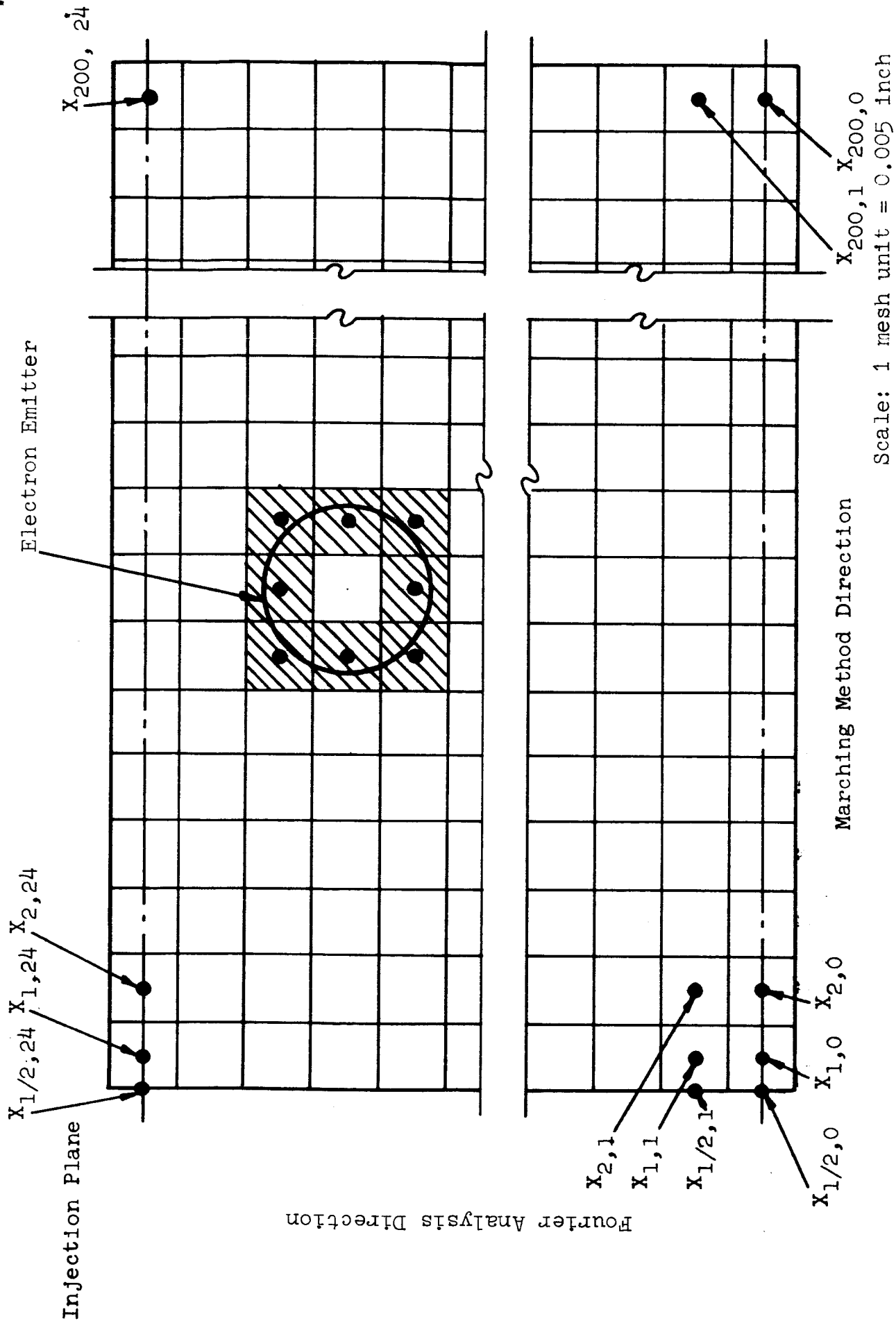
GRID MESH DEFINED OVER HALF PERIOD IN THE X-Y PLANE

Fig. 2-2

Scale: 1 mesh unit = 0.005 inch

7

The following assumptions have been made in the computer
model:
1. The system is periodic in the transverse direction with an axis of symmetry in each period.
2. Non-relativistic mechanics prevail in the consideration of particle motion.
3. The effect of direct collisions between ion-ion, electron-electron, and ion-electron is neglected.
4. The electric fields remain constant within a small time interval Δt.
5. The charge enclosed in a small mesh is uniformly distributed in the mesh.

2.2 PROCEDURE FOR SOLVING POISSON'S EQUATION

It has been mentioned before that Fourier analysis in the
transverse (y) direction and the marching method along the x-
axis are used for solving Poisson's equation. The potential
and space-charge density at mesh point (i,j), are expressed as

$$\varphi_{i,j} = \sum_{k=0}^{K-1} U_{i,k} \cos 2\pi k \frac{y_j}{b} \tag{2-1}$$

and

$$\rho_{i,j} = \sum_{k=0}^{K-1} \bar{\rho}_{i,k} \cos 2\pi k \frac{y_j}{b} \quad , \tag{2-2}$$

where

$$U_{i,k} = \frac{2}{K} \sum_{y_j} \varphi_{i,j} \cos 2\pi k \frac{y_j}{b} \qquad (2\text{-}3)$$

and

$$\bar{\rho}_{i,k} = \frac{2}{K} \sum_{y_j} \rho_{i,j} \cos 2\pi k \frac{y_j}{b} \quad . \qquad (2\text{-}4)$$

In Eqs. (2-1) through (2-4) $k \neq 0$ and $k \neq 24$, K = total number of mesh points in the transverse direction; for $k=0$ and $k=24$, the right hand sides of Eqs. (2-3) and (2-4) should be divided by 2. $U_{i,k}$ and $\bar{\rho}_{i,k}$ are the Fourier transforms of $\varphi_{i,j}$ and $\rho_{i,j}$, respectively.

For normalization purposes,

$$\varphi(i,j) = -\frac{8}{9} \left(\frac{\Delta x}{\ell}\right)^2 \left(\frac{\ell}{L}\right)^2 \frac{\varphi_0}{(\omega_p \Delta t)^2} V_{i,j} \qquad (2\text{-}5)$$

is assumed, where Δx = mesh size, ℓ = distance between accel and decel planes, L = distance between ion source and accel plane, φ_0 = voltage between ion source and accel plane, ω_p = electron plasma radian frequency and Δt = the unit-time interval. Using Eqs. (2-1) through (2-5), we obtain

$$X_{i-1,k} + X_{i+1,k} - \left(4-2\cos 2\pi k \frac{\Delta y}{b}\right) X_{i,k} = q^* \sum_{y_j} N(x_i, y_j) \cos 2\pi k \frac{y_j}{b} ,$$

$$(2\text{-}6)$$

where

$$V_{i,j} = \sum_{k=0}^{K-1} X_{i,k} \cos 2\pi k \frac{y_j}{b} \quad , \tag{2-7}$$

$$q^* = \frac{1}{KN} \left(\frac{\ell}{\Delta x}\right)^2 \frac{a}{\ell} (\omega_p \Delta t)^2 \quad , \tag{2-8}$$

$N(x_i, y_j)$ = total number of ions-minus-electrons in the i-jth rectangle, a = width of ion beam (in half period) at the accel plane, and N = total number of ions between accel and decel planes, if they would drift with the same velocity as that at the accel plane*. It may be mentioned here that, in defining the parameter N, the decel plane is assumed to be located at x=ℓ. However, for the case of arbitrarily shaped electron emitters, this plane is not defined specifically; nevertheless, these parameters are used merely for normalization purposes (although it will be necessary to select appropriate values for these parameters). A mean value of the x-coordinate will be used for the electron emitter. This is considered appropriate because otherwise new normalization may require significant changes in the present computer program.

It has been mentioned before that the marching method is used to solve Poisson's equation for each Fourier harmonic; the Fourier harmonics are then grouped together through a systematic procedure to give the actual voltage distribution. For application of the marching method the left hand side of Eq. (2-6) is factorized to give

---

* This definition is used strictly for normalization purposes.

$$\psi_{i+1/2,k} - \beta\psi_{i-1/2,k} = q^* \sum_{y_j} N(x_i, y_j) \cos 2\pi k \frac{y_j}{b} \qquad (2\text{-}9)$$

and

$$X_{i+1,k} = \frac{X_{i,k}}{\beta} + \psi_{i+1/2,k} \quad , \qquad (2\text{-}10)$$

where β is the larger root of the algebraic equation given by

$$\beta^2 - 2(2 - \cos 2\pi k \frac{\Delta y}{b})\beta + 1 = 0 \quad . \qquad (2\text{-}11)$$

Starting from the extreme position of the charged particle, ψ's are evaluated while marching toward the accel plane, and X's are evaluated while marching away from the accel plane; Eqs. (2-9) and (2-10) are used in this procedure. It can be shown that, beyond the farthest particle, $\psi_{i,k}=0$, and one need not worry about solving the potential distribution beyond this plane.

In evaluating the potential distribution, the electron emitter is held at zero potential, and the potential at "infinity" (actually the farthest location in the simulation) is obtained at each time interval. The zeroth harmonic of this potential with a change in sign gives the ship potential with respect to infinity. Thrust is also calculated at each time step by using Maxwell's stress tensor.

2.3 PROCEDURE FOR UPDATING ELECTRONS AND IONS

By using the normalization defined in Eqs. (2-5), (2-7), and (2-8), the equations of motion of electrons and ions are also normalized in a convenient manner, and are given for electrons by

$$\frac{x_{n+1}}{\Delta x} - 2 \frac{x_n}{\Delta x} + \frac{x_{n-1}}{\Delta x} = 2 \frac{\partial V(x,y)}{\partial x/\Delta x} \qquad (2\text{-}12)$$

and

$$\frac{y_{n+1}}{\Delta y} - 2 \frac{y_n}{\Delta y} + \frac{y_{n-1}}{\Delta y} = 2 \frac{\partial V(x,y)}{\partial y/\Delta y} \qquad (2\text{-}13)$$

and for ions by

$$\frac{x_{n+1}}{\Delta x} - 2 \frac{x_n}{\Delta x} + \frac{x_{n-1}}{\Delta x} = - \frac{m}{M} \frac{2\partial V(x,y)}{\partial x/\Delta x} \qquad (2\text{-}14)$$

and

$$\frac{y_{n+1}}{\Delta y} - 2 \frac{y_n}{\Delta y} + \frac{y_{n-1}}{\Delta y} = - \frac{m}{M} \frac{2\partial V(x,y)}{\partial y/\Delta y} \qquad (2\text{-}15)$$

where suffix n refers to the nth unit time interval and M/m = the ion-to-electron-mass ratio. It may be mentioned here that three terms in the Taylor's series expansion for $V(x,y)$ are used to evaluate the electric fields used for updating the particles at each time step. The displacements at the first unit-time interval are obtained by directly integrating the equations of motion.

2.4 SIMULATION OF INJECTION PLANE

2.4.1 INTRODUCTION

It is necessary to distinguish the difference between the injection plane x=0 and accel plane. In the first configuration that was studied under this contract, namely, the configuration reported on in Quarterly Report[4] No. 3, the injection plane in our computer model did not correspond to the accel plane of the actual system. In this case, the injection plane represented a plane to the right of the accel plane in the actual configuration. However, in the second engine design that was analyzed, namely, Sellen's configuration, and in all other geometries studied with this program under the previous contract, the accel and injection planes were the same plane.

2.4.2 VOLTAGE DISTRIBUTION

The simulation of the voltage distribution along the injection plane is accomplished by taking the potential distribution along the injection plane which is specified as input, and converting these potentials into an equivalent normalized charge. This equivalent normalized charge is added to the space charge in the column of mesh squares just to the right of the injection plane. This equivalent normalized charge, which is constant with respect to time, is added every time step. For more details on this method, see Quarterly Report[5] No. 1, Section 5.1.

2.4.3 VELOCITY DISTRIBUTION

In addition to specifying the distribution of potential along the injection (accel) plane, one must input the initial conditions for the ions entering at the injection plane. For

the first time step, the equations of motion of ions, namely, Equations (2-14) and (2-15) cannot be used, because the coordinates of the ion at the previous time step are not known. The updating of the ion is accomplished by using direct integration of the equations of motion. The resulting equations for the x and y coordinates are

$$
\frac{x_1}{\Delta x} = \frac{\dot{x}_o}{\dot{x}_{o,id}} \frac{N_i}{N} \frac{\ell}{\Delta x} - \frac{1}{4} \frac{(\partial\varphi/\partial x)_o}{(\partial\varphi/\partial x)_{o,id}} \frac{\varphi_d}{\varphi_o} \frac{\ell}{\Delta x} \left(\frac{N_i}{N}\right)^2
$$

$$
- \frac{1}{12} \left(\frac{N_i}{N}\right)^3 \left(\frac{\ell}{\Delta x}\right)^2 \left(\frac{\ell}{L} + \frac{\varphi_d}{\varphi_o}\right) \left[\frac{(\partial^2\varphi/\partial x^2)_o}{(\partial^2\varphi/\partial x^2)_{o,id}} \frac{\dot{x}_o}{\dot{x}_{o,id}} \right.
$$

$$
\left. + \frac{(\partial^2\varphi/\partial x\partial y)_o}{(\partial^2\varphi/\partial x^2)_{o,id}} \frac{\dot{y}_o}{\dot{x}_{o,id}} \right] \quad , \tag{2-16}
$$

and

$$
\frac{y_1}{\Delta y} = \frac{y_o}{\Delta y} + \frac{\dot{y}_o}{\dot{x}_{o,id}} \frac{N_i}{N} \frac{\ell}{\Delta x} - \frac{1}{4} \frac{(\partial\varphi/\partial y)_o}{(\partial\varphi/\partial x)_{o,id}} \frac{\varphi_d}{\varphi_o} \frac{\ell}{\Delta x}\left(\frac{N_i}{N}\right)^2 - \frac{1}{12}\left(\frac{N_i}{N}\right)^3\left(\frac{\ell}{\Delta x}\right)^2\left(\frac{\ell}{L} + \frac{\varphi_d}{\varphi_o}\right)
$$

$$
\left[\frac{(\partial^2\varphi/\partial y^2)_o}{(\partial^2\varphi/\partial x^2)_{o,id}} \frac{\dot{y}_o}{\dot{x}_{o,id}} + \frac{(\partial^2\varphi/\partial x\partial y)_o}{(\partial^2\varphi/\partial x^2)_{o,id}} \frac{\dot{x}_o}{\dot{x}_{o,id}} \right] , \tag{2-17}
$$

where

$$
\omega_p \Delta t = \frac{N_i}{N} \left(\frac{M}{2m}\right)^{1/2} \frac{2\ell}{3L} \quad . \tag{2-18}
$$

14

In Eqs. (2-16) and (2-18), $\dot{x}_o$ and $\dot{y}_o$ are actual velocity components at t=0, $\dot{x}_{o,id}$ is the ideal x-component of velocity* at t=0, m is the electron mass, η is the absolute value of electron charge to its mass, and the suffix o,id refers to the ideal value at the injection plane. Using the ideal (linear) potential distribution in the gun and accel-decel regions as shown in Fig. 2-3, it can be shown that

$$\left(\frac{\partial\varphi}{\partial x/\Delta x}\right)_{o,id} = \frac{\varphi_d}{\ell/\Delta x} \qquad (2\text{-}19)$$

$$\left(\frac{\partial^2\varphi}{\partial x^2}\right)_{o,id} = \frac{\varphi_o}{(\Delta x)^2} \frac{\Delta x}{\ell} \left(1 + \frac{\ell}{L}\right) \qquad , \qquad (2\text{-}20)$$

where $\varphi_d > 0$.

Thus, the initial conditions for the ions that need to be specified are

$$\frac{y_o}{\Delta y} \quad , \quad \frac{\dot{x}_o}{\dot{x}_{o,id}} \quad , \quad \frac{\dot{y}_o}{\dot{x}_{o,id}} \quad , \quad \frac{(\partial\varphi/\partial x)_o}{(\partial\varphi/\partial x)_{o,id}} \quad , \quad \frac{(\partial\varphi/\partial y)_o}{(\partial\varphi/\partial x)_{o,id}}, \frac{\varphi_d}{\varphi_o} \quad ,$$

the second derivates of φ were actually not considered in computations. The derivation of these equations is dealt with in detail in Quarterly Report No. 1, Section 5.2.

---

* This ideal velocity is computed on the basis that only the x-component velocity contributes to the kinetic energy.

Ion Source   Accel Plane   Decel Plane

φ_o

φ_d

L ℓ
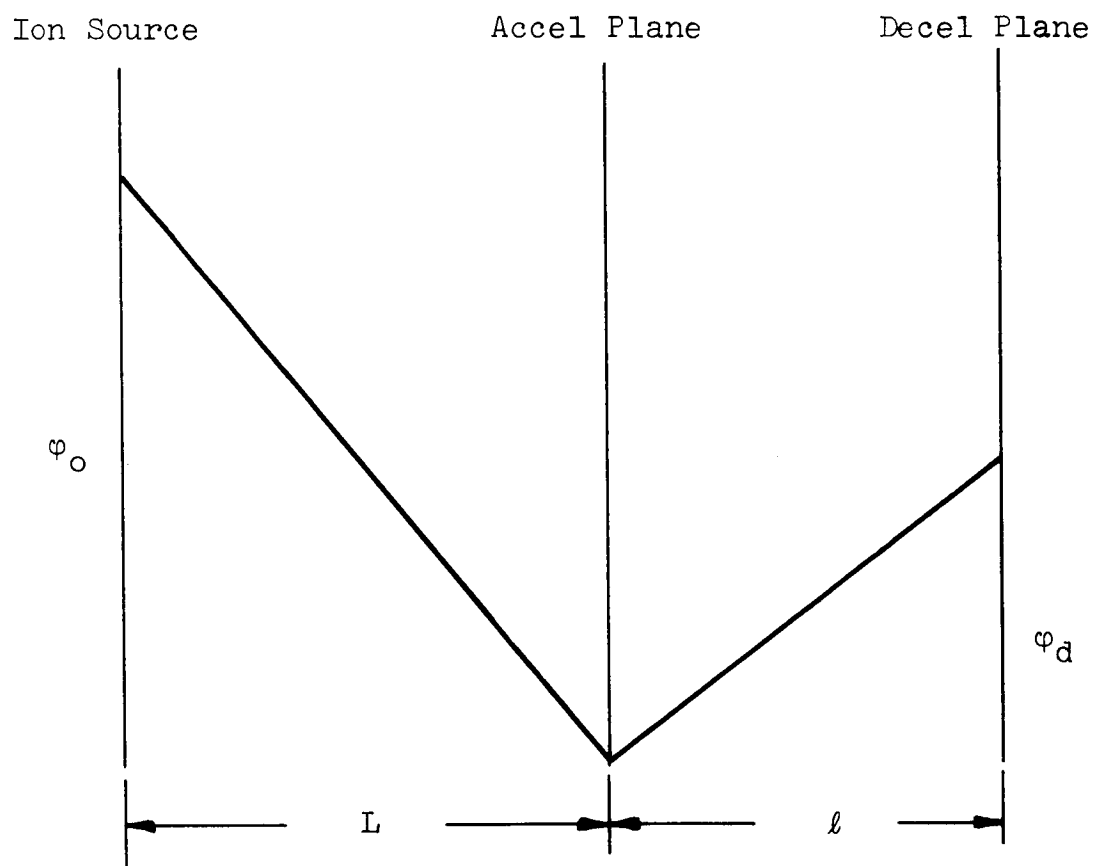
IDEALIZED (LINEAR) POTENTIAL DISTRIBUTION IN THE GUN AND
ACCEL-DECEL REGIONS USED FOR NORMALIZATION

Fig. 2-3

16

2.5 SIMULATION OF THE CYLINDRICAL (CIRCULAR) ELECTRON EMITTER

2.5.1 INTRODUCTION

In principle, it is possible to study any shape of electron emitter situated anywhere in the 200 x 24 grid mesh. However, there are in reality some restrictions on the size of the emitter which are due to the limitations in the available computer memory. There is relatively little computer storage left because a large number of mesh points (5000) and large number of charged particles (4400) are being used in this analysis. For these reasons, it was necessary to restrict the total number of mesh points used to simulate the electron emitter (decel system) to 10; but there are no restrictions on the placement of the electron emitter in our system. It can be placed even at the exit plane of our system, i.e., $x/\Delta x = 200$.

It was considered appropriate to simulate the case where the electron emitter's configuration is cylindrical, i.e., the representation in the x-y plane is circular. The choice of a particular design affects: (1) determination of electron emission conditions, (2) ion and electron interception on the electron emitter, and (3) calculation of the capacitance matrix used in the potential solver.

2.5.2 ELECTRON EMISSION CONDITIONS

Emission of electrons is restricted to the exterior of the cylinder. Physically, electrons are emanating from all points on the exterior surface of the cylinder. In this simulation, electrons are ejected from equally spaced points along a portion of or from the entire perimeter of the circular cross-section. The electrons are emitted from the electron emitter with random velocity components according to the Maxwellian velocity distribution. The derivation of the electron emission conditions and related details are given in Quarterly Report No. 1, Section 3.2.

2.5.3 PARTICLE INTERCEPTION CONDITIONS

The three tests derived to check for particle interception on a cylindrical electron emitter with radius R_c and center at (X_c, Y_c) are discussed in this section. Figure 2-4 shows two successive points (X_i, Y_i) and (X_{i+1}, Y_{i+1}) of an ion or electron trajectory. Also, defined are the vectors $\bar{r}_i$ and $\bar{r}_{i+1}$ with initial point at (X_c, Y_c) and terminating at (X_i, Y_i) and (X_{i+1}, Y_{i+1}), respectively. Note that both (X_i, Y_i) and (X_{i+1}, Y_{i+1}) are shown outside of the cylinder. The first test that obviously should be made is to check whether (X_{i+1}, Y_{i+1}) is inside the cylinder, i.e., is

$$(X_{i+1} - X_c)^2 + (Y_{i+1} - Y_c)^2 \leq R_c^2 \quad , \qquad (2\text{-}21)$$

and if so, declare the particle intercepted. If this test indicates that (X_{i+1}, Y_{i+1}) is outside of the cylinder, another test must be made to check if the line segment joining (X_i, Y_i) and (X_{i+1}, Y_{i+1}) or extension in either direction intersects the cylinder. This test can be expressed mathematically as

$$R_c^2 \left[(X_{i+1} - X_i)^2 + (Y_{i+1} - Y_i)^2 \right] \geq \left[(X_i - X_c)(Y_{i+1} - Y_c) \right.$$
$$\left. - (X_{i+1} - X_c)(Y_i - Y_c) \right]^2 \quad . \qquad (2\text{-}22)$$

If a particle does not satisfy Eq. (2-22), it is not intercepted. If a particle does satisfy Eq. (2-22) another test is applied, namely

$$\left| (X_i - X_c)^2 + (Y_i - Y_c)^2 - (X_{i+1} - X_c)^2 - (Y_{i+1} - Y_c)^2 \right|$$
$$\leq (X_{i+1} - X_i)^2 + (Y_{i+1} - Y_i)^2 \quad . \qquad (2\text{-}23)$$

18
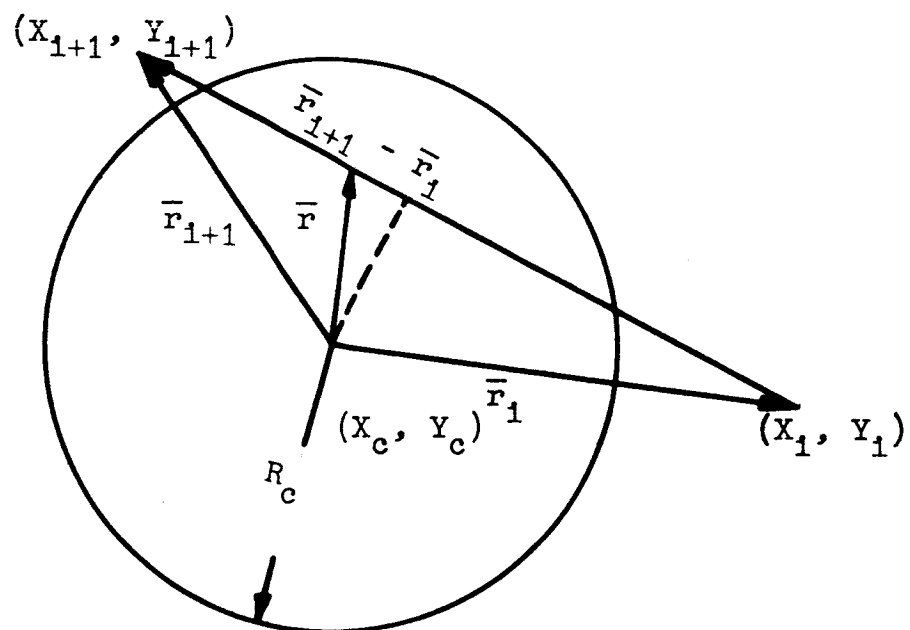
GEOMETRY AND NOTATION USED IN DETERMINING
TESTS FOR PARTICLE INTERCEPTION

Fig. 2-4

This test checks to see if the successive particle positions lie on opposite sides or the same side of the cylinder. If Equation (2-23) is satisfied, the particle is intercepted; if this condition is not met, no interception occurs.

To reduce amount of computer time needed to check as many as 4400 particles per time step for interception on the electron emitter, a rough check is made to eliminate all those particles not in the neighborhood of the emitter from the three tests presented above. The bounds of a rectangle enclosing the emitter, namely RECTL, RECTR, RECTB, and RECTT are inputted (this rectangle is also used in the formulation of normalized thrust). This rough check can be written as

$$RECTL \leq X_{i+1} \leq RECTR, \quad RECTB \leq Y_{i+1} \leq RECTT \quad . \tag{2-24}$$

Thus, this is actually the initial test on the particles.

2.5.3 EVALUATION OF CAPACITANCE MATRIX

The role played by the so-called "capacitance matrix" is described in Section 6 of the Final Report[1], Analysis of Electron-Ion Mixing in Ion Engines, Contract No. NAS3-2503. To summarize that description, the capacitance matrix is needed in the procedure to simulate the effects of the boundary constraints at the decel system (electron emitter) in the solution of Poisson's equation. The correct potential distribution is found by superimposition of appropriate values of compensating charges on the actual charges produced by ions and electrons. The compensating charges are calculated by premultiplying the uncorrected potential matrix by the capacitance matrix. The uncorrected potential matrix is defined as the matrix composed of the potentials at the locations of the boundary constraints, calculated while ignoring the boundary constraints (set at zero volts).

The evaluation of the capacitance matrix is similar to that calculated before, the only difference being the new geometry for the electron emitter (decel grid). The locations of boundary constraints do not necessarily lie along a vertical line (plane in space). As mentioned in Section 2.5.1, the decel grid geometry is arbitrary to the extent that it can be specified by approximately 10 discrete mesh points. Figure 2-2 illustrates the accel-decel system with a cylindrical electron emitter geometry. Eight mesh points on the cylinder are locations where boundary constraints exist. To consider the effect of these boundary constraints, an arbitrary charge (in our case unit charge was chosen for convenience) is placed at one of these eight mesh points. Then Poisson's equation is integrated with zero voltage on the accel grid, using Fourier analysis and the marching method, to obtain the potentials at each of the eight points. Unit charge is placed in succession at each of the eight points, and voltages are obtained at all eight points for each repositioning of the unit charge. The result is an 8 x 8 symmetric matrix known as the "inverse capacitance matrix". Inverting this matrix, which is obtained relatively fast on the IBM 7094 computer because the matrix is not very large, yields the capacitance matrix. This matrix is calculated only once for each different electron emitter geometry, and a magnetic tape is used to store the coefficients. These coefficients are inputted to the computer at the beginning of a production run.

2.6 SIMULATION OF THE QUADRANGULAR ELECTRON EMITTER

2.6.1 DEFINITION OF THE QUADRANGULAR GEOMETRY

The second basic configuration that was simulated under this contract was a closed geometry consisting of connected line segments. It was determined that, because of limitations in computer execution time and restrictions in computer memory, this type of geometry would be limited to a maximum

of four sides, thus the quadrangular nomenclature. It was
also decided that electron emission would be restricted to the
exterior surface as it was in the case of the cylindrical
emitter. This implies that only one side of each line seg-
ment composing the electron emitter will be emitting. A
gamut of designs is possible with this definition. A straight
line emitter with emission from two sides can be defined by
two segments going between the same end points. (See Fig.
2-5a.) A triangular electron emitter and a general quad-
rangular emitter can be defined (see Fig. 2-5b and 2-5c).
We also decided to make it possible to shield one or more
of the segments from emission, i.e., define zero emission
along these segments.

The input variables which are needed to describe any
quadrangular geometry are:

(1) NVER - number of vertices or corners of the geometry
(NVER equals the number of connected straight line
segments also. NVER $\leq$ 4. The number associated with
each vertex increases as one travels counterclockwise
about the emitter.)

(2) $\left[XVER(N), YVER(N), N=1,\ldots, NVER \right]$ - coordinates of the
vertices.

(3) $\left[NEPS(N), N=1,\ldots, NVER \right]$ - number of emission points
along each side (the total number of emission points
around the entire circumference, i.e.,

$$\sum_{N=1}^{NVER} NEPS(N) \leq 15 \quad ,$$

which is the same bound as was applied for the cyclindri-
cal emitter case).
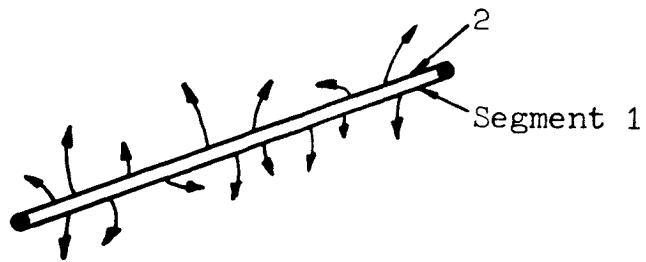
(a)
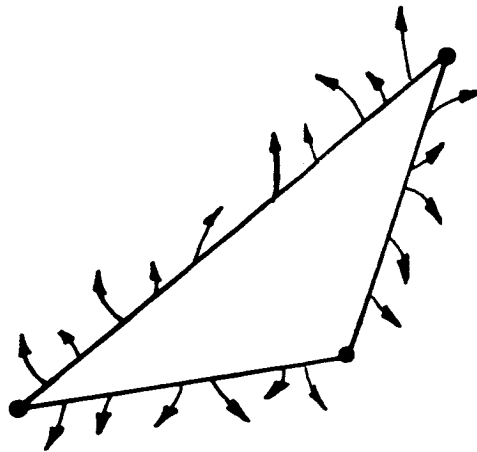
(b) Triangular Emitter
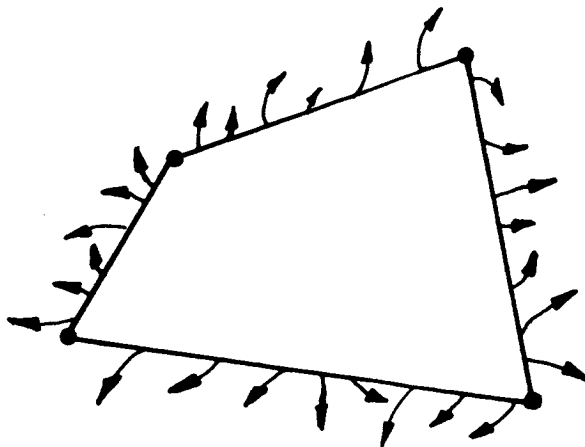
(c) Quadrangular Emitter

VARIOUS ELECTRON EMITTER CONFIGURATIONS COMPOSED OF CONNECTED SEGMENTS

Fig. 2-5

(4) RECTL, RECTR, RECTB, RECTT - left, right, bottom
and top bounds of a rectangle which includes the
electron emitter and on which a rough test for
particle interception on the electron emitter
will be made.

2.6.2 ELECTRON EMISSION CONDITIONS

Let us now formulate the logic needed for describing the
emission of electrons from a quadrangle. One necessary con-
dition is that there is no emission from the vertices or
corners. The reason for this condition is that the tangential
and normal directions at the vertices are not known, which in
turn makes it impossible to define the velocity components at
the time of emission.

For that reason, to find the coordinates of the emission
points XE(M), YE(M) along side N, one first calculates

$$\Delta X = \left[XVER(N+1) - XVER(N) \right] / NEPS(N) \qquad (2\text{-}25)$$
$$\Delta Y = \left[YVER(N+1) - YNER(N) \right] / NEPS(N) \quad . \qquad (2\text{-}26)$$

Then XE(M) and YE(M) can be calculated:

$$XE(1) = XVER(N) + \Delta X/2 \qquad (2\text{-}27)$$
$$YE(1) = YVER(N) + \Delta Y/2 \qquad (2\text{-}28)$$
$$XE(M) = XVER(N) + \Delta X \quad M=2, \ldots, NEPS(N) \qquad (2\text{-}29)$$
$$XE(M) = YVER(N) + \Delta Y \quad M=2, \ldots, NEPS(N) \quad . \qquad (2\text{-}30)$$

As in the case of the cylindrical electron emitter, the
electrons are emitted with random velocity components accord-
ing to the Maxwellian velocity distribution.

2.6.3 PARTICLE INTERCEPTION CONDITIONS

As was mentioned in Section 2.6.1, the quadrangular elec-
tron emitter is composed of connected straight line segments.
Thus, the interception of an electron or ion on the electron
emitter occurs when the particle trajectory intersects one of
the segments comprising the emitter.

As in the case of the cylindrical emitter, the first test
selects those particles whose present position (X, Y) is within
the rectangle bounded by RECTL, RECTR, RECTB, RECTT and which
encloses the electron emitter.

Next, we must examine whether or not the trajectory as
defined by the straight line segment connecting the past posi-
tion (XP, YP) and (X, Y) actually intersects one of the seg-
ments of the electron emitter, namely, the segment connecting
$\left[\text{XVER(N)}, \text{YVER(N)}\right]$ and $\left[\text{XVER(N+1)}, \text{YVER(N+1)}\right]$. Let us express
each of these segments in equation form. For this we need to
determine the slopes of each segment. Let S(N) be the slope
of the emitter segment and ST be the slope of the trajectory.
These parameters to be written as

$$S(N) = \left[\text{YVER(N+1)} - \text{YVER(N)}\right]/\left[\text{XVER(N+1)} - \text{XVER(N)}\right] \qquad (2\text{-}31)$$
$$ST = (Y\text{-}YP)/(X\text{-}XP) \qquad (2\text{-}32)$$

The equations of these straight lines can be written as

$$y - YP = ST\ (x\text{-}XP) \qquad (2\text{-}33)$$
$$y - YVER(N) = S(N)\left[x\text{-}XVER(N)\right] \qquad (2\text{-}34)$$

Except for the case where ST=S(N), Eqs. (2-33) and (2-34) can
be solved simultaneously for x and y. Obtaining values for x
and y does not imply interception has occurred. Figure 2-6
shows three possible arrangements where, although the lines
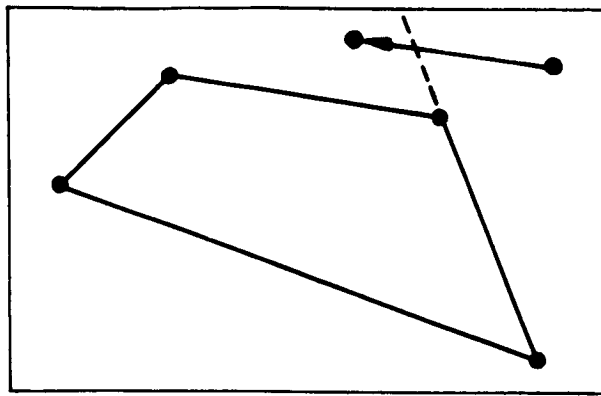
(a)
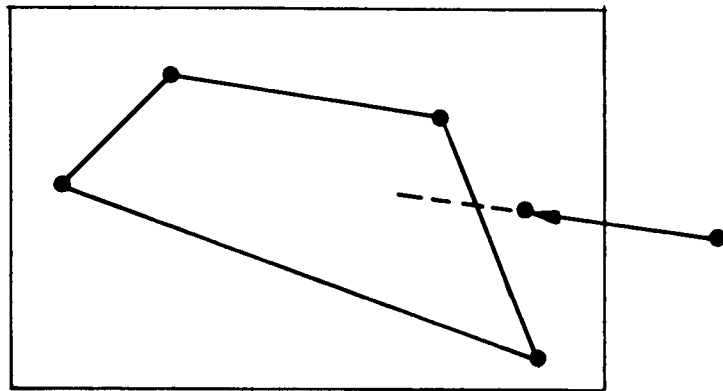
(b)
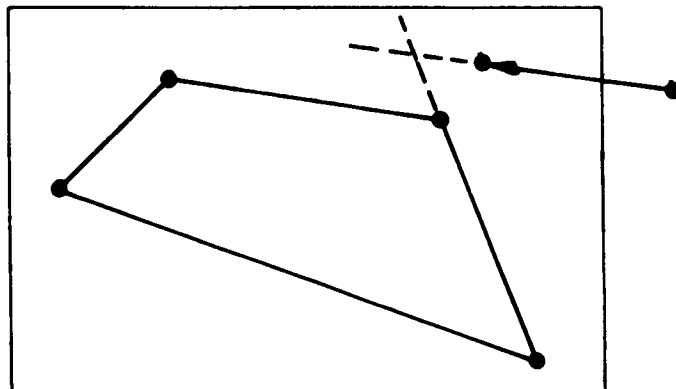
(c)

SEVERAL CONFIGURATIONS SHOWING INTERSECTION OF LINES
BUT NO PARTICLE INTERCEPTION

Fig. 2-6

intersect, there is no interception on the electron emitter. Thus, to insure interception on the emitter, (x, y) must satisfy the following set of conditions:

$$X \leq x \leq XP \quad \text{or} \quad XP \leq x \leq X \tag{2-35}$$

$$\text{and} \quad Y \leq y \leq YP \quad \text{or} \quad YP \leq y \leq Y \tag{2-36}$$

$$\text{and} \quad XVER(N) \leq x \leq XVER(N+1) \quad \text{or} \quad XVER(N+1) \leq x \leq XVER(N) \tag{2-38}$$

$$\text{and} \quad YVER(N) \leq y \leq YVER(N+1) \quad \text{or} \quad YVER(N+1) \leq y \leq YVER(N) \tag{2-39}$$

The reason for the choice shown in Eqs. (2-35) through (2-38) is that sometimes $X \leq XP$, but other times $X \geq XP$, etc. We have shown the tests for interception of a particle trajectory as defined by (X, Y) and (XP, YP) with the Nth segment of the emitter. Obviously, this same technique is applied to check for interception on the (N+1)st segment of the emitter if no interception is found on the Nth segment and if N<NVER. If N=NVER, all possible segments have been checked for interception on the emitter.

2.7 CALCULATION OF NORMALIZED THRUST

It is necessary to take into account both the inertial and electrostatic forces in computing the thrust, because the injection plane potential is not constant. The potential distribution depends on the ion beam, geometrical configuration and the voltages applied to the other electrodes in the system.

The electrostatic contribution of the total thrust results from the normal forces experienced on the surface of the injection plane and the electron emitter. To minimize the computer time needed to calculate the thrust, it was considered appropriate to use the rectangle enclosing the electron emitter as a basis for the computation of electrostatic force on the emitter. This rectangle has left, right, bottom, and top bounds of RECTL, RECTR, RECTB, RECTT, respectively.

The inertial contribution to the total thrust is due to the movement of ions across the injection (accel) plane and the movement of electrons from and to the electron emitter.

In Quarterly Report[6] No. 2, Section 2, expressions for the actual and ideal values of thrust due to electrostatic and inertial forces are derived. The total normalized thrust is given by

$$T^* = \frac{1}{F_1 F_2} \frac{a}{\ell} \frac{1}{N} \left[\sqrt{\frac{M}{m}} \left(\frac{\delta x}{\Delta x} \right)_{ions} + \left(\frac{\delta x}{\Delta x} \right)_{electrons} \right]$$

$$- \frac{1}{F_1 F_2} \frac{1}{2} \left(\frac{\Delta x}{\ell} \right)^2 \frac{1}{(\omega_p \Delta t)^2} \Bigg\{$$

(Equation is continued on the next page.)

$$\left[\sum_{j} \left(\frac{2\partial V}{\partial x/\Delta x} \right)^2 - \left(\frac{2\partial V}{\partial y/\Delta y} \right)^2 \right]_{\text{ion-injection plane}}$$

$$+ \left[\sum_{j} \left(\frac{2\partial V}{\partial x/\Delta x} \right)^2 - \left(\frac{2\partial V}{\partial y/\Delta y} \right)^2 \right]_{\text{RECTR}}$$

$$- \left[\sum_{j} \left(\frac{2\partial V}{\partial x/\Delta x} \right)^2 - \left(\frac{2\partial V}{\partial y/\Delta y} \right)^2 \right]_{\text{RECTL}}$$

$$- 2 \left[\sum_{i} \left(\frac{2\partial V}{\partial x/\Delta x} \right) \left(\frac{2\partial V}{\partial y/\Delta y} \right) \right]_{\text{RECTT}}$$

$$\left. + 2 \left[\sum_{i} \left(\frac{2\partial V}{\partial x/\Delta x} \right) \left(\frac{2\partial V}{\partial y/\Delta y} \right) \right]_{\text{RECTB}} \right\} \qquad (2\text{-}39)$$

where

$$F_2 = \frac{1}{12} \left(\frac{4}{9} \right)^2 \left(\frac{\ell}{L} \right)^4 \frac{1}{(\omega_p \Delta t)^2} \qquad (2\text{-}40)$$

and

$$F_1 = - \left(\frac{\phi_d}{\phi_o} \right)^2 + \frac{M}{m} \left(\frac{2m}{M} \right)^{1/2} \left(\frac{\ell}{L} \right)^3 \frac{2}{81} \frac{a}{\ell} \frac{1}{\omega_p \Delta t} \quad . \qquad (2\text{-}41)$$

Equation (2-41) corresponds to the ideal thrust contributed by electrostatic and inertial forces due to ions only; F_1 is used for normalization in Eq. (2-39).

2.8   TEMPERATURE CALCULATIONS

In the previous electron-ion mixing studies for the case of ideal accel grid, some calculations regarding the cooling of electrons were made at different segments of the beam and at different time intervals. These calculations led to the belief that there is some energy exchange between ions and electrons. It was thought desirable to improve the accuracy of these calculations. For this reason, the pertinent equations to be used

for evaluating the temperature of both ions and electrons have
been derived. These temperatures depend upon σ, the mean square
fluctuation in velocity, which is given by

$$\sigma = \overline{v^2} - (\overline{v})^2 \quad . \tag{2-42}$$

The normalized electron temperature $(T_e^*)_n/T$ at the nth time
step is given by

$$\frac{(T_e^*)_n}{T} = \left(\frac{e\varphi_o}{kT}\frac{m}{M}\right)\left(\frac{N}{N_1}\right)^2 \left(\frac{\Delta x}{\ell}\right)^2 (\sigma_e)_n \left(\frac{\Delta t}{\Delta x}\right)^2 \quad , \tag{2-43}$$

where

$$(\sigma_e)_n\left(\frac{\Delta t}{\Delta x}\right)^2 = \frac{\sum\limits_p \left\{\left[\frac{x_{n+1}}{\Delta x} - \frac{x_n}{\Delta x} - \frac{\partial V}{\partial x/\Delta x}\right]^2 + \left[\frac{y_{n+1}}{\Delta y} - \frac{y_n}{\Delta y} - \frac{\partial V}{\partial y/\Delta y}\right]^2\right\}}{P_{e,n}}$$

$$- \frac{\left[\sum\limits_p \left(\frac{x_{n+1}}{\Delta x} - \frac{x_n}{\Delta x} - \frac{\partial V}{\partial x/\Delta x}\right)\right]^2 + \left[\sum\limits_{p=1}^{p} \frac{y_{n+1}}{\Delta y} - \frac{y_n}{\Delta y} - \frac{\partial V}{\partial y/\Delta y}\right]^2}{P_{e,n}^2} \tag{2-44}$$

In Eq. (2-43), T is the actual absolute temperature of the
electron emitter, and $P_{e,n}$ is the total number of electrons in
the given space being analyzed at the nth time step in Eq.
(2-44). Similarly, the normalized ion temperature is given by

$$\frac{(T_i^*)_n}{T} = \left(\frac{e\varphi_o}{kT}\right)\left(\frac{N}{N_1}\right)^2 \left(\frac{\Delta x}{\ell}\right)^2 (\sigma_i)_n \left(\frac{\Delta t}{\Delta x}\right)^2 \quad , \tag{2-45}$$

where

$$(\sigma_1)_n \frac{\Delta t}{\Delta x}^2 = \frac{\sum_p \left\{ \left[\left(\frac{x_{n+1}}{\Delta x} - \frac{x_n}{\Delta x} \right) + \frac{m}{M} \frac{\partial V}{\partial x / \Delta x} \right]^2 + \left[\left(\frac{y_{n+1}}{\Delta y} - \frac{y_n}{\Delta y} \right) + \frac{m}{M} \frac{\partial V}{\partial y / \Delta y} \right]^2 \right\}}{P_{1,n}}$$

$$- \frac{\left[\sum_p \left(\frac{x_{n+1}}{\Delta x} - \frac{x_n}{\Delta x} \right) + \frac{m}{M} \frac{\partial V}{\partial x / \Delta x} \right]^2 + \left[\sum_p \left(\frac{y_{n+1}}{\Delta y} - \frac{y_n}{\Delta y} \right) + \frac{m}{M} \frac{\partial V}{\partial y / \Delta y} \right]^2}{P_{1,n}^2} . \quad (2\text{-}46)$$

$P_{1,n}$ is the total number of ions in the given space being analyzed at the nth time step. For more details on the derivation of these temperature equations, see Quarterly Report No. 1, Section 6.0.

3.0 SIMULATION OF HIGH-VOLTAGE ION BEAM CONFIGURATION

3.1 INTRODUCTION

The first of the two configurations that were studied under this contract is discussed in Section 3 and will be referred to as the High-Voltage Ion Beam Configuration or Configuration 1. The simulation of this geometry presented a slight problem, because the electron emitter and decel grid were not the same electrode as the computer model had been designed for originally. However, this problem was overcome by first choosing the injection plane in the computer model just to the right of the decel grid in the actual physical system. Also a bias had to be applied between the injection plane and the electron emitter to keep electrons from moving towards the emitter. This problem occurs, because the dc voltages are scaled in our simulation but the thermal voltage is not.

The input data for Configuration 1 as given to us by Jones[3] is presented in Section 3.2. The problems in simulating this configuration with low mass ions are discussed in Section 3.3. The results of some initial test cases, which were run to establish the primary current for neutralization, are also explained in Section 3.3. In Section 3.4 the results from the production runs made with the electron emitter withdrawn from the ion beam are summarized. Information obtained from calculations made with the emitter immersed in the ion beam is presented in Section 3.5. Conclusions are discussed in Section 3.6.

3.2 INPUT DATA

The ion-gun configuration for generating the input data for the neutralizer program is shown in Fig. 3-1. The various electrodes, equipotentials, and ion trajectories are also shown in this figure. The scales along the x and y

ION GUN GEOMETRY, ENTRANCE PLANE AND NEUTRALIZERS
(All Voltages in Kilovolts)

Fig. 3-1

Scale: 1 mesh unit ≈ 0.005 inch

33

axes correspond to those in the computer model. The trajectories were calculated by using Hamza's[7] program with the simulation of zero x-component electric field at the exit (x=60). The other pertinent data were provided by Jones[3]. The configuration shown in Fig. 3-1 includes the accel and decel grids. The electron emitter was not simulated in obtaining the ion trajectories. The electron emitter is to be placed on the right side of the decel grid (which is at zero potential) at a convenient location; the choice of the location depends upon the compromise in the coupling between the ion beam and the electron emitter, and erosion of the emitter surface due to ion bombardment, because of ion exchange or otherwise. As a starting point, a circular cross-section emitter of radius 1.2 units with center at (60.5,21), corresponding to the scales in Fig. 3-1, was selected. We shall refer to this as the withdrawn emitter. This required fixing of the potential at points with coordinates (59.5,20), (59.5,21), (59.5,22), (61.5,22), (61.5,21), (61.5,20), (60.5,20) and (60.5,22). These eight points are located around the outer surface. The simulation of the circle with boundary constraints at the eight points in the x-y coordinate system is shown in Fig. 2-2. No rigid requirement at the center (60.5,21) was imposed, although the solution of Poisson's equation resulted in nearly zero (0.001 or even less) voltage also at this point. Later, after obtaining results with the withdrawn emitter, we immersed the emitter in the beam with center at (60.5,0). We shall refer to this as the immersed emitter. The x=53 plane was selected as the injection plane. This was quite convenient because any shift of the injection plane to the left would have necessitated a boundary constraint at the various points of the decel grid, thus increasing the size of the capacitance matrix.

The potential distribution along the injection plane (x=53 in Fig. 3-1 and x=0 in computer model) is given in Table I as a function of y.

y (Mesh Unit)	Potential (Volts)
0	-959.1
1	-955.7
2	-947
3	-933
4	-913.6
5	-885.8
6	-849.9
7	-806.6
8	-756.6
9	-701.6
10	-648.3
11	-608.5
12	-557.3
13	-495.4
14	-423.8
15	-343.5
16	-255.5
17	-160.5
18	- 59.1
19	- 32
20	- 21.8
21	- 16.5
22	- 13.5
23	- 11.4
24	- 10
25	- 9.3
26	- 9.1

VARIATION OF POTENTIAL ALONG y-AXIS AT x=53

TABLE I

The relative space-charge density as a function of y along
the injection plane, obtained from the ion trajectories in
Figure 3-1, is plotted in Figure 3-2. This data indicates
the distribution with respect to y of the particles to be
injected across the injection plane. Figures 3-3 and 3-4
show the variation of the x and y velocity components
across the injection plane, respectively.

3.3 PROBLEMS IN SIMULATION OF LOW-MASS IONS

It has been mentioned earlier[1,5,6] that the neutralizer
program for ion-mixing study uses low-mass ions. The values
of ion-to-electron-mass ratio of 64, 144, and 256 have been
used in the earlier studies. This is primarily due to the
limited accuracy in the x- and y-coordinates in the computer
memory because of the packing technique discussed earlier[1].
There are some other advantages (such as early diagnosis for
ion instability, etc.) in using low-mass ions. This results
in a considerable saving of computer time and memory. The
neutralization mechanism for the actual case (cesium or mercury
ions) is determined as a result of extrapolation of the data
obtained from low-mass ratios. For neutralization, considera-
tion of two things is important: (1) the total number of elec-
trons and ions, and (2) electron and ion currents. A micro-
scopic equalization of the number density and current for
electrons and ions would be ideal for space-charge neutraliza-
tion; however, because of random motion of the electrons, one
can best achieve macroscopic neutralization over a few debye
lengths.

It can be argued from the discussion in the above
paragraph that number density and velocity are the two para-
meters one would like to conserve in going from high-mass
ions to low-mass ions. Thus in the case of low-mass ions,
which are simulated in the neutralization studies, the voltages
applied on the various grids (electrodes) are correspondingly

Scale: 1 mesh unit ≍ 0.005 inch
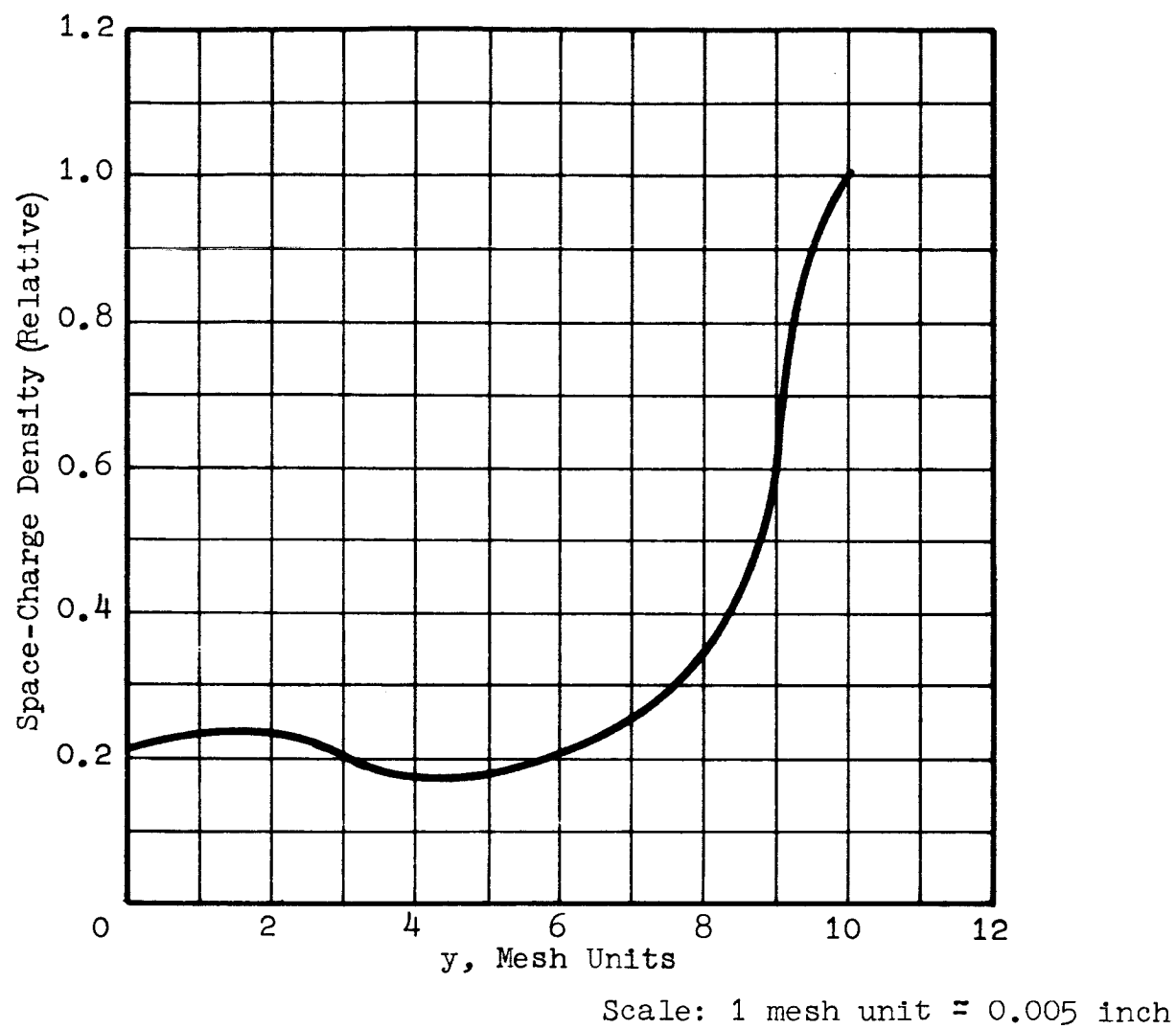
SPACE-CHARGE DENSITY VERSUS y AT THE INJECTION PLANE

Fig. 3-2
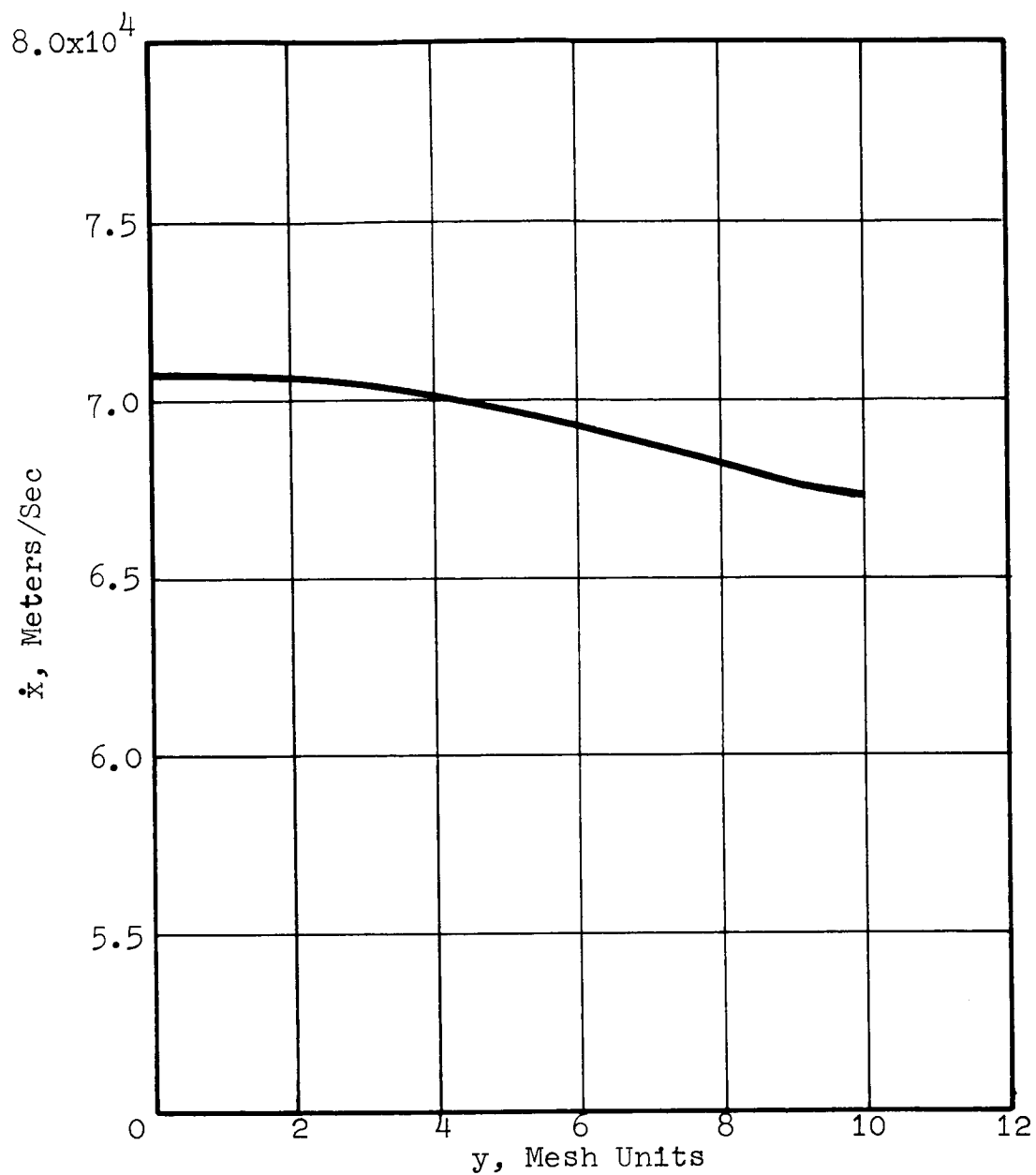
x-COMPONENT VELOCITY DISTRIBUTION AT THE INJECTION PLANE

Fig. 3-3
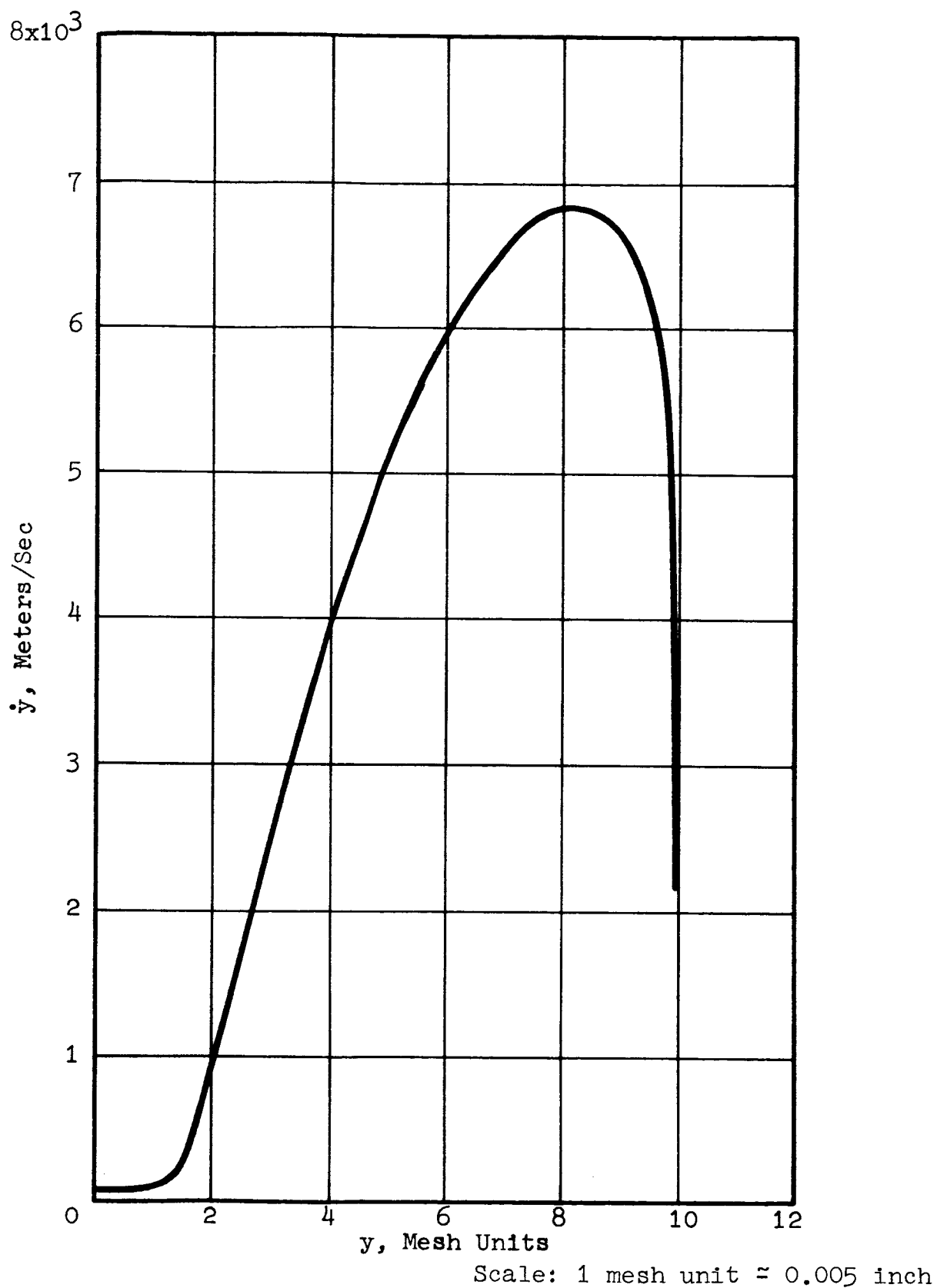
y-COMPONENT VELOCITY DISTRIBUTION AT THE INJECTION PLANE

Fig. 3-4

39

reduced. Under such conditions the voltage difference between the electron emitter and the decel electrode is not enough to prevent the thermal electrons from reaching the decel electrode. This imposes a problem in the study of neutralization because, in such a case, most of the electrons move toward the injection plane; all particles crossing the injection plane from right to left are absorbed and deleted from the program. This problem was not of importance in earlier studies because (1) under normal conditions the electron flow to the near electrode is extremely small and (2) in the previous studies, electron emitter and decel plane were assumed identical, so that the voltage difference between the decel plane and injection plane (accel grid), even for the case of low-mass ions, was much larger than the thermal equivalent voltage for electrons emitted from the decel grid (electron emitter). Because of the shift of the injection plane from the accel plane in the previous formulations to a plane near the decel plane, as discussed above, it was necessary to impose artificially some other conditions which would not change the physical significance of the neutralization mechanism and would prevent electron motion to the left of the injection plane. This problem, if not considered properly, can lead to incorrect understanding of the neutralization mechanism.

It was decided, after studying various schemes[5], to bias the injection plane negative with respect to the emitter. The value of the bias voltage should be just enough to prevent electrons from reaching the injection plane. The bias value would vary for different values of the ion mass so that the extrapolated value of the bias for the actual case (cesium or mercury) should be zero or negligible. (Ion mass has to be infinite in order to reduce this extrapolated bias to a zero value.) This technique is considered relatively simple and does not alter the physics of the neutralization mechanism. Tables II and III give variations

40

M/m	φ_o(Volts)	φ_d(Volt)	Bias (Volts)
64	0.625	0.3125	1250
144	1.406	0.3125	555
256	2.5	0.3125	312.5
**256 x 10^3	2500	0.3125	0.3125

VARIATION OF φ_o, φ_d AND REQUIRED BIAS* AS A FUNCTION OF M/m

(V_d=0.5)

TABLE II

M/m	φ_o(Volts)	φ_d(Volt)	Bias (Volts)
64	0.625	0.1875	750
144	1.406	0.1875	333
256	2.5	0.1875	187.5
**256 x 10^3	2500	0.1875	0.1875

VARIATION OF φ_o, φ_d AND REQUIRED BIAS* AS A FUNCTION OF M/m

(V_d=0.3)

TABLE III

---

*   This bias refers to the voltage distribution for the
    cesium ion case.

** The value of M/m=256 x 10^3 nearly corresponds to cesium
    ion mass.

of bias, actual beam potential (φ_o), and the difference (φ_d) between potentials at the injection plane and the electron emitter as a function of mass ratio for two different values of V_d (normalized φ_d). Since the voltage across the injection plane is not constant, φ_d = the minimum voltage difference which exists between the electron emitter and various points along the injection plane. The value of φ_d is selected appropriately so that the corresponding value of V_d is just enough to prevent electrons crossing the injection plane. As mentioned earlier, this problem arises only in the vicinity of the electron emitter because the voltage near the y=0 axis is high enough to prevent electrons crossing the injection plane in the vicinity of y=0.

The expression for the normalized potential V is given by

$$V_{ij} = - \frac{1}{4} \left| \frac{\ell}{\Delta x} \right|^2 \left| \frac{N_i}{N} \right|^2 \frac{M}{m} \frac{\varphi_{ij}}{\varphi_o} \quad , \qquad (3\text{-}1)$$

where the various parameters have been referred to in the earlier reports[1,5]. For the present case $\ell/\Delta x = 7.5$ and $N_i/N = 1/30$ were used in evaluating V_{ij} for the data shown in Tables II and III. (This value of N_i/N was selected in the previous studies[1] on the basis of various compromises.) It may be visualized from the data in Table II (or III) and Eq. (3-1) that the thermal equivalent voltage of 0.2 volt (electron emitter temperature = 2300°K) corresponds to a normalized voltage of about 0.32. (Normalized voltage is a dimensionless quantity.) It appears then that the normalized V_d used in Tables II and III may not be enough to prevent electrons crossing the injection plane. This difficulty was circumvented by allowing emission from the downstream surface of the electron emitter only. Furthermore, the electrons emitted toward the y=0 axis would have less chance to cross the injection plane. It may be mentioned here that, because of the random velocity distribution of the emitted electrons, the emitter surface is completely surrounded by electrons which

form a virtual cathode. This will be discussed in detail in Section 3.4. From the results of both test and production runs for two different values of the bias of voltage, it was found that the physical nature of the neutralization mechanism is not altered.

3.4 RESULTS WITH ELECTRON EMITTER WITHDRAWN

3.4.1 INTRODUCTION

Several test runs were made to determine the emission requirements for the electron emitter. Test runs with various values of N_e/N_i were made which are discussed in detail[4] in Quarterly Report 3. To summarize, the net charge (number of electrons minus number of ions) versus time plots indicated that a value of $N_e/N_i = 12$ should be used for this configuration. As has been pointed out N_e/N_i is not a very good indication of the electron current since many of the electrons emitted return immediately to the cathode and are collected. However, the relatively large value of $N_e/N_i = 12$ as compared to 3 for the emitter simulated under the previous contract[1] indicates poor coupling between the ion beam and the electron emitter. After the establishment of emission requirements of the electron emitter, some general data was obtained for a large number of time steps. The effect of the mass ratio (ion-to-electron-mass ratio) was studied by considering three values of mass ratio (64, 144, and 256). The data includes trajectories of ions and electrons, net charge as a function of time, ship potential and thrust variations as a function of time, equipotentials, density of the charged particles, and temperature calculations. For the case of $M/m = 144$, two investigations were made for two values of the bias voltage (333 and 555 volts). These results are briefly discussed in the following paragraphs.

In the calculations discussed in Sections 3.4 and 3.5 the following parameters are held constant:

$$N_i = 3, \quad N = 90, \quad \frac{\ell}{\Delta x} = 7.5, \quad \frac{a}{\ell} = 1.33, \quad \frac{e\varphi_o}{kT} = 0.1 \frac{M}{m} \ .$$

The value of ℓ/L is varied for each M/m so that the value of $\omega_p \Delta t$ is the same (0.2828) in all cases. For all the data discussed in Section 3.4, $N_e/N_i = 12$ and $-3\pi/4 < \theta < \pi/4$; i.e., the electron emission was restricted to half of the surface, but the interception test was made for the complete surface. Unless otherwise specified, the bias value is the same as in Table III.

3.4.2 TRAJECTORIES

Figures 3-5 and 3-6 show the typical ion trajectories x versus time, for two values of M/m; namely, 256 and 64. Because of high-mass, ion trajectories are nearly straight lines. The periodic bunching or crossing of trajectories is essentially due to the fact that the ions are not emitted at a constant x-component velocity across the injection plane. In the present data there are 17 injection points, and 3 ions are emitted every time step. This case is similar to that of a velocity modulation at the injection plane like that in a klystron at a frequency corresponding to 17/3 time steps. The resulting trajectories are similar to the Applegate diagram[8], except in this case the trajectories are modified because of the fluctuating fields which result from the presence of electrons. For the case of $M/m=64$, some additional bunching of ions is indicated in the results shown in Fig. 3-6. This is due to the fact that low-mass ions are more susceptible to fluctuating fields. The results for $M/m=144$ (for two values of the bias voltage) are similar to those shown in Fig. 3-5. The acceleration of the first few ions shown in the two figures is due to the fact that (1) the emission cycle is started from the center of the beam where the x-component velocity is maximum, and (2) there is some acceleration due to the electron pressure. The acceleration due to the electron pressure was shown to be inversely proportional to the value of the ion mass, from the previous calculations[1].

Figures 3-7 and 3-8 show the ion trajectories, y versus x, for the two values of M/m: 256 and 64, respectively. As mentioned in the previous results[1] the reflection from the top, $y=24$ (and the bottom, $y=0$) is due to the periodic nature of the model assumed in this analysis. Because of symmetry only half a period is shown in these figures. The reflected ions are actually ions from the neighboring cell. Because of the reduced ion mass, the fluctuations in the y-direction for the
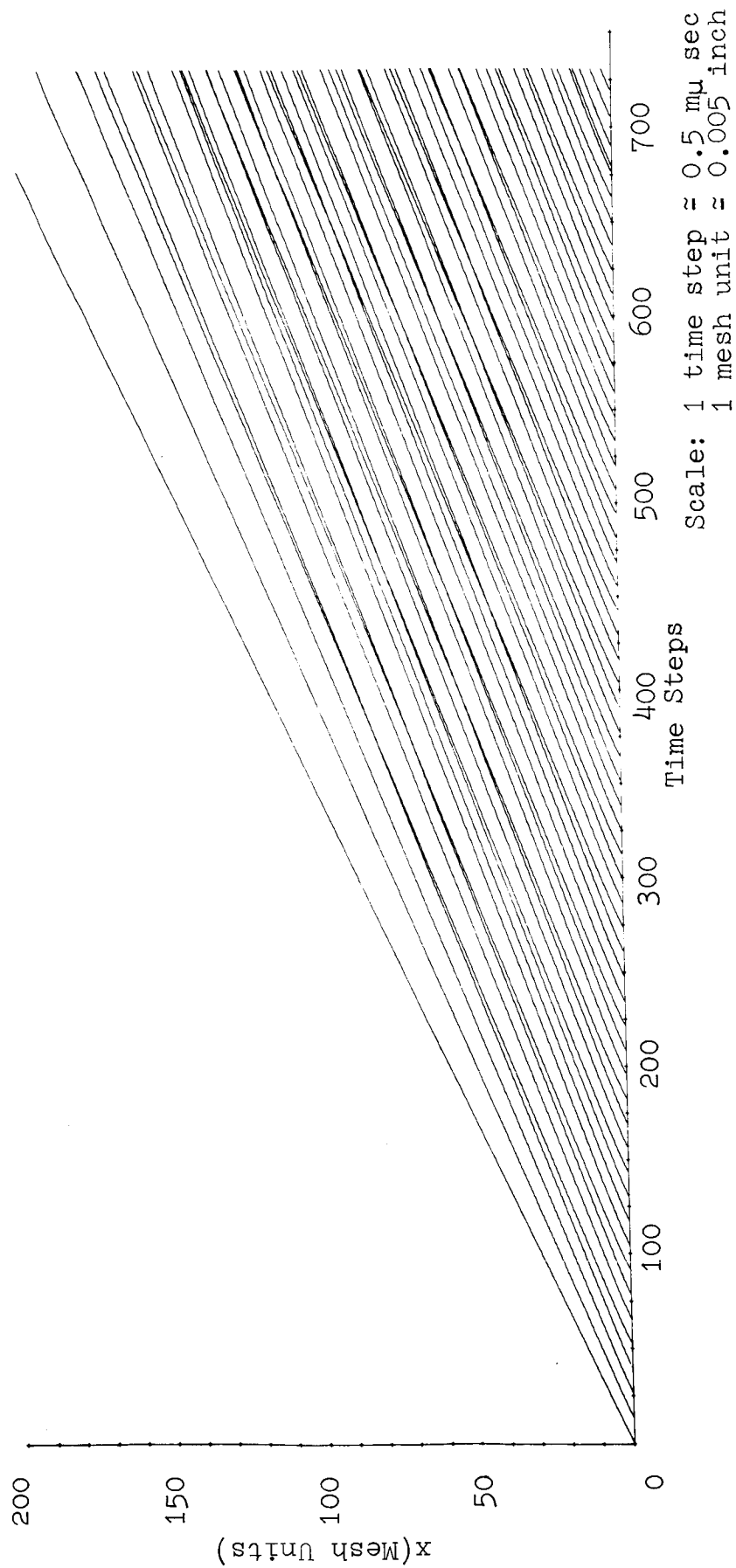
ION TRAJECTORIES: x VERSUS TIME, M/m=256

Fig. 3-5

Scale: 1 time step ≅ 0.5 mμ sec
1 mesh unit ≅ 0.005 inch

x(Mesh Units)

Time Steps

46
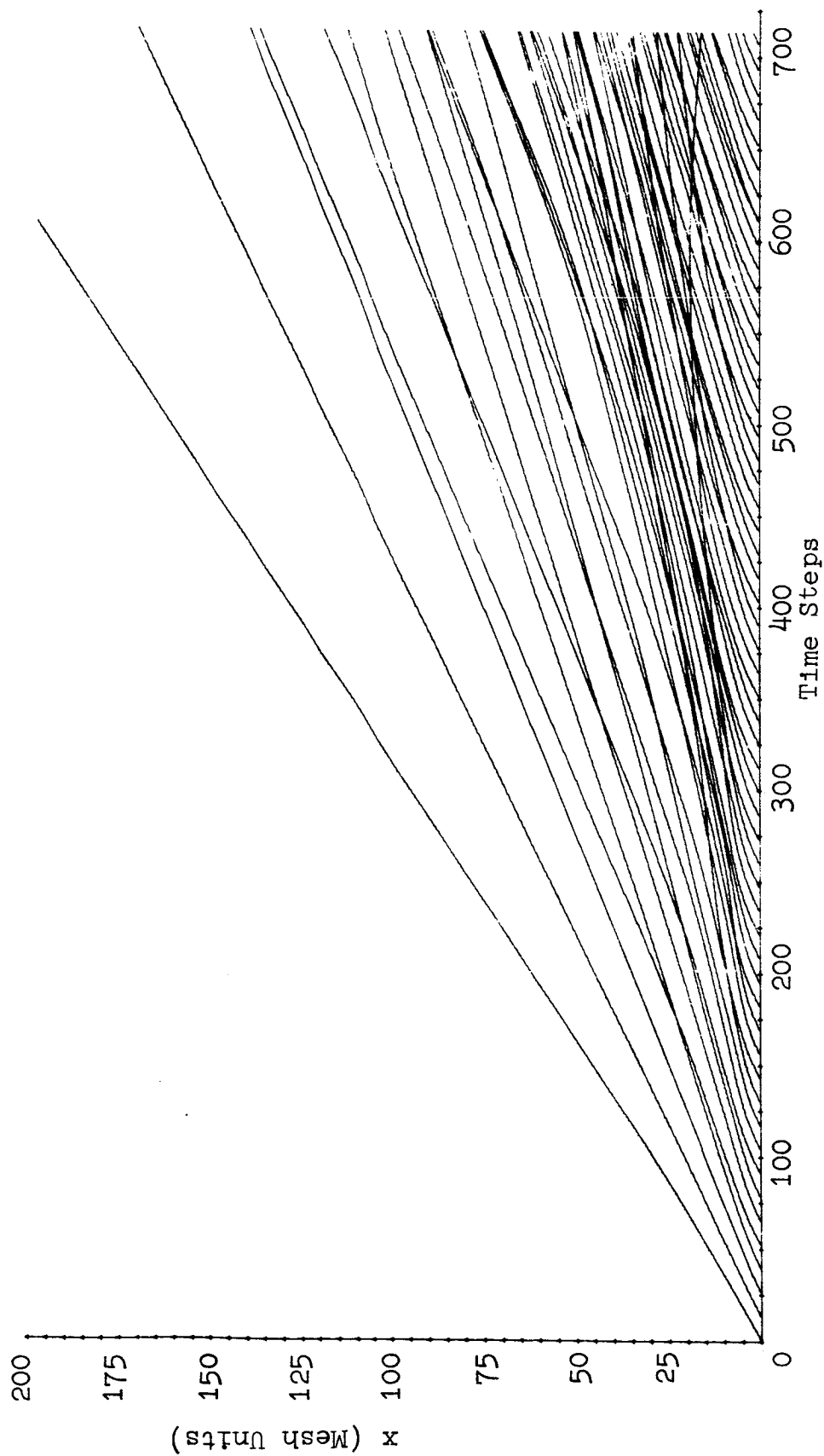
ION TRAJECTORIES: x VERSUS TIME, M/m=64

Fig. 3-6

Scale: 1 mesh unit ≈ 0.005 inch
       1 time step ≈ 0.5 mμ sec.

47
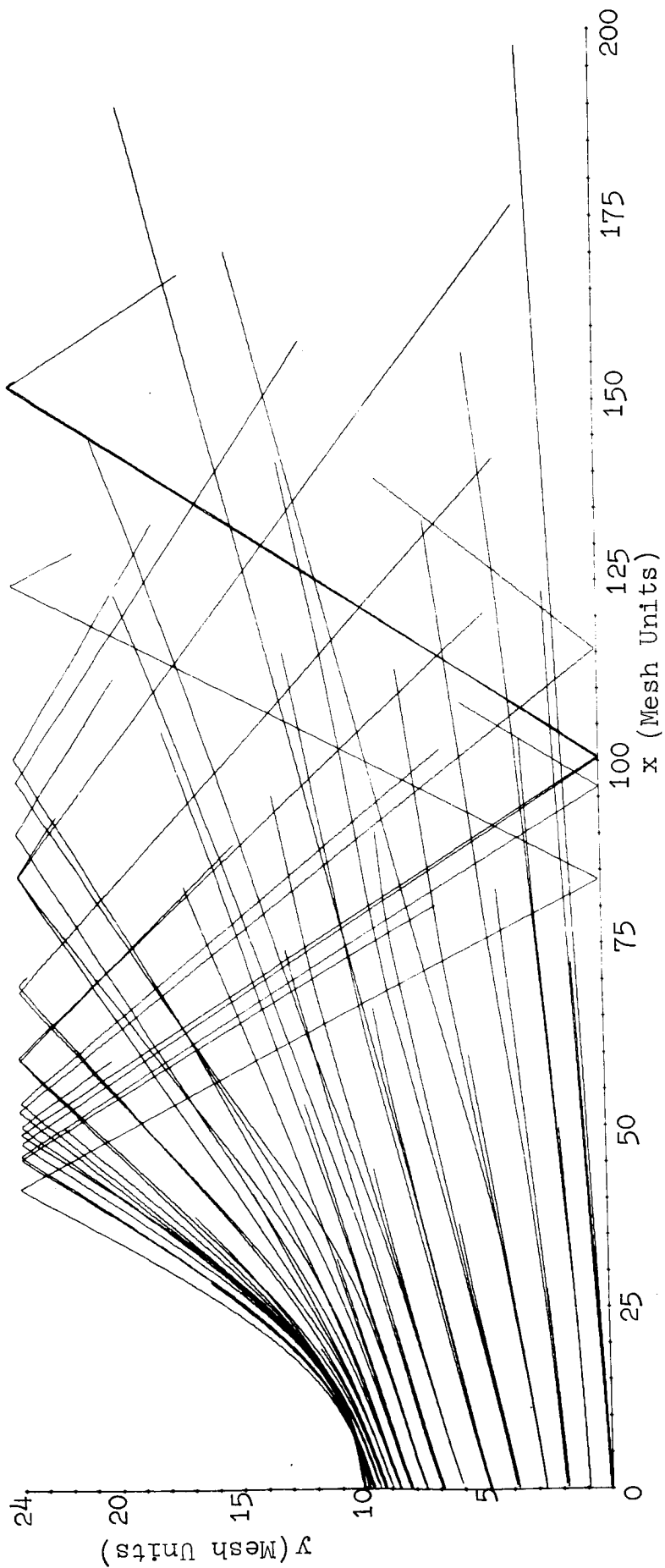
ION TRAJECTORIES: y VERSUS x , M/m=256

Fig. 3-7

Scale: 1 mesh unit ≈ 0.005 inch

x (Mesh Units)

y (Mesh Units)

48
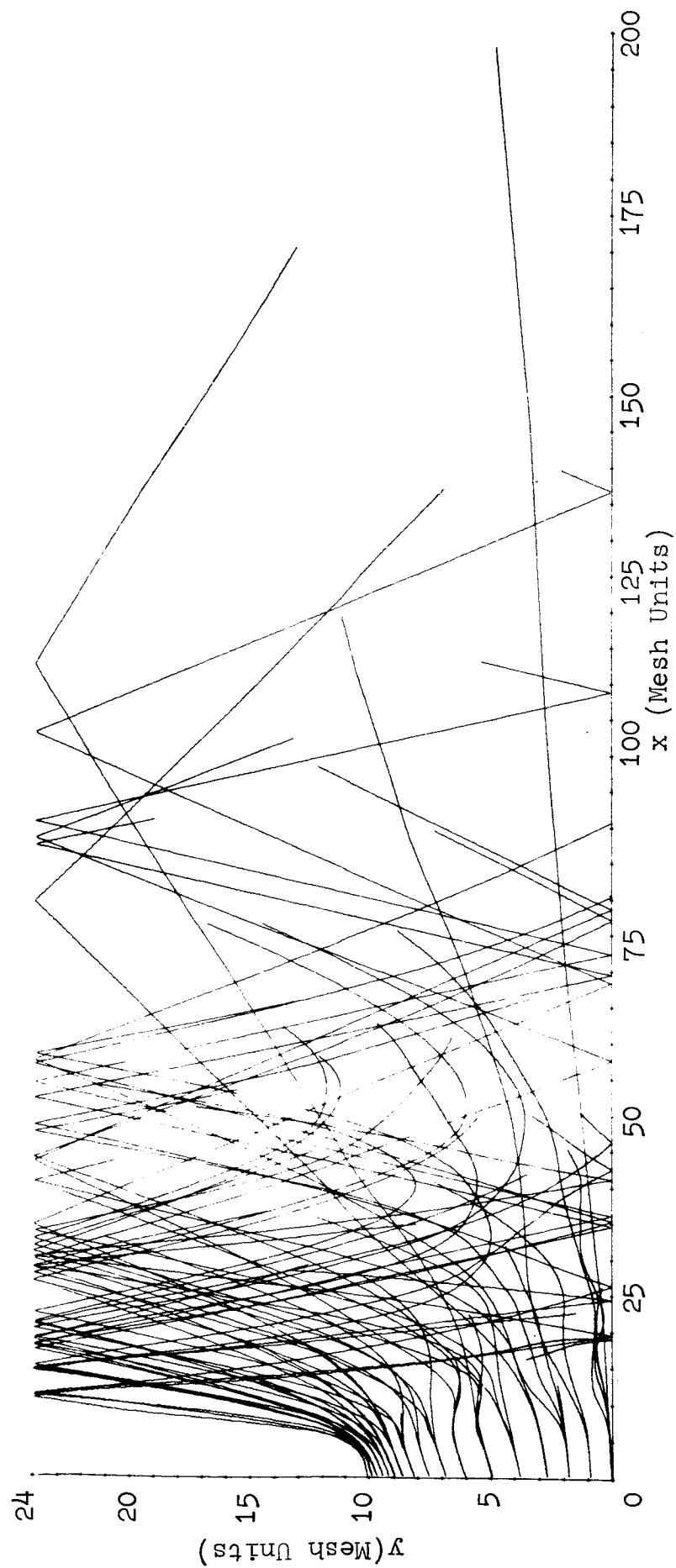
ION TRAJECTORIES: y VERSUS x, M/m=64

Scale: 1 mesh unit ≅ 0.005 inch

Fig. 3-8

case of M/m=64 are more than those for the case of M/m=256.
The results for the case of M/m=144 are similar to those shown
in Fig. 3-7, except that there is more beam divergence because
of low-mass ions. The y-component injection velocity is small,
and ions also experience fluctuating fields; this is more evi-
dent in the plots shown in Fig. 3-8. In general, there is
always a positive potential region (after some small transient
period) in the center, because the ions are concentrated in the
central region, particularly near the injection plane. This is
indicated by the reflection of ions in the trajectories shown
in Fig. 3-8. This type of reflection is not noticed for the
other cases due to (1) heavy mass and (2) the ions from the
neighboring cell enter the plasma region farther from the emit-
ter location, where the ion beam density is reduced and this
region is fairly neutralized. In the earlier studies[1] such
reflection of ions (M/m=64) did not occur, because the coupling
in those models was high, neutralization occurred almost instan-
taneously, and the ions from the neighboring cell (reflected
ions) experienced negligible space-charge field.

The reflection of ions in the central region and their
response to field fluctuations as noticed in plots shown in
Fig. 3-8 indicate a rapid thermodynamic equilibrium of ions
and electrons. This is further evidenced from the temperature
calculations discussed in Section 3.4.4.

Figure 3-9 shows the electron trajectories, x versus time,
for the case of M/m=144; the results for the other cases are
similar to those shown in this figure. It is noticed as in the
previous studies that the electrons oscillate back and forth.
Fast-velocity electrons go beyond the ion beam and are reflected
back due to the reflecting potential developed at the plasma
edge[9]. This implies that the electrons are very mobile and tend
to compensate the positive charge wherever it is created in
space. Because of the finite response time, the electron motion
becomes oscillatory. However, the overall envelope of the elec-
tron cloud seems to move at a nearly constant velocity.

Farthest Ion

x (Mesh Units)

Time Steps   Scale: 1 mesh unit ≅ 0.005 inch
                      1 time step ≅ 0.5 mµ sec.
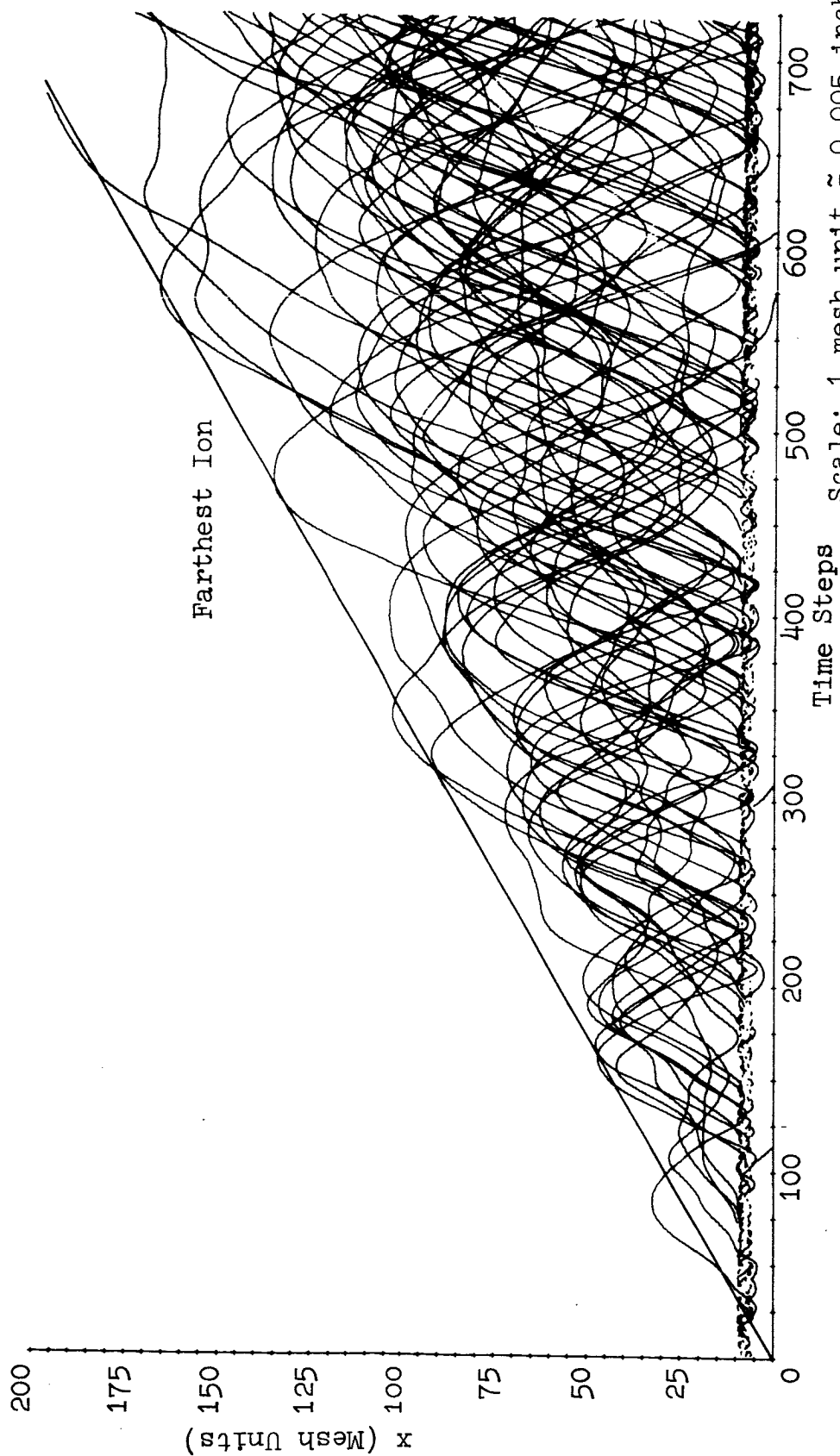
ELECTRON TRAJECTORIES: x VERSUS TIME, M/m=144, BIAS=333 VOLTS

Fig. 3-9

The broken lines in the vicinity of x=7.5 indicate the emission and interception of the electrons at the emitter surface. Electrons are emitted from half of the surface but the interception test is made for the complete surface. The trajectories reaching the x=0 axis indicate a fraction of total number of electrons crossing the injection plane. The minimum voltage difference between the emitter and injection plane is approximately the thermal equivalent voltage. This would allow about 37 percent of the total number of emitted electrons to cross the injection plane. However, this number in the present studies is extremely small because (1) emission is artificially simulated from half surface only, (2) the average voltage difference between the emitter and injection plane is more than the minimum value, and (3) the ions, at later time intervals, develop a positive potential in the central region, which pulls electrons.

Figure 3-10 shows the typical electron trajectories, y versus x, for the case of M/m=256. The electron emitter is of circular shape; it appears as an ellipse because of the difference in scales along the x- and y-axes. Although electrons are emitted from only half the surface, yet electrons form a cloud or "virtual cathode" about the entire emitter. In comparing the data shown in Fig. 3-5 with the data shown in this figure, it is clearly noted that electrons follow ions very closely. Again, as mentioned previously[1], the entire space is covered by electrons which travel with appreciable transverse motion. The x-component velocity for the complete cloud is, however, nearly equal to the ion velocity. Some trajectory plots for a relatively small number of electrons in the previous results[9,10] have indicated that the electron motion in the y-direction is very nearly specified by the electron plasma frequency with a small drift along the x-axis. Electron trajectories for the cases M/m=64 and M/m=144 are similar to these results.

Electron Cloud Around Emitter
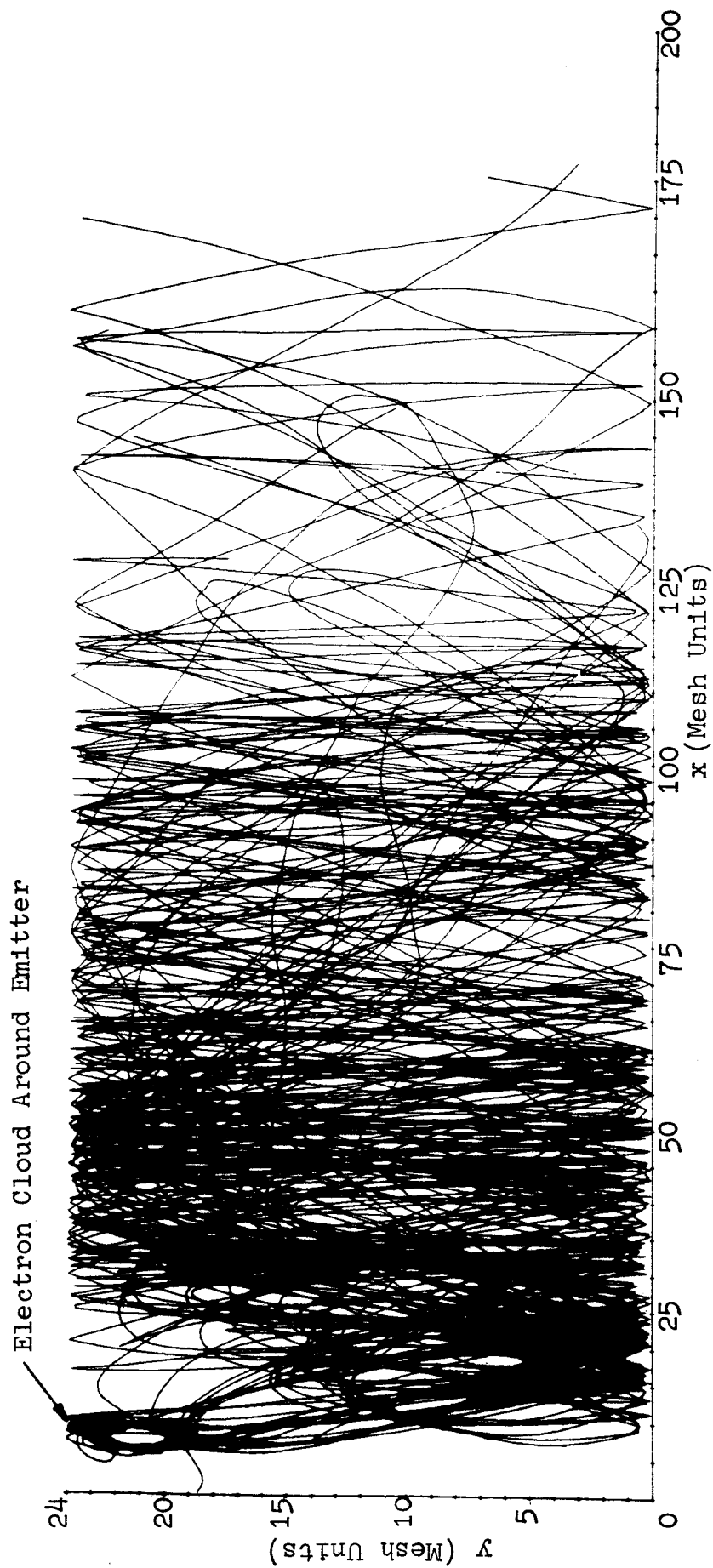
ELECTRON TRAJECTORIES, y VERSUS x, M/m=256

Scale: 1 mesh unit ≃ 0.005 inch

Fig. 3-10

53

3.4.3 SHIP POTENTIAL AND THRUST

One of the useful criteria for establishing the degree of neutralization of an ion beam in an ion engine is the variation in the ship potential and thrust as a function of time. Figure 3-11 shows the variation of the normalized ship potential as a function of time (for the case of $M/m=144$) for two different values of bias voltages discussed earlier, i.e., 333 volts and 555 volts. As indicated on the figure, it can readily be seen that there is not much difference in the two plots and that in both cases the ship potential fluctuates around a steady-state level. The large fluctuations near 700 time steps are caused by particles leaving the exit plane, which we removed from computer memory. Thus, these fluctuations are not physical. The program was later corrected to take into account the charge which passes the exit plane. We assume that the particles drift at their exit velocity and consider the fundamental charge harmonic of these particles in calculating the potential distribution. Results obtained after this correction was made are presented in Sections 3.5.3, 4.3.3, and 4.4.2.

Table IV presents a comparison of data obtained from the ship potential for the bias voltages of 333 and 555 volts. These values were found by fitting a sinusoidal variation to each of the two curves in Fig. 3-11. In other words, we Fourier-analyzed these curves graphically to determine the characteristics of the fundamental frequency. The values for the steady-state level and amplitudes of oscillation were found by multiplying the computer results by the normalization constant, φ_0, which in this case was 2500 volts. These values correspond to the values in the case of cesium ions. In this analysis, we neglected the non-physical fluctuations near 700 time steps.
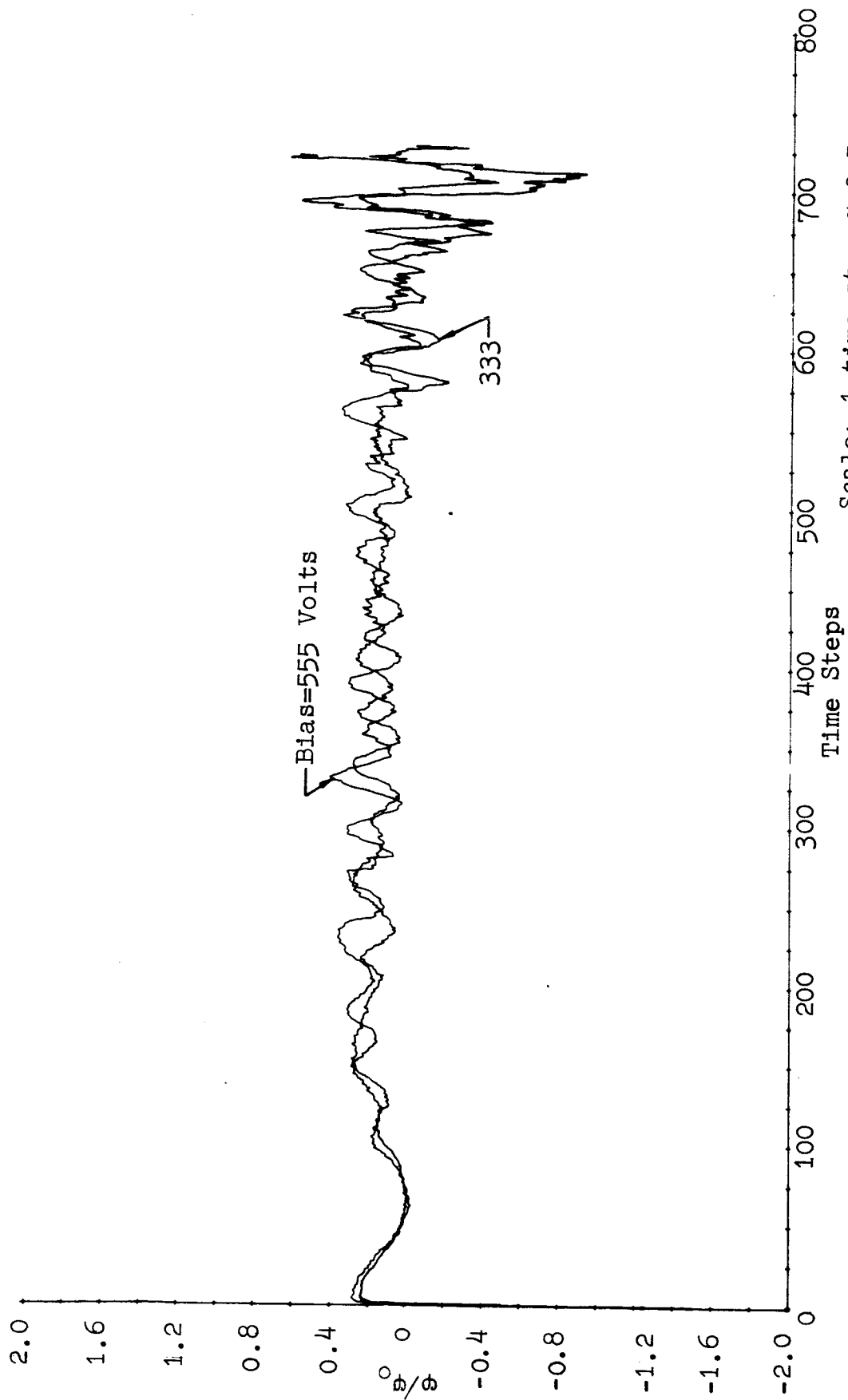
NORMALIZED SHIP POTENTIAL VERSUS TIME, M/m=144

Fig. 3-11

55

Bias (Volts)	Steady-State Level (Volts)	Amplitude of Oscillation (Volts)	Number of Time Steps in a Period
333	430	310	30
555	450	312	33

COMPARISON OF SHIP POTENTIAL FOR TWO DIFFERENT
VALUES OF THE BIAS VOLTAGE

TABLE IV

Note that the variation of bias (so long as it is reasonably small, as in the present computations) does not seem to alter the physics of the neutralization mechanism. For the case of the larger bias (555 volts), the electron barrier is increased; this results in the escape of a smaller number of electrons from the sheath surrounding the electron emitter. The reduction in the total number of electrons reduces the electron plasma frequency, and thus the total number of time steps in a period is increased.

It is interesting to mention here that $\omega_p \Delta t = 0.2828$ in these calculations. The value of the electron plasma frequency was obtained from the assumption[5] that there are as many electrons as ions and that ions travel in straight

lines starting from the injection plane. This value of the
electron plasma frequency is thus determined when the elec-
trons are trapped in between y=0 and y=10 planes. (In these
calculations ions are injected from y=0 to y=10.1.) The
present results indicate that eventually the whole space is
filled with electrons. Thus, the electron density is reduced
by a factor 2.4 from the ideal value used in the normalization.
This corresponds to a reduction in the electron plasma fre-
quency by a factor of 1.55; that is, the number of time steps
in a plasma period is increased by 1.55. According to this
estimate, the number of time steps in a plasma period should
be approximately 34.4. This is very close to what has been
observed in the variation of the ship potential. The slight
decrease in this number from the calculations discussed above,
as noticed in the results, is probably due to the facts that
(1) there are more electrons than ions and (2) particles do
not spread over the entire space. (In the above calculations,
it is assumed that electrons spread over from y=0 to y=24.)
In a practical case, the contributions to the plasma frequency
from the heavy ions would be negligible. These results indicate
that, in general, the ship potential fluctuates at the plasma
frequency. In order to detect these fluctuations, a high fre-
quency probe is necessary.

Figure 3-12 shows the variation of the normalized ship
potential as a function of time for three different values
of M/m. Again, the large fluctuations at later time inter-
vals are due to limitations in the present program (particles
leaving the exit plane are deleted from the program) as
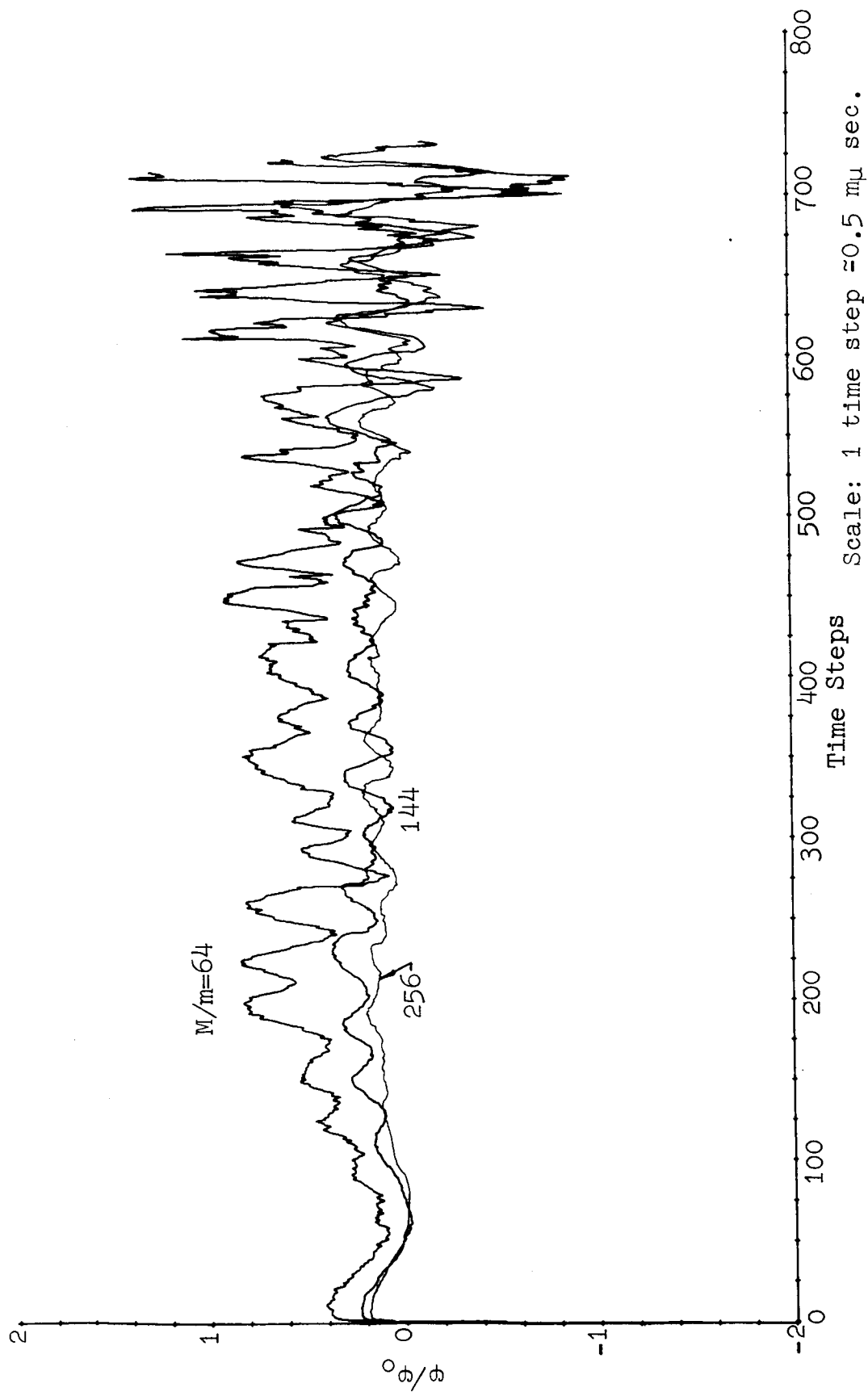
NORMALIZED SHIP POTENTIAL VERSUS TIME: VARIATION WITH MASS RATIO

Fig. 3-12

58

discussed above. As may be noticed, both the steady-state level and the amplitude of oscillations are reduced as the value of M/m is increased. Table V shows a comparison of data obtained from the ship potential for three different values of M/m. The voltage values are calculated for the case of cesium ions from the respective data for different values of M/m.

M/m	Steady-State Level (Volts)	Amplitude of Oscillations (Volts)	Number of Time Steps in a Period
64	1325	375	26.2
144	430	310	30
256	300	200	33

COMPARISON OF SHIP POTENTIAL FOR
DIFFERENT VALUES OF M/m

TABLE V

An extrapolation to the practical case of heavy ions indicates negligible values for both the steady-state level and the amplitude of oscillations. These results are similar to those obtained earlier[1] for the idealized configuration.

In interpreting the above results, particularly the steady-state level, it is necessary to realize that the injection plane is at a negative potential with respect to the

emitter and that the effect of the negative potential extends in space, implying that the emitter is at a positive potential with respect to infinity. At later time intervals, the presence of ions tends to develop a positive potential zone in the central region even though there are more electrons in the complete space. A good many electrons surround the emitter so that the number of electrons in the total space is not enough to neutralize the ion beam adequately. (This is due to poor coupling between the ion beam and the electron emitter.) At such an instance, the instantaneous value of the ship potential can become negative as indicated in Figs. 3-11 and 3-12 at later time intervals.

Figure 3-13 shows the variation of the normalized thrust as a function of time for two different values of M/m, namely 64 and 256. The thrust variation for the case of M/m=144 with a bias voltage of 333 volts (and 555 volts also) was similar to that for the case of M/m=256 shown in Fig. 3-13. The fine periodicity in these plots (17/3 time steps per period) is due to the fact that there are 17 injection points and only 3 ions are injected at each time step. The injection velocities and the fields for these injection points are different, and thus contributions to thrust from the injected particles would be different at different time steps. The maximum value of thrust in this periodicity is obtained for the conditions existing in the center of the beam. As may be noticed from Fig. 3-13, the steady-state level is increased, and the fluctuations are decreased (for the normalized thrust) as the value of M/m is increased. This conclusion is again similar to that derived from the earlier calculations[1].
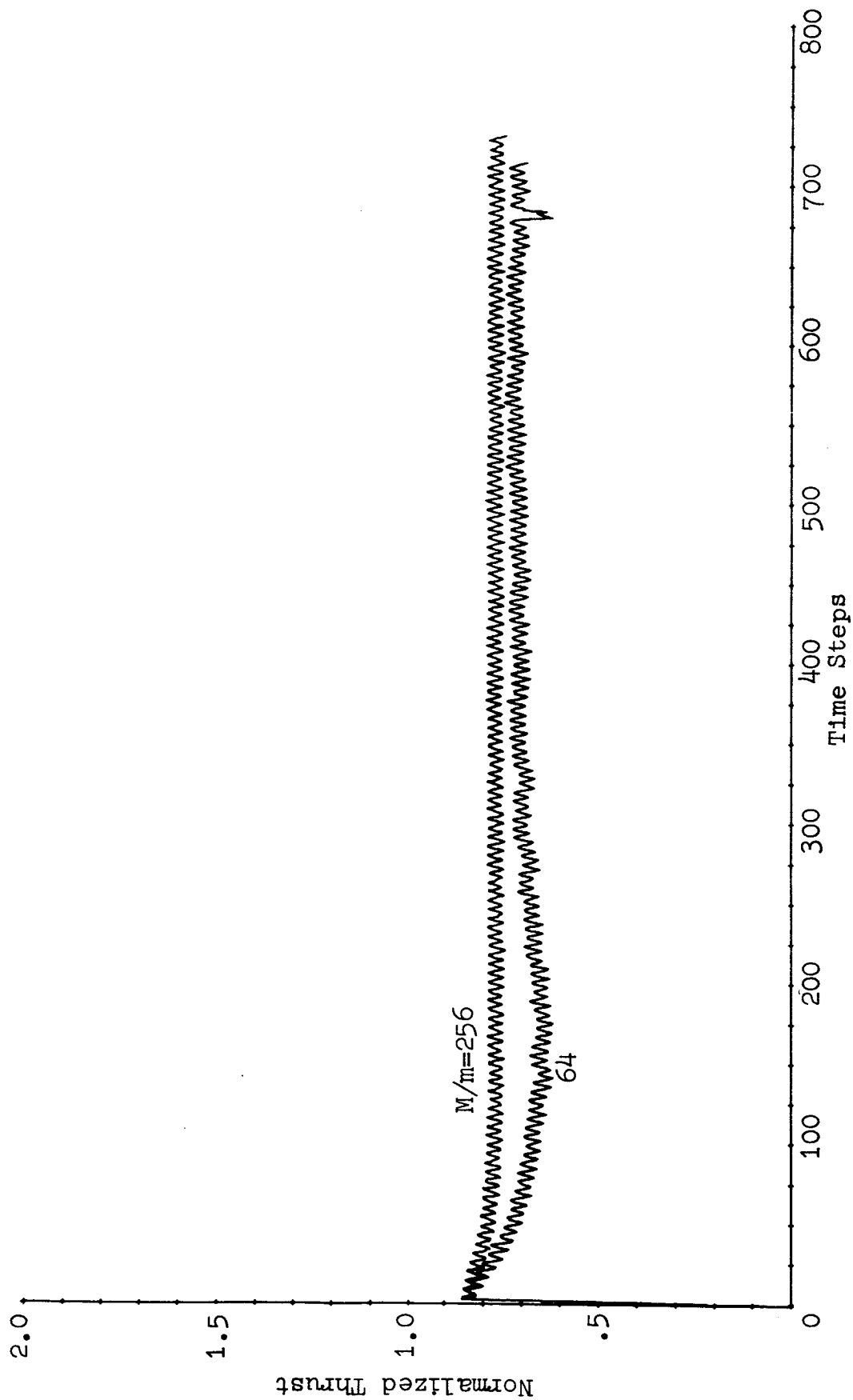
NORMALIZED THRUST VERSUS TIME: VARIATION WITH MASS RATIO

Fig. 3-13

Scale: time steps ≈ 0.5 mμ sec.

3.4.4 TEMPERATURE CALCULATIONS

It has been mentioned earlier that one of the aims of
the electron-ion mixing program was to evaluate temperature
of both electrons and ions as a function of space and time.
This has been of particular interest because Sellen, et al[2],
have noticed considerable amount of cooling of electrons along
the beam away from the source. In Sellen's experiments, the
ion beam and the electron emitter are well coupled and the
plasma potential is very nearly the same as that of the elec-
tron emitter. The present configuration under study is not
similar to the configuration from which Sellen obtained re-
sults, so somewhat different results might be expected.

The formulation for temperature calculations both for
electrons and ions has been given in Section 2.8. Because of
computer memory restrictions, it was necessary to limit the
computation of temperature to five locations in space. For
this purpose, it is necessary that there should be a suffi-
cient number of particles in each location so that the
statistical techniques can be applied without an appreciable
error. Each location corresponds to a vertical strip 5 mesh
units wide (in the x-direction) and 24 mesh units in the y-
direction. All the particles located in these 120 mesh rec-
tangles are considered in evaluating the temperature at the
corresponding time interval. Typically, there are 40 or more
particles of each species in a segment under equilibrium
conditions. In the following, the temperature calculations
for different cases mentioned earlier are discussed. The
normalized temperature (with respect to the electron-emitter
temperature) is plotted versus x. The results are shown only
at the five locations mentioned above, a horizontal line indicat-
ing the computed temperature of a particular species at a certain
time step as shown in these plots.

Figure 3-14 shows the variation of the normalized temperature as a function of x at different time steps for the case where M/m=144 and bias voltage is 333 volts. Both electron and ion temperatures are plotted; ion temperatures are plotted in dashed lines while electron temperatures are plotted in solid lines. Ions injected initially at x=0 correspond to a zero temperature. For a few time steps there are no data shown. This implies that at the particular time instant there were practically no particles (ion or electron) in the next strip. In the vicinity of the electron emitter, a virtual cathode (under space-charge limited conditions) is formed and only fast velocity electrons can escape this barrier. The electron temperature in the emitter strip is less than the emitter temperature*. The high-velocity electrons correspond to a high temperature in their own reference, and, moreover, there is formation of a positive potential region slightly down-stream from the emitter. Thus, the electrons pick-up some more energy. This results in an increase in temperature of the electrons. From the data at various time steps (200, 300, 400, 500, 600, and 700), the average electron temperature in the second strip (x-coordinate of the centroid=28.5) is approximately 3.4 times the emitter temperature. The corresponding normalized ion temperature in this segment is about 0.5.

In general, there is a good mixing of electrons and ions also from the thermodynamic point of view. After having attained high temperatures[11], the electrons begin to cool down as they drift in the x-direction. Similarly, the ions starting with a zero temperature develop some randomization and their temperature is increased. From a comparison of plots for ion and electron temperatures at a given time step, it can be

---

*   It can be shown that, for the Maxwellian velocity distribution used here, the electron temperature $\simeq 0.465T$ (T=emitter temperature) when there is no other energy exchange mechanism involved.
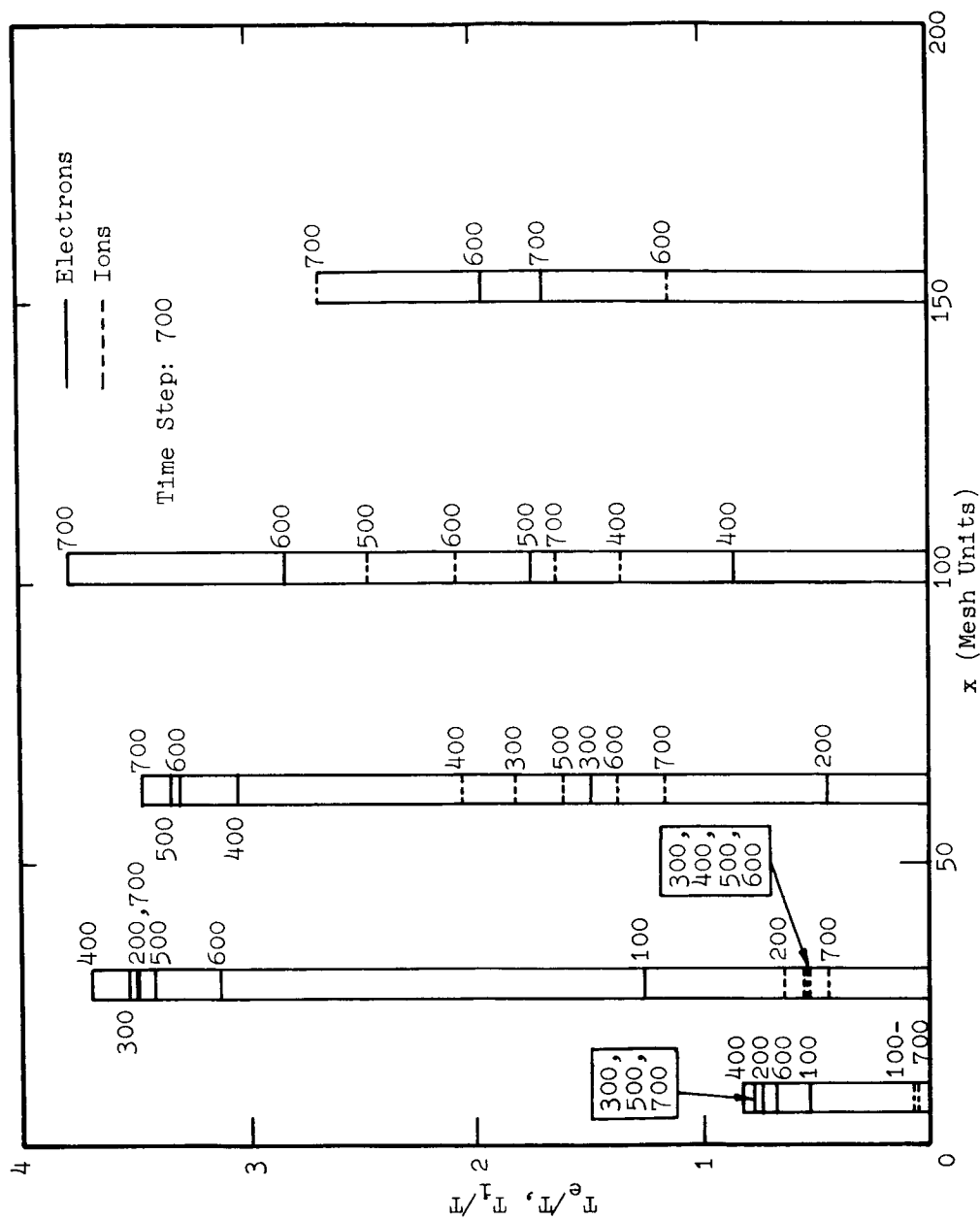
Scale: 1 mesh unit $\approx$ 0.005 inch
1 time step $\approx$ 0.5 mμ sec.

NORMALIZED TEMPERATURE VERSUS x, M/m=144, BIAS=333 VOLTS

Fig. 3-14
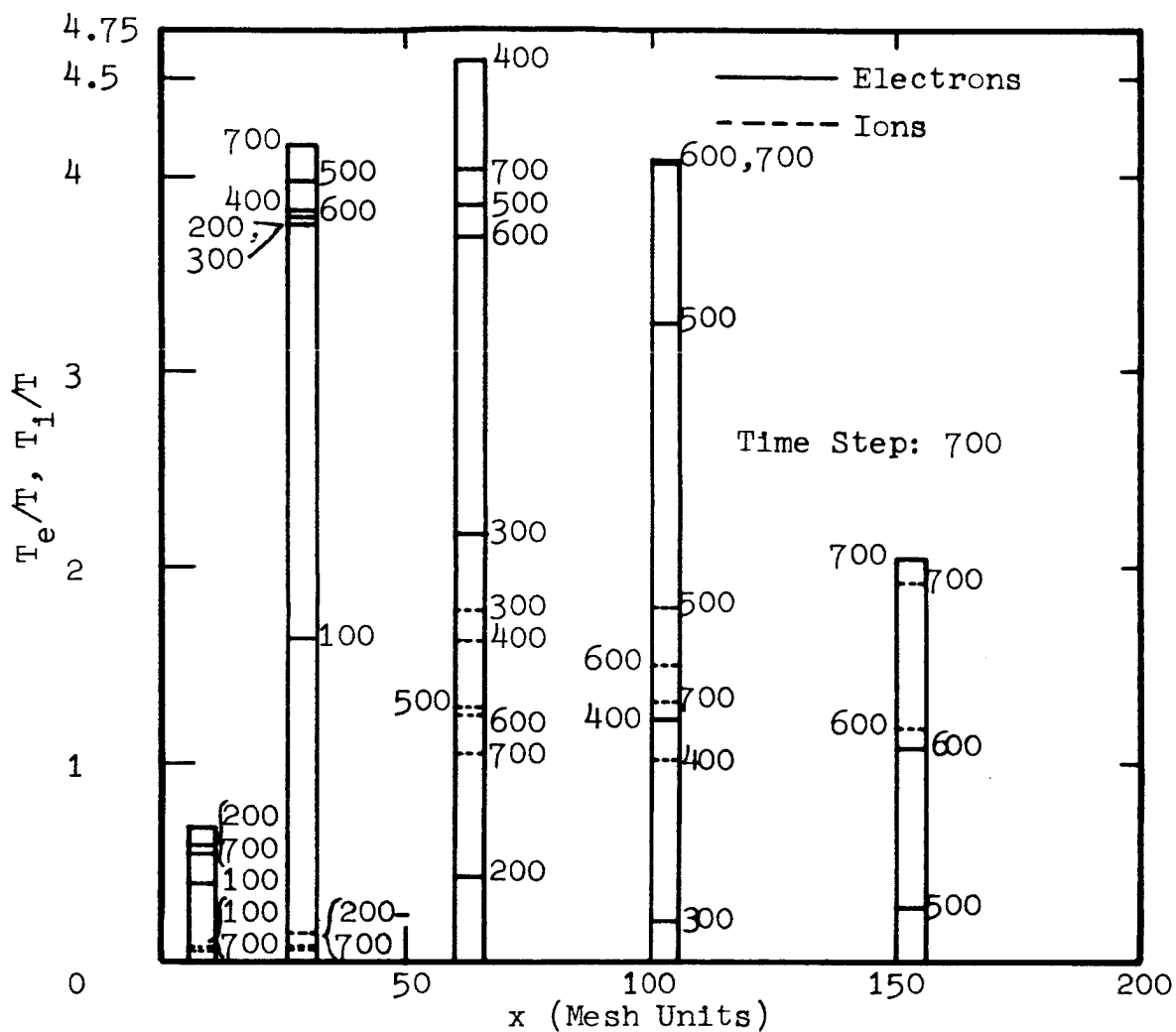
Electrons
Ions

Time Step: 700

x (Mesh Units)

T_e/T, T_i/T

noticed that there is always a tendency to reach a stage of equilibrium where the two temperatures are nearly equal. In some cases there may be a crossing; however, the grain size in this calculation is too coarse for us to discuss this crossing.

Figure 3-15 also shows the electron-and-ion temperature plots for $M/m=144$, but with bias voltage of 555 volts. Because of the increase in bias voltage, the initially emitted electrons have to cross a higher barrier, through which only the high velocity electrons can escape. The average electron temperature in the second strip is nearly the same as in the previous case, except that there are more fluctuations in the second case; for example, the electron temperature at 400 time steps is increased by about 11 percent in the second case. This results in a corresponding increase in the ion temperature also. In general, there is a good correlation between ion and electron temperatures at different time steps for the two cases. This indicates that there is a good mixing of electrons and ions.

Figures 3-16 and 3-17 show the corresponding plots for $M/m=256$ and 64, respectively. These results are, in general, of the same type as discussed before. For the case of $M/m=64$, there is evidently more rapid mixing of electrons and ions, particularly because ions are lighter and are more susceptible to fluctuating fields created by randomly moving electrons. As a result of this behavior, the maximum electron temperature in this case is less than that in the previous cases.

NORMALIZED TEMPERATURE VERSUS x, M/m=144, BIAS=555 VOLTS

Fig. 3-15

Scale: 1 mesh unit ≈ 0.005 inch
1 time step ≈ 0.5 mμ sec.

Scale: 1 mesh unit ≃ 0.005 inch
1 time step ≃ 0.5 mμ sec.

NORMALIZED TEMPERATURE VERSUS x, M/m=256

Fig. 3-16
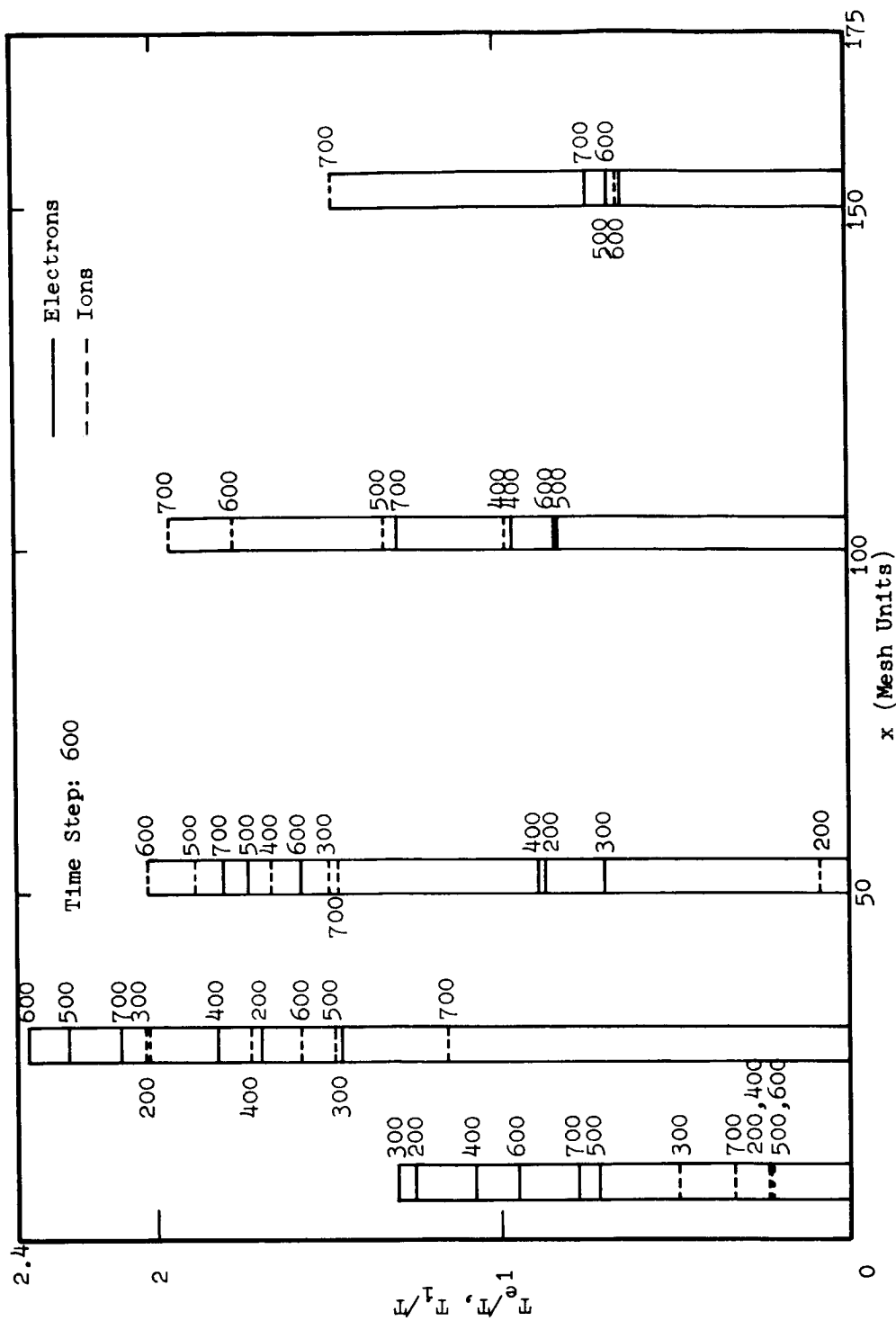
NORMALIZED TEMPERATURE VERSUS x, M/m=64

Fig. 3-17

Scale: 1 mesh unit ≈ 0.005 inch
       1 time step ≈ 0.5 mμ sec.

3.4.5 FRACTIONAL EXCESS CHARGE

One of the most important criteria for ion-beam neutralization is the equalization of both the negative and positive charges. At the beginning of the contract period, we calculated for this configuration the net negative charge, i.e., total number of electrons minus the total number of ions within our 200 by 24 grid mesh, as a function of time. In Quarterly Report No. 3, Section 5.5, plots of net negative charge versus time for this configuration were presented and discussed. Unfortunately, these results are not completely correct because an error was found in the scheme for detection of ions and electrons leaving the grid mesh. Also, it was later suggested that the calculation of a relative or fractional excess charge, i.e., (number of electrons - number of ions) / (number of ions) would be more useful and meaningful than the net negative charge as defined above. We proceeded to correct the error and modify the program to compute the fractional excess charge at each time step.

Figure 3-18 shows the fractional excess charge plotted as a function of time for the case where M/m=144 and bias voltage is 333 volts. Note that there are usually slightly more electrons than ions which try to compensate for any build-up of positive charge in the grid mesh. However, the electronic charge after only 90 time steps is only about one percent in excess of the ionic charge, and is even less than one percent in excess for time steps greater than 90. This is certainly one excellent indication of beam neutralization for this case. Similar results for fractional excess charge versus time were found with cases where M/m=64 and M/m=144. However, it took longer for the curve to approach the zero level in the case where M/m=64.

69

FRACTIONAL EXCESS CHARGE VERSUS TIME

Scale: 1 time step ≈ 0.5 mμ sec.
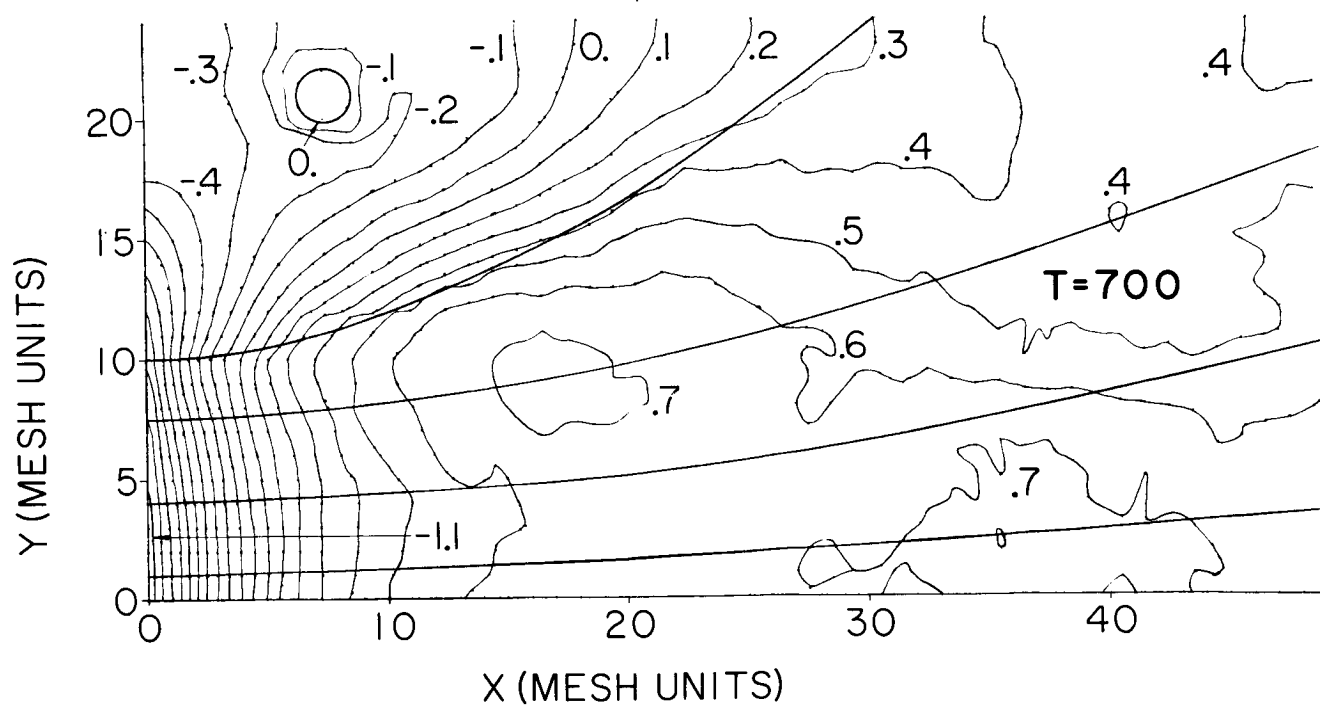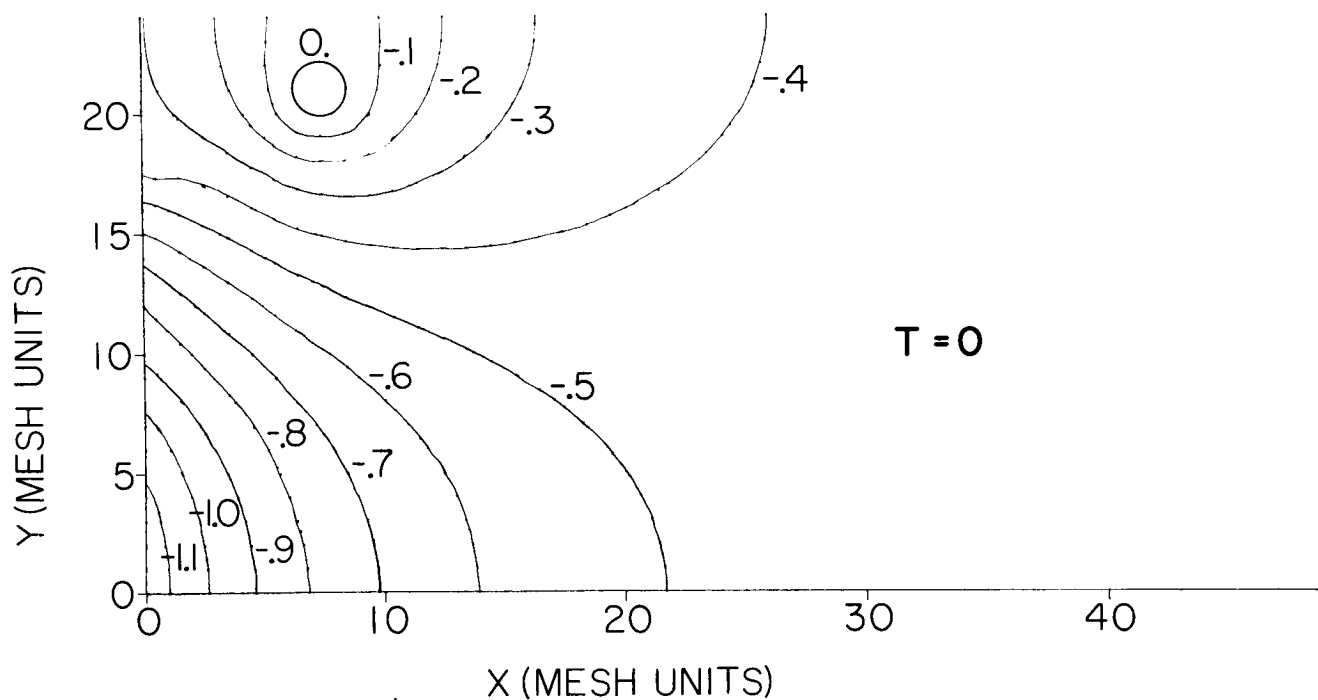
Fig. 3-18

70
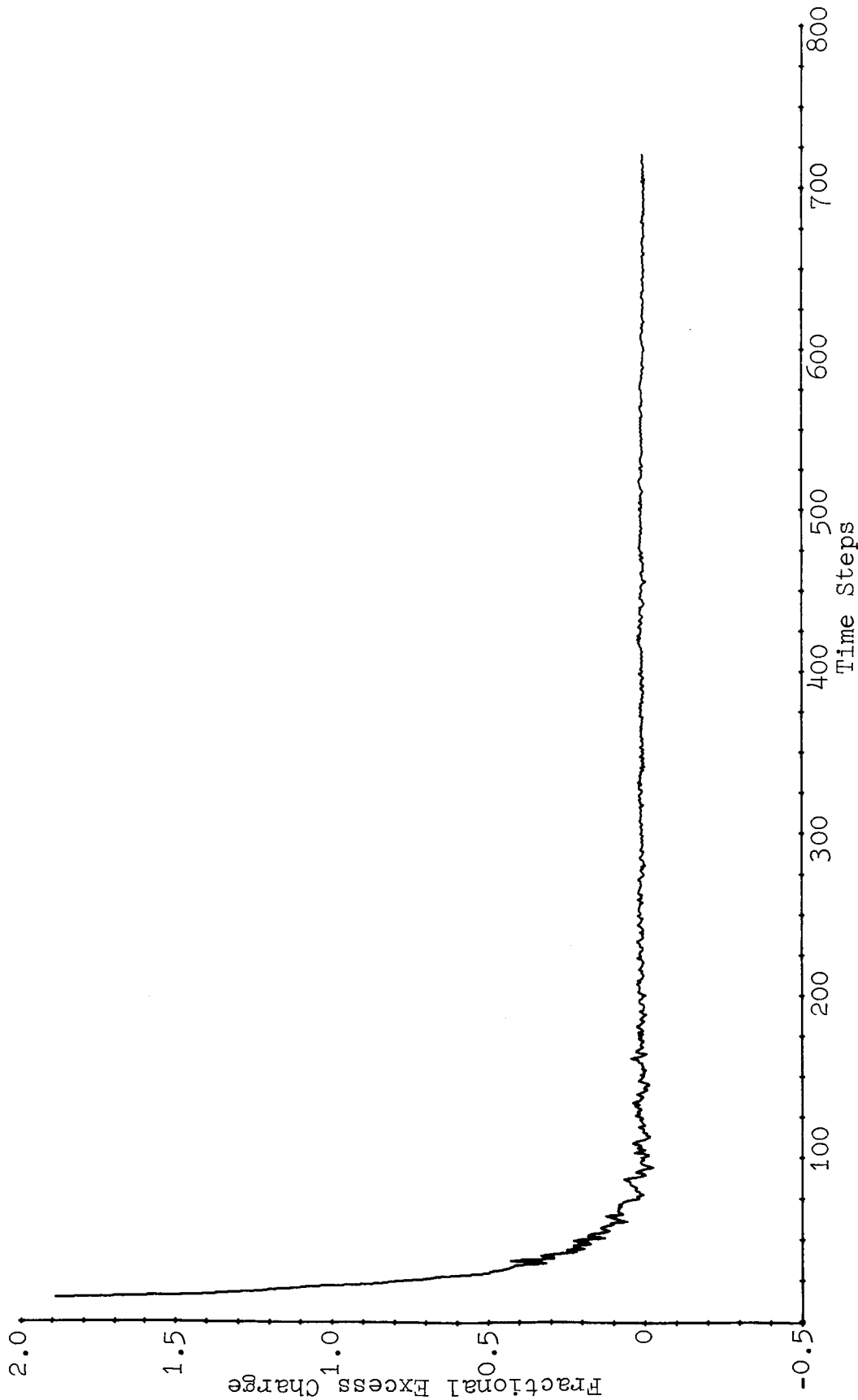
3.4.6 EQUIPOTENTIALS

Figure 3-19 shows the equipotentials near the injection plane at 0 and 700 time steps for the case where M/m=144 and bias=333 volts. (The ion beam is also indicated on the plot at 700 time steps.) Several important features can be noticed from these plots. First, the equipotential lines are drawn taut parallel to the injection plane when the plasma has been formed; this condition causes less lens effect. This contradicts the assumption used in calculating the ion trajectories within the gun region, namely, that the equipotentials become parallel to the beam axis at the injection plane[7]. Secondly, a strongly positive hump at the center of the ion beam is observed. This is the self-formed "anode" which serves to extract electrons from the virtual cathode and draws them into the beam. Thus, the system sets up its own electron diode.

Figure 3-20 shows the equipotentials in the entire region at 300 and 700 time steps for the same case as Figure 3-19. Clearly, the beam and plasma advance as time increases. As in Figure 3-19, the positive hump along the center of the beam is seen. However, neutralization seems to be occurring as this hump decreases in height between T=300 and T=700. Bubbles or islands which continually move and change shape are shown in Figure 3-20. This condition implies the plasma, although neutralized in the whole, is not microscopically neutralized. Instability of the plasma is also indicated by this condition. Similar equipotential plots were obtained for the case where the bias was increased from 333 to 555 volts.

EQUIPOTENTIALS NEAR INJECTION PLANE (WITHDRAWN NEUTRALIZER)

Fig. 3-19

Scale: 1 mesh unit = 0.005 inch
1 norm volt = 1110 volts

72
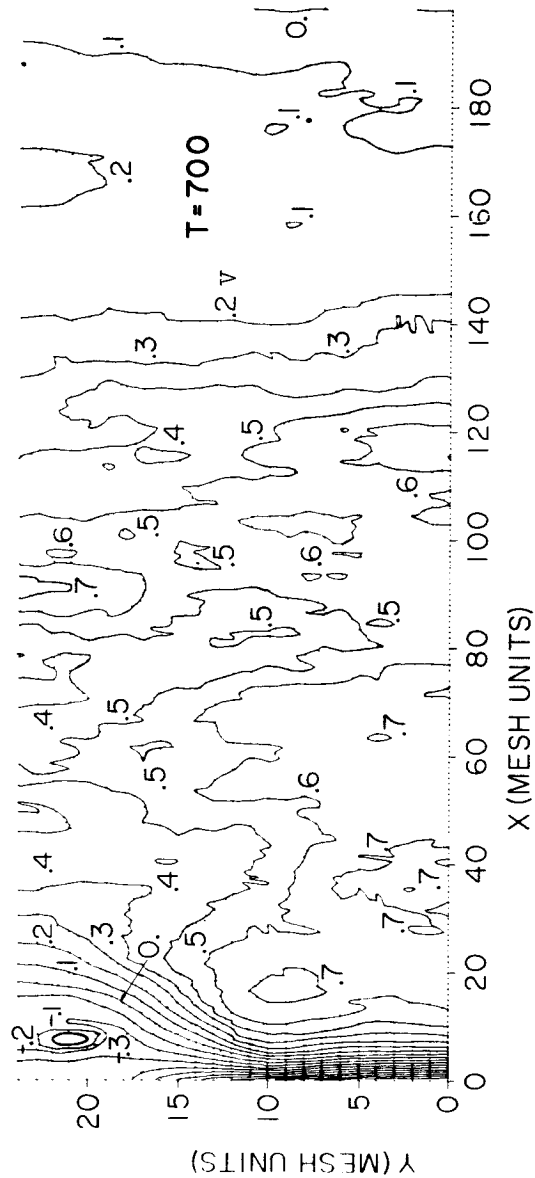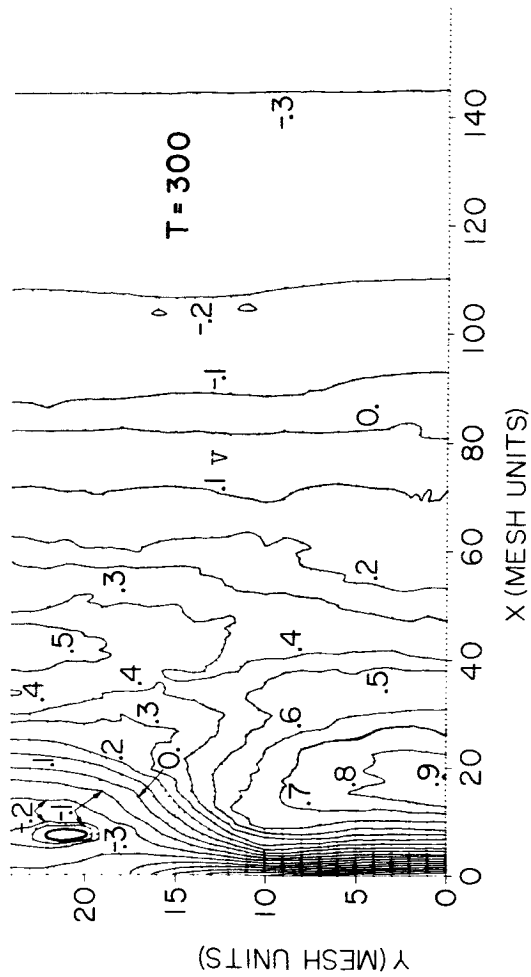
EQUIPOTENTIALS IN ENTIRE REGION (WITHDRAWN NEUTRALIZER)

Scale: 1 mesh unit ≃ 0.005 inch
1 norm. volt ≃ 1110 volts

Fig. 3-20

3.5 RESULTS WITH ELECTRON EMITTER IMMERSED

3.5.1 INTRODUCTION

After obtaining results for Configuration 1 with the electron emitter withdrawn, we immersed the emitter within the beam with center at (60.5, 0). Also, corrections had been made to include the effect of the charged particles that had moved to the right of the exit plane in the calculation of the potential distribution. A run was made for the case where $M/m=144$, $N_e/N_i=12$, bias=333 volts and electron emission was permitted over the whole perimeter of the emitter. The remaining sub-sections in Section 3.5 will present these results and compare them with those obtained using the withdrawn emitter.

3.5.2 TRAJECTORIES

Fig. 3-21 illustrates ion and electron trajectories for the Configuration 1 with emitter immersed. A somewhat unexpected lens effect is shown. The neutralizer represents a potential peak to the ion beam, which crosses the entrance plane through a considerable central potential depression due to the accel electrodes. The ions, therefore, tend to circumvent the emitter, cross over behind it, and thus develop appreciable divergence. Figure 3-21 also indicates that the electrons adjust their densities to suit the ions. Once again, the electron sheath or "virtual cathode" has been formed.

3.5.3 SHIP POTENTIAL AND THRUST

Figure 3-22 is a plot of the normalized ship potential versus time. The period of the fluctuations is approximately 37 time steps which corresponds closely to the number of time steps in the electron plasma frequency, which was calculated in Section 3.4.3 to be 34.4. The amplitude of these fluctuations is 281 volts as compared to 310 for that obtained with the withdrawn emitter. There are no longer any wild fluctuations when the

74
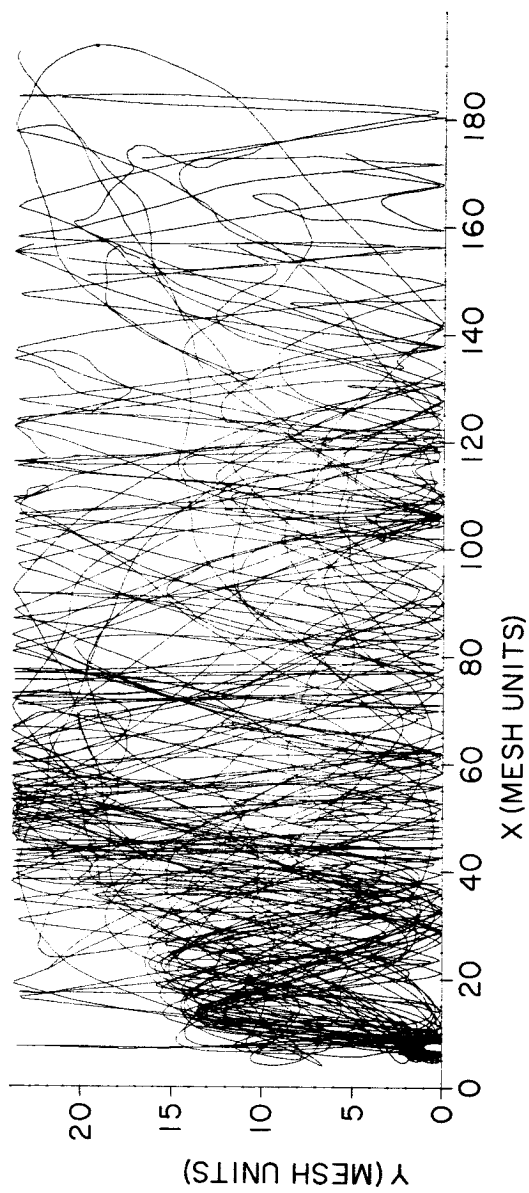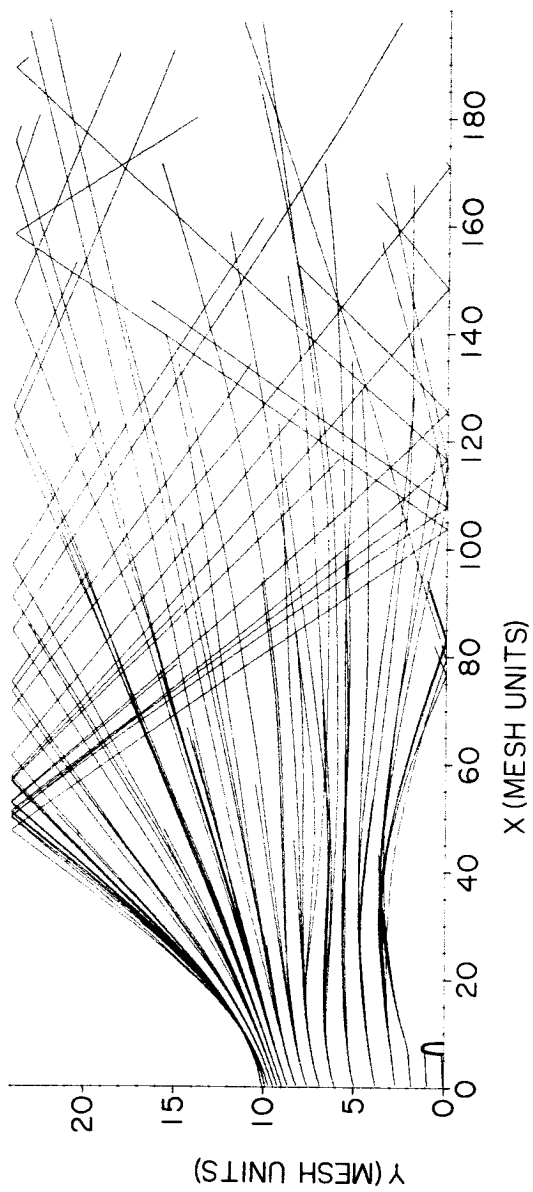
ION AND ELECTRON TRAJECTORIES (IMMERSED NEUTRALIZER)

Fig. 3-21

Scale: 1 mesh unit ≃ 0.005 inch
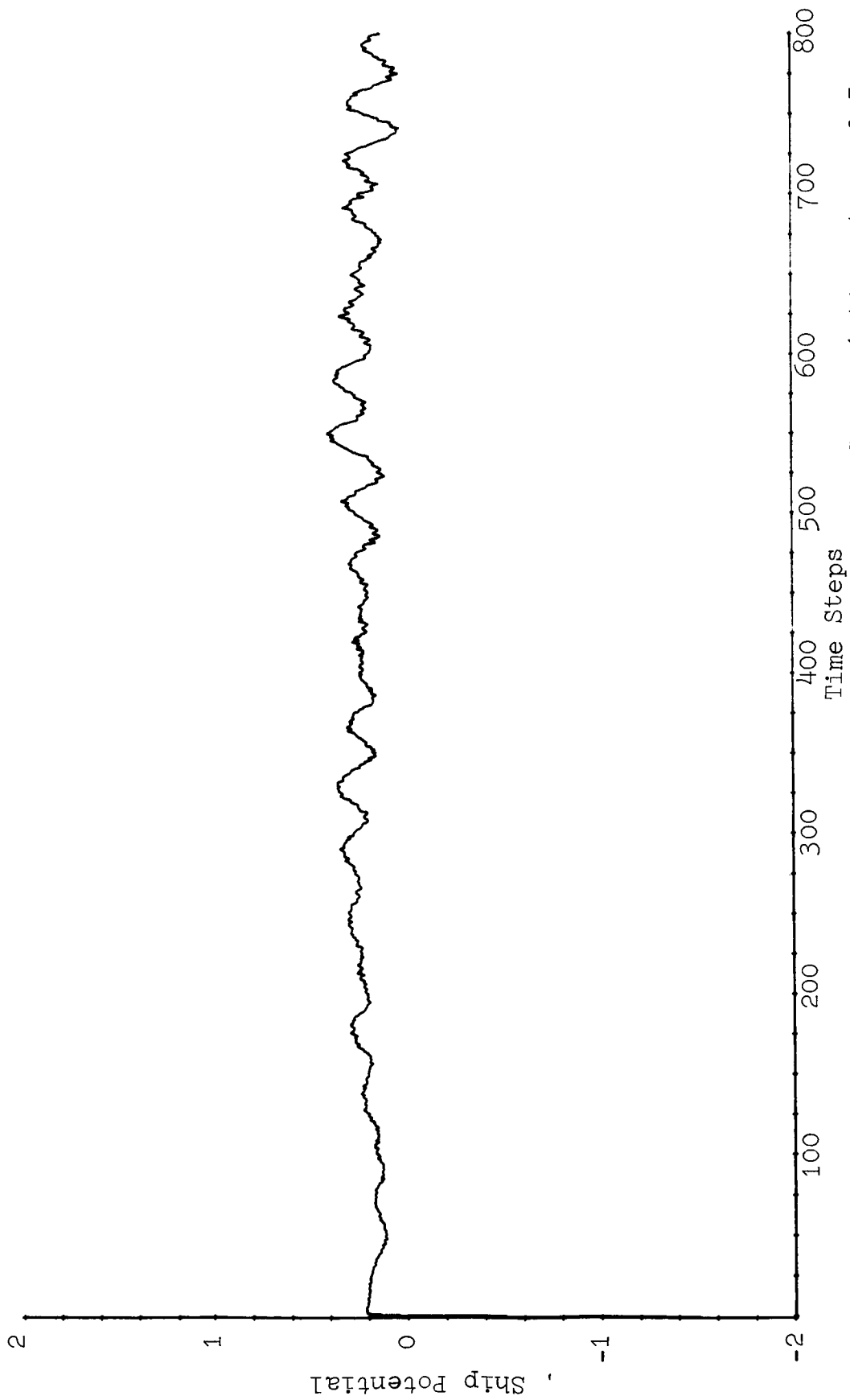
Fig. 3-22

SHIP POTENTIAL VERSUS TIME PLOT

Scale: 1 time step ≅ 0.5 mμ sec.

particles cross the exit plane, indicating that the inclusion of the net charge to the right of the exit plane in the calculation of potentials was important. The variation of normalized thrust as a function of time is similar to the results discussed in Section 3.4.3.

3.5.4 TEMPERATURE CALCULATIONS

Figure 3-23 is a plot of the normalized ion and electron temperatures versus x for various time steps. Comparing these results with those where the emitter is withdrawn (Fig.3-14), we can conclude that the temperatures for the immersed emitter are only one fourth as high as those temperatures for the withdrawn emitter. The reason for this is that the electrostatic coupling between the electrons and the beam is good for the immersed emitter. Once again, there is good mixing of electrons and ions from thermodynamic considerations. The ions develop random motion, the electrons cool down, and thus the tendency to reach equal temperatures is seen.

3.5.5 FRACTIONAL EXCESS CHARGE

Figure 3-24, illustrating the fractional excess charge plotted as a function of time for the immersed emitter, is very similar to the curve for the withdrawn emitter (Fig.3-18). As in Fig. 3-18, electronic charge is slightly greater than the ionic charge. However, the fractional excess charge for the immersed emitter is stabilized around zero in half the time it took for the withdrawn emitter. This fact indicates that neutralization occurs much sooner for the immersed neutralizer case. In other words, the electron current and ion beam are well coupled.

NORMALIZED TEMPERATURE VERSUS x, M/m=144,
BIAS=333 VOLTS, IMMERSED EMITTER

Fig. 3-23

78

FRACTIONAL EXCESS CHARGE VERSUS TIME

Scale: 1 time step ≈ 0.5 mμ sec.

Fig. 3-24

79
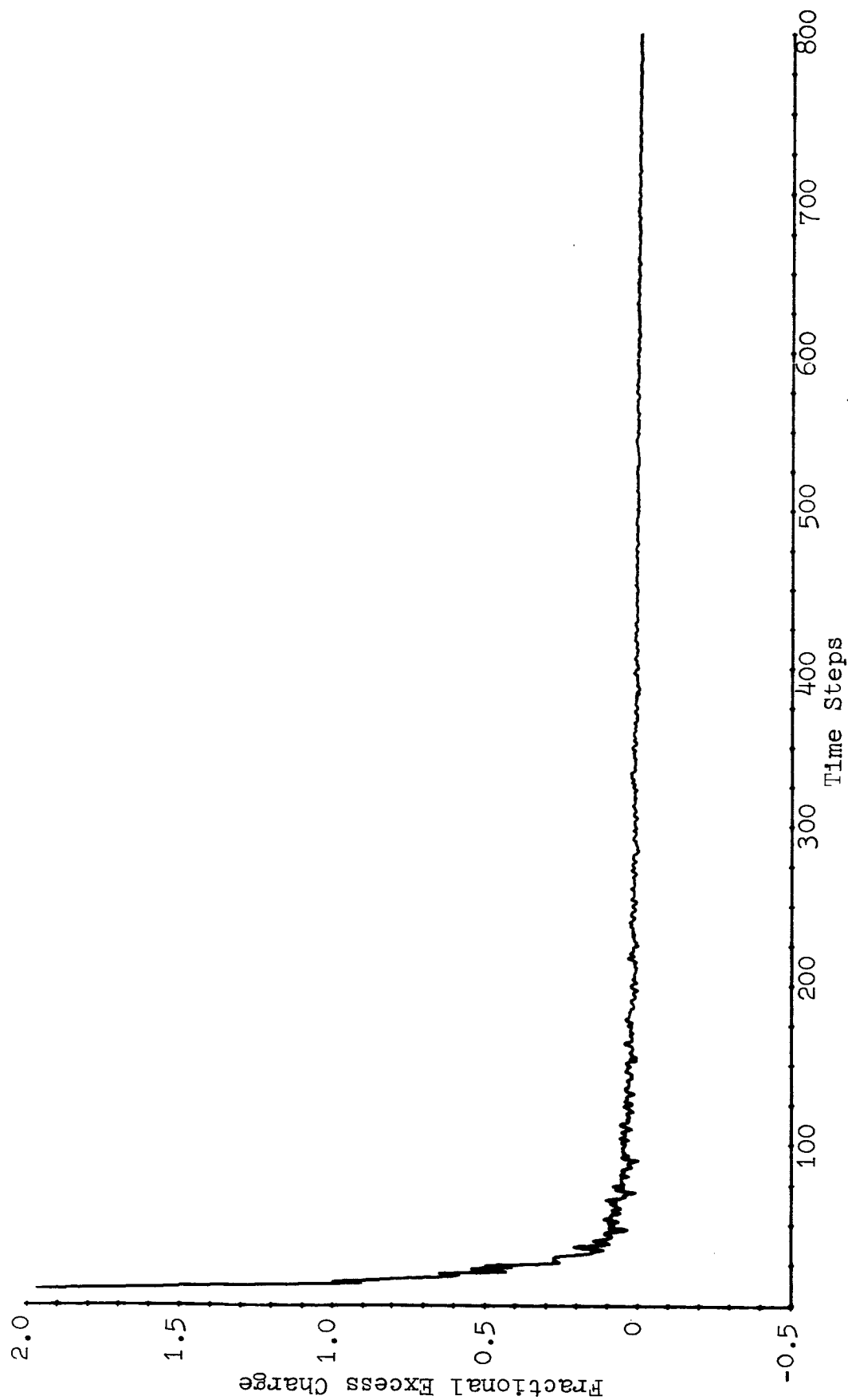
3.5.6 EQUIPOTENTIALS

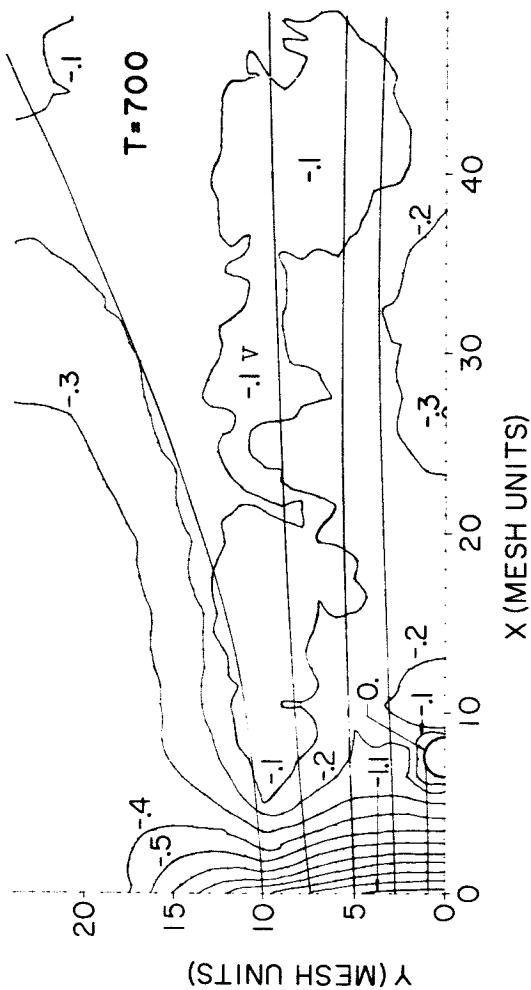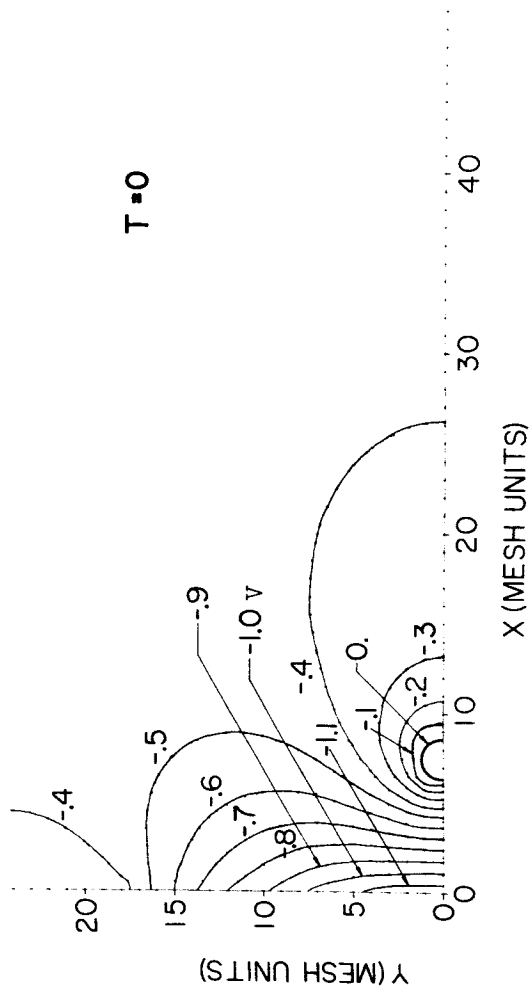The plot of equipotentials near the injection plane before and after the formation of a plasma for the immersed emitter is given in Fig. 3-25. As in the withdrawn emitter case, the equipotentials are pulled parallel to the injection plane. Thus, the edge of the plasma set up by the electrons and ions forms a near planar sheath. Downstream from the emitter, the plasma is at a fairly uniform potential.

Figure 3-26 shows the equipotentials in the entire region at 300 and 700 time steps. The advance of the nearly neutral plasma is evident. This plasma is much flatter with respect to potential than is the plasma for the case of the withdrawn neutralizer for the same time steps. This implies neutralization occurs faster for the emitter immersed than for the neutralizer withdrawn. Once again, the bubbles or islands, indicating plasma instability, are present.

3.6 CONCLUSIONS

The neutralization mechanism was investigated for high voltage ion beams under several conditions. This investigation was made for three values of ion-to-electron-mass ratio and extrapolation was made to the case of heavy ions. Because of the fact that the voltage difference between the injection plane and the electron emitter was only a few volts, it was necessary for simulation of the low-mass ions to introduce some artificial bias on the injection plane so as to cut down the electron movement towards the injection plane. (This injection plane was not the same as the accel plane which was simulated in previous computations.) Plasma oscillations at the electron plasma frequency are noticed in the ship potential, and the magnitude of these oscillations is reduced as the ion mass is increased. Thrust is reduced because of divergent beam at the injection plane.

EQUIPOTENTIALS NEAR INJECTION PLANE (IMMERSED NEUTRALIZER)

Scale: 1 mesh unit ≈ 0.005 inch
1 norm. volt ≈ 1110 volts

Fig. 3-25

81

T=300

T=700

X (MESH UNITS)

X (MESH UNITS)

Y (MESH UNITS)
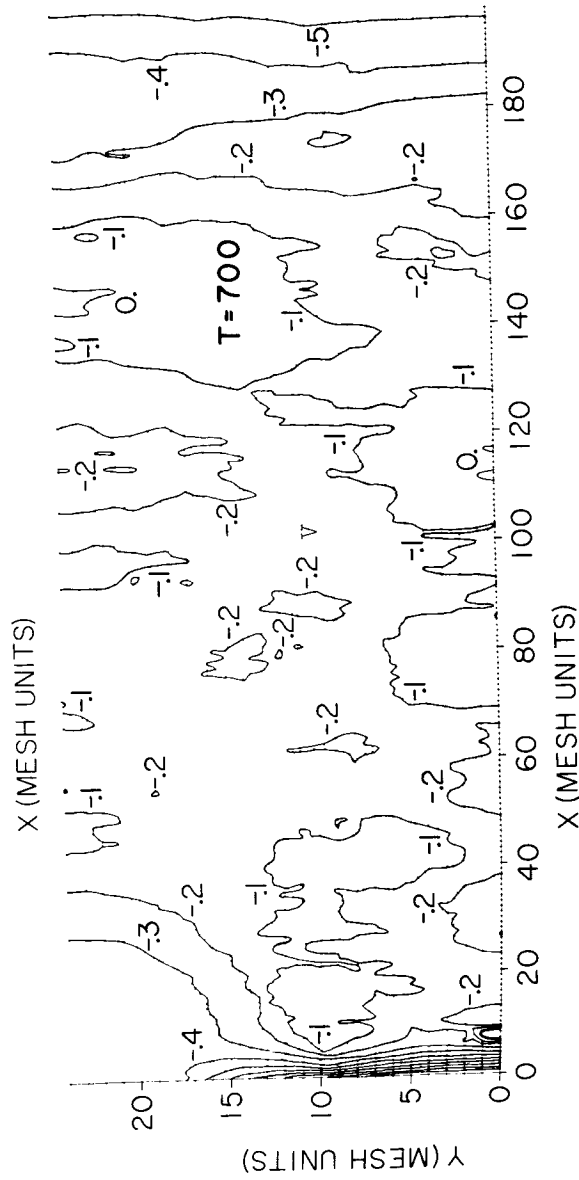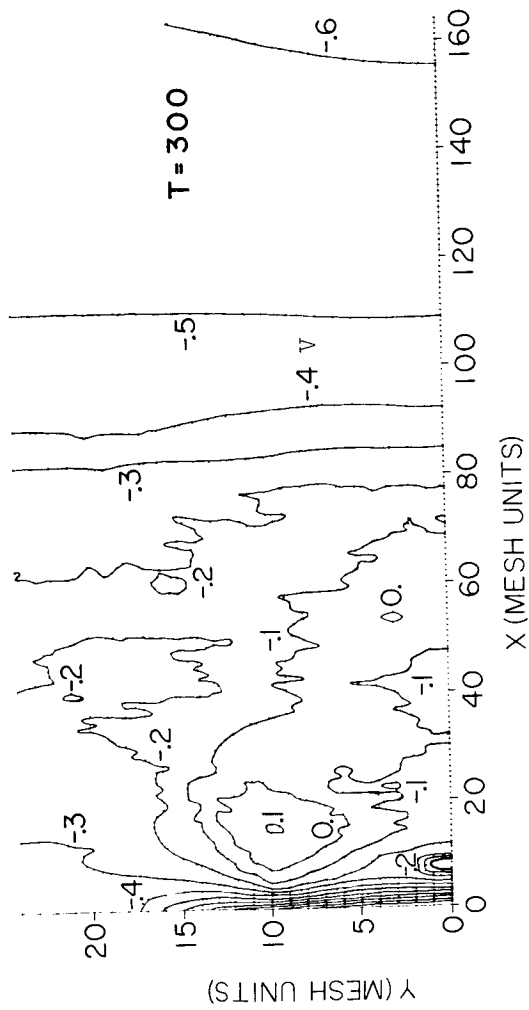
Y (MESH UNITS)

Scale: 1 mesh unit ≈ 0.005 inch
1 norm. volt ≈ 1110 volts

EQUIPOTENTIALS IN ENTIRE REGION (IMMERSED NEUTRALIZER)

Fig. 3-26

An immersed emitter presents a better coupling to the ion beam and charged neutrality is achieved sooner than in the case of a withdrawn emitter even with less primary electron current. Electron temperature is first increased along the ion beam and then is reduced, indicating adequate mixing of electrons and ions. Temperatures for the case of the immersed emitter are much lower than for the case of the withdrawn emitter, indicating a better coupling between the emitter and the ion beam in the former case.

Plasma potential is not stabilized; this may be primarily due to the fact that the particles have not been traced for a sufficiently long time because of computer limitations. This indicates that the electron velocities are not stabilized within the transient period during which the particles are traced; charge neutrality is, however, achieved about 200 time steps after the engine is started.

4.0   SIMULATION OF LOW-VOLTAGE ION BEAM CONFIGURATION

4.1   INTRODUCTION

The second of the two configurations studied under the contract is discussed in Section 4.0 and will be referred to as the low-voltage ion beam configuration, configuration 2, or Sellen's[11] geometry. The simulation of this geometry presented several small problems. The physical model was that of a cylindrical geometry studied in a tank, while our computer model is used to study planar (x-y) geometries which are periodic in the y-direction. Thus, it was not possible to simulate the actual r-z voltages accurately throughout the entire region in our x-y model. Also the voltages are scaled down by the same order of magnitude for both low and high voltage ion beams in the computer model. This creates difficulties when low mass ions are used since the electron thermal energy is not scaled in the computer model. The simulation aims at representing realistic velocity ratios, and therefore, with unrealistic mass ratios $(m_i = 144\ m_e)$ employs unrealistic energy or voltage ratios. As mentioned earlier, low-ion-mass simulation is made for computer economy reasons.

4.2   INPUT DATA

Figure 4-1 shows the actual physical configuration with which Sellen[11] performed experiments. The tank wall was approximated at 18 inches from the axis for reasons of convenience. This tank was held at 100 volts positive with respect to the accel grid. Sellen found that the plasma adeoptd the electron emitter voltage (107 volts positive with respect to the accel grid implying that the space tank played a negligible role.

Tank Wall (100 Volts)

NOTE: Voltage reference is changed to suit
simulation on the resistor network.

18"

Accel Grid (0 Volts)

Genode (350 Volts)

.4"

.7"

.55" .047"

.125"

Center Line

Electron Emitter (107 Volts,
Diameter .012")
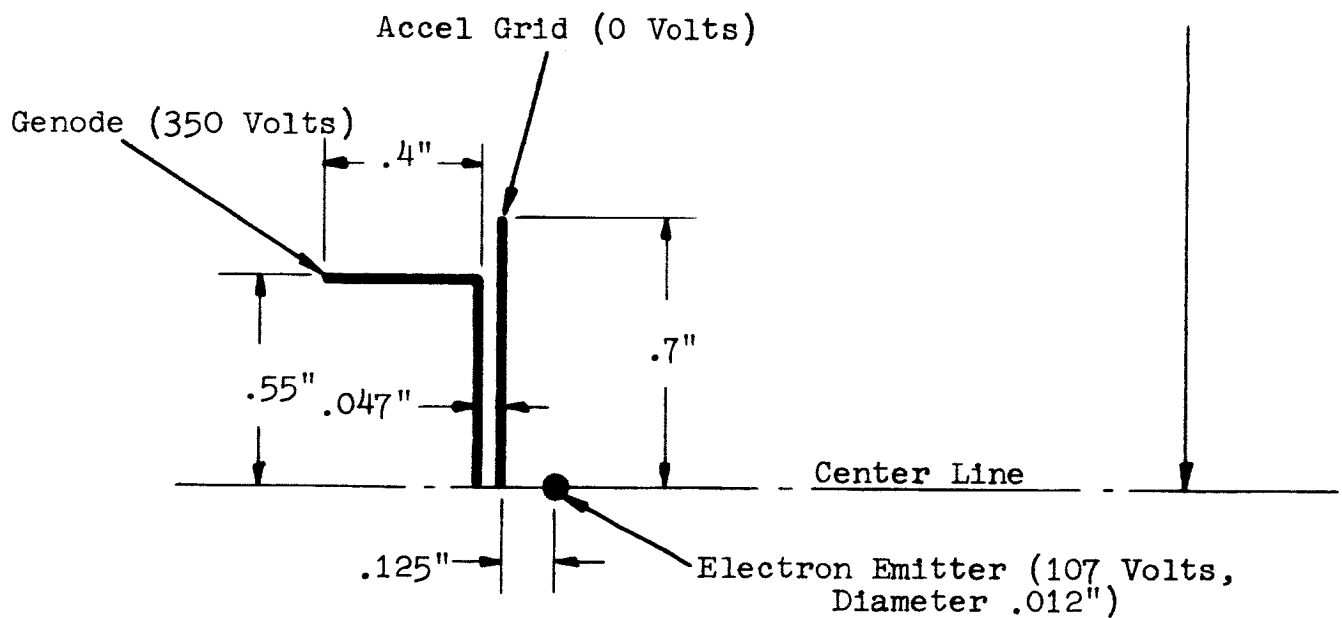
LOW VOLTAGE ION-BEAM CONFIGURATION (SELLEN'S GEOMETRY)

Fig. 4-1

Unfortunately, it is impossible to simulate on the computer long regions in order to make a suitable comparison between the analytical and experimental results. The computer model corresponds to about 25 cm of physical length with 2.5 meshes between the accel grid and the electron emitter.

The geometry shown in Fig. 4-1 was first simulated on the axially-symmetric (r-z) Litton Precision Resistance Network Analogue and the dc potential distribution was determined. The resistance netowrk has a 51 x 26 array of nodes, between which precision resistances are connected. Because of the small spacing between the genode and accel grids, and the accel grid and electron emitter, the region to the right of the accel plane was simulated once again on the resistance network using a three times expanded scale. The potentials along a plane coincident with the accel grid, obtained from the previous network simulation, were used as boundary conditions. Figure 4-2 illustrates the normalized equipotentials resulting from the second resistance network simulation.

These same boundary conditions along the injection (accel) plane were used in the computer model. Slight modifications were made to adjust for the fact that there are 26 mesh points in the transverse direction on the resistance network, while there are 25 mesh points in the y-direction in the computer model. The actual potential distribution to be kept fixed along the injection (accel) plane as a function of y is given in Table VI.

The beam is injected across the accel plane from $y=0$ to $y=10$ mesh units with a normalized injection velocity of 1.182 entirely x-directed. The injection velocity is normalized with respect to that for a 250 volt beam. In addition, the normalized field components in the x and y directions at the accel plane are 1 and 0, respectively.

86
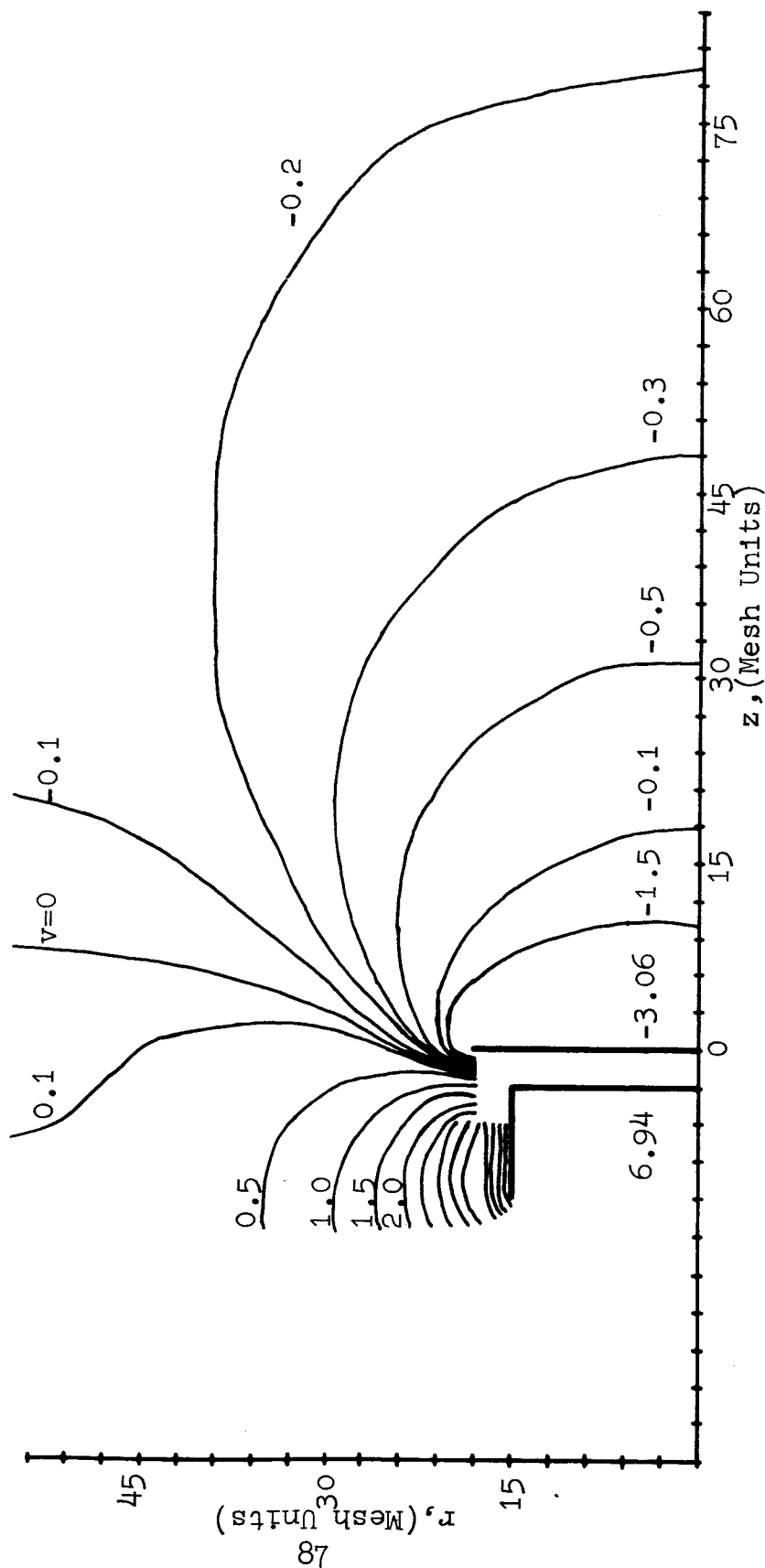
EQUIPOTENTIALS FROM SIMULATION ON r-z RESISTANCE NETWORK

[Electron Emitter at 0 volt is located at (2.5,0); approximated Sellen's Geometry]

Scale: 1 mesh unit ≈ 0.05 inch

Fig. 4-2

y (Mesh Units)	Potential (Volts)
0	-107
1	
2	
3	
4	
5	
6	
7	
8	
9	
10	
11	
12	
13	
14	
15	- 40
16	- 35
17	- 30
18	- 25
19	- 20
20	- 15
21	- 10
22	- 5
23	0
24	5

VARIATION OF POTENTIAL ALONG INJECTION PLANE

TABLE VI

The electron emitter (decel grid) is simulated by fixing
zero normalized potential at (2.5, 0). However, the emission
and interception on the emitter are defined in terms of a
circle with center at (2.5, 0) and radius 0.25 mesh unit.
The actual emitter radius is 0.006 inch which corresponds to
0.12 mesh unit. However, from several test cases in which
the emitter radius was varied, it was found that the minimum
dimension that could be used was 0.25 mesh units; for values
less than 0.25, the interception area proved too small, and
many electrons went upstream and crossed the accel grid. This
problem enters because the potential difference between emitter
and injection plane is reduced appreciably in the scaled version
for low mass ion. Several other test cases were made where
the ratio N_e/N_i was varied. A value of 6 was found to be
optimal. The other parameters that were held constant in
this study are: $\ell/L=0.5$, $M/m=144$, $N_i=3$, $N=30$, $a/\ell=4$, and
$\ell/\Delta x=2.5$. The value of the time step, $\omega_p \Delta t$, is equal (0.2828)
to what it was for the high voltage ion beam configuration
discussed in Section 3.0.

4.3   RESULTS

4.3.1   Introduction

It was mentioned earlier that initially the voltage dis-
tribution along the accel plane obtained from simulation of
Sellen's geometry on the r-z resistor network, was used as a
boundary condition for the voltage distribution along the
injection plane of the computer simulation. Several test
cases were made to optimize the electron emission. In general,
electron emission slightly larger than ion emission should be
sufficient, but because of computer limitations one tries to
reach the equilibrium stage as early as possible; this is
achieved by optimizing the primary electron emission to a

value much larger than the ion emission. Needless to say, the unwanted electrons fall back on the cathode and the net electron current is very nearly equal to the ion current. The first production run yielded fairly good neutralization but the plasma potential did not stabilize and potential fluctuations in space and time were noticed. In scaling from high-mass ion to low-mass ion, the velocity is kept invariant but then the kinetic energies of the ions and electrons are not scaled appropriately. Because of the small voltages in the practical case, the electron velocities used in the study might appear to be too large in the computer simulation; because of the large velocities some electrons overshoot the ion beam and depress the potential in space. This results in larger (positive) values of the ship potential with some fluctuations. The demand and supply of the electrons are well maintained, but unless their velocities are also controlled, one may notice fluctuations in plasma potential which eventually reflect in the ship potential variation. Later the electron emitter temperature was reduced by a factor of two. This resulted in a slight deficit of electrons during the early period, but a charge balance was achieved eventually. The ship potential was reduced, but remained positive, and fluctuations were higher than in the earlier case.

The studies discussed above suggested that although there was charge neutralization, the electrons did not reach the stage of being tamed to go along with the ions at the same velocity and thereby maintain neutrality. If the program is run for a long time and contributions from all the electrons (including those leaving the system) are appropriately taken into accound, neutralization should be achieved eventually. This could not be done because of computer limitations. An examination of the space-charge free potential distribution in space

indicated that it was not close to that in the r-z configuration; perhaps much higher negative voltages in the simulated program delayed the neutralization. The system does not have fast response to correct for deviations from the steady-state values. Later a voltage distribution along the injection plane was modified to give potential distribution in space (at least in the region of the ion beam) much closer to that in the r-z geometry. Again this comparison is for space-charge free configurations; this resulted in less negative voltages in space (space-charge free case) than in the previous case, and the production run made with these boundary conditions resulted in fast charge neutralization; however, the plasma was again not stabilized, although smaller fluctuations were noticed. These results are summarized in the following sections. The first few sections refer to the earlier potential distribution discussed above.
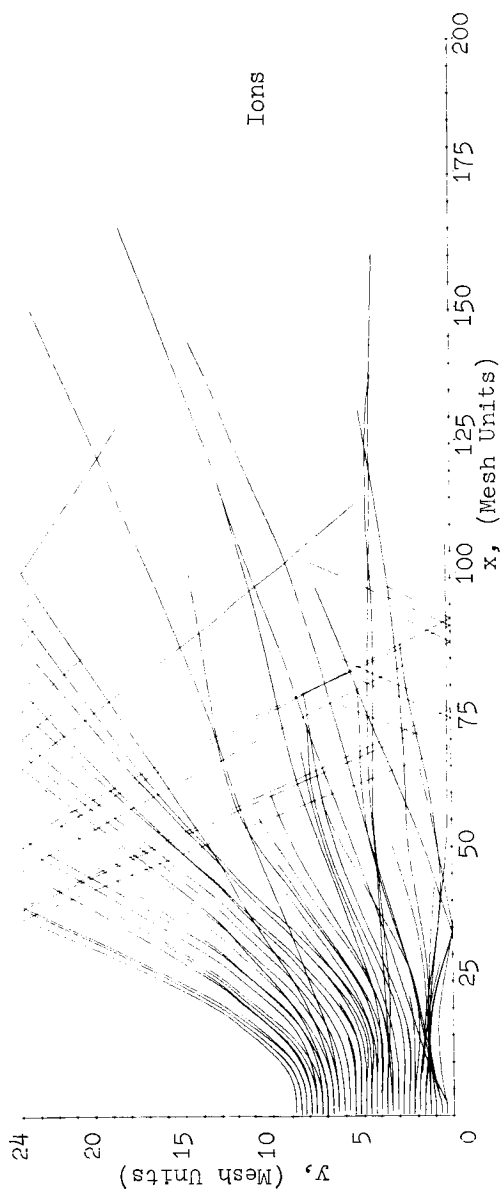
4.3.2 Trajectories

Figure 4-3 illustrates a sampling of the ion and electron trajectories, y versus x, for the case where $e\varphi_0/kT=28.8$. As* was evidenced in the results for the high voltage ion beam configuration, the inner ions circumvent the immersed emitter, causing considerable divergence. Also, the electrons are dense where there are ions, a condition demonstrating their tendency to stay within the beam and propagate downstream with it.

Several high-energy electrons visible in Fig. 4-3 shoot downstream ahead of the beam and are reflected back due to the potential barrier set up by their self-charge.

Figure 4-4 shows the same sample of ions and electrons plotted in the x versus time domain (for the case where $e\varphi_0/kT=28.8$). The ion trajectories are nearly straight because

---

* In these studies M/m=144. φ_1/φ_0 referred to in the plots corresponds to the ratio of decel to accel potentials.

ION AND ELECTRON TRAJECTORIES, y VERSUS x, $\varphi_1/\varphi_o=0.428$, $e\varphi_o/kT=28.8$
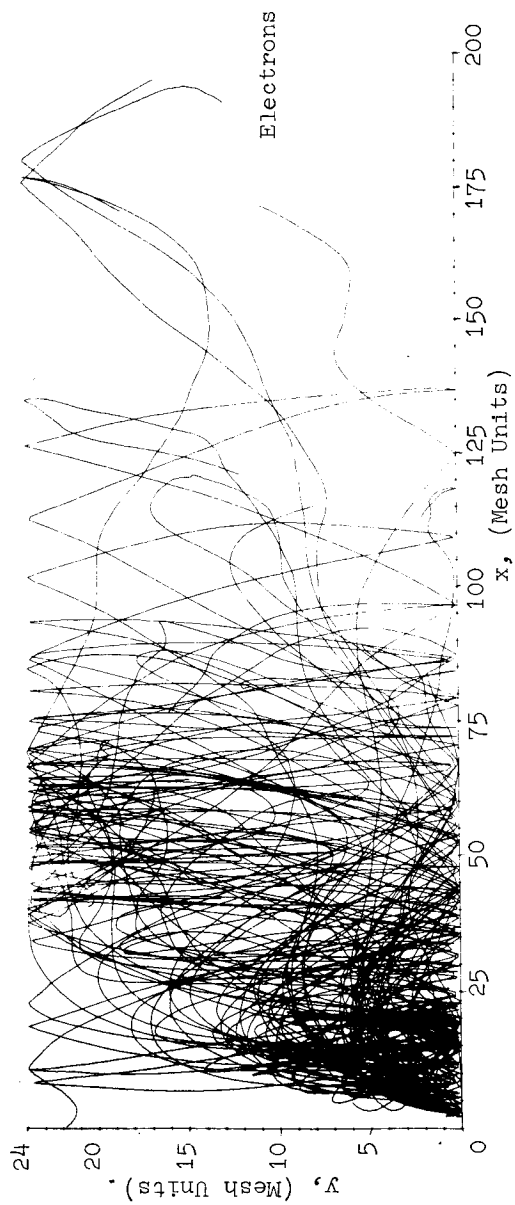
Scale: 1 mesh unit ≃ 0.05 inch

Fig. 4-3
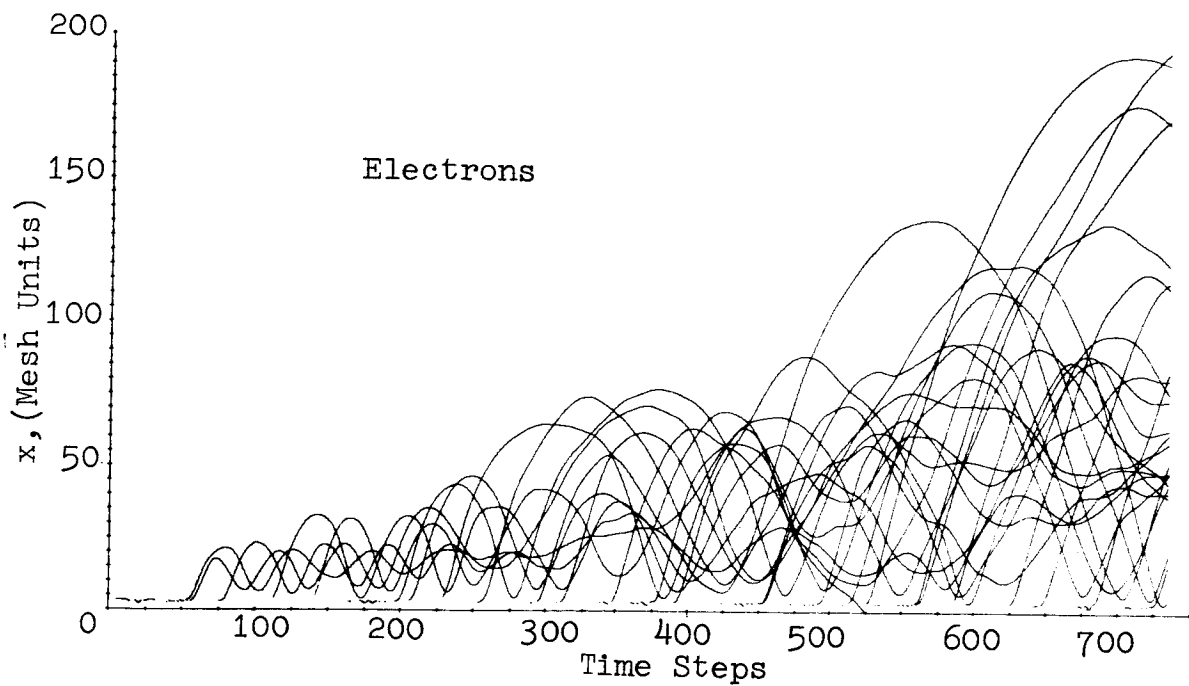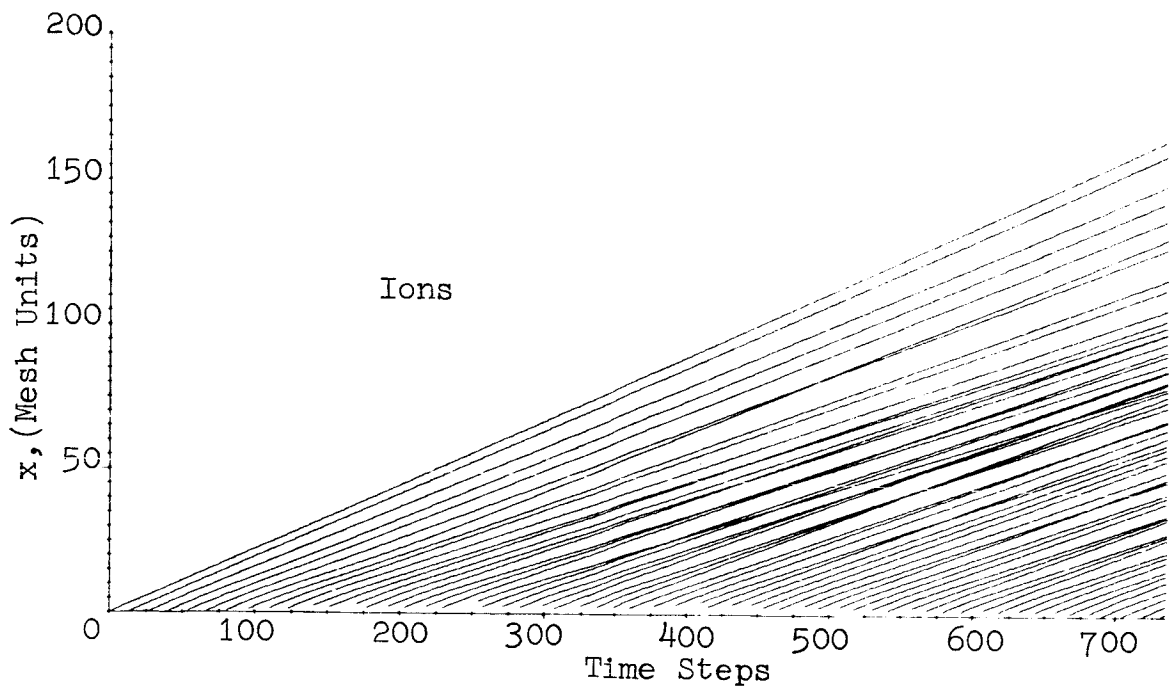
Scale: 1 mesh unit ≃ 0.05 inch
1 time step ≃ 14 m_μ sec.

ION AND ELECTRON TRAJECTORIES, x VERSUS TIME,
$\varphi_1/\varphi_0 = 0.428$, $e\varphi_0/kT = 28.8$

Fig. 4-4

93

of their heavy mass relative to the electrons. The crossovers indicate that the ions, although crossing the injection plane with the same velocity, are affected by the instantaneous electric fields created by the space charge and accelerate or decelerate accordingly. These crossovers would not be visible in trajectories of ions with realistic mass ratios. Similar results were obtained for the case of $e\varphi_0/kT=14.4$.
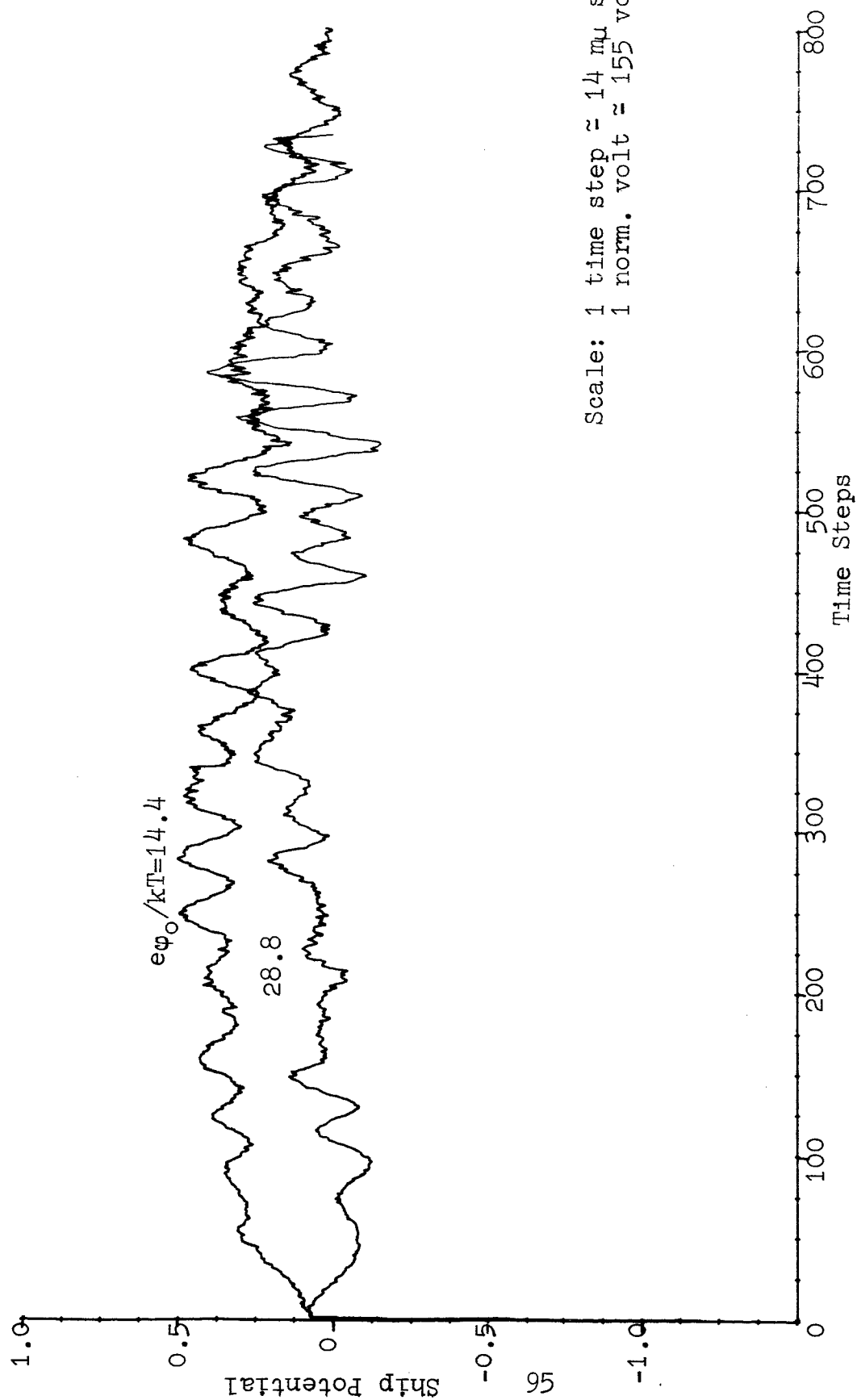
4.3.3 Ship Potential and Thrust

Figure 4-5 shows the normalized ship potential plotted as a function of time for two cases, namely $e\varphi_0/kT=14.4$ and 28.8. Note that the steady state level for the case of $e\varphi_0/kT=14.4$ is greater than that for the case of $e\varphi_0/kT=28.8$. However, the dc levels for both cases tend after 700 time steps to approach the value of .2, which corresponds to about 70 volts. The average amplitude of the fluctuations for both cases is approximately equal to 26 volts; and the oscillation frequency in both cases is nearly that of the electron plasma.

Figure 4-6 shows the variation of the normalized thrust as a function of time for the two cases. It is interesting to note that the normalized thrust is always greater than one, for these cases, while it was always less than one for the runs made using configuration 1 (see Section 3.4.3). The reason for this difference is that the ions had a sizeable transverse or y-velocity component when crossing the injection plane in configuration 1; however, for Sellen's geometry the velocity of the ions at the injection plane is directed entirely longitudinally or parallel to the x-axis. Another conclusion that can be drawn from the plots shown in Fig. 4-6 is that the normalized thrust for the case of the lower emitter temperature is greater than for the case of the higher emitter temperature. This condition could be caused by greater electrostatic forces around the emitter for the case where $e\varphi_0/kT=28.8$ than for the case where $e\varphi_0/kT=14.4$. This is due to the fact that the low energy

94

SHIP POTENTIAL VERSUS TIME, $\varphi_1/\varphi_0=0.428$

Fig. 4-5

Scale: 1 time step $\simeq$ 14 mμ sec.
       1 norm. volt $\simeq$ 155 volts

$e\varphi_0/kT=14.4$

28.8

Ship Potential

Time Steps

95
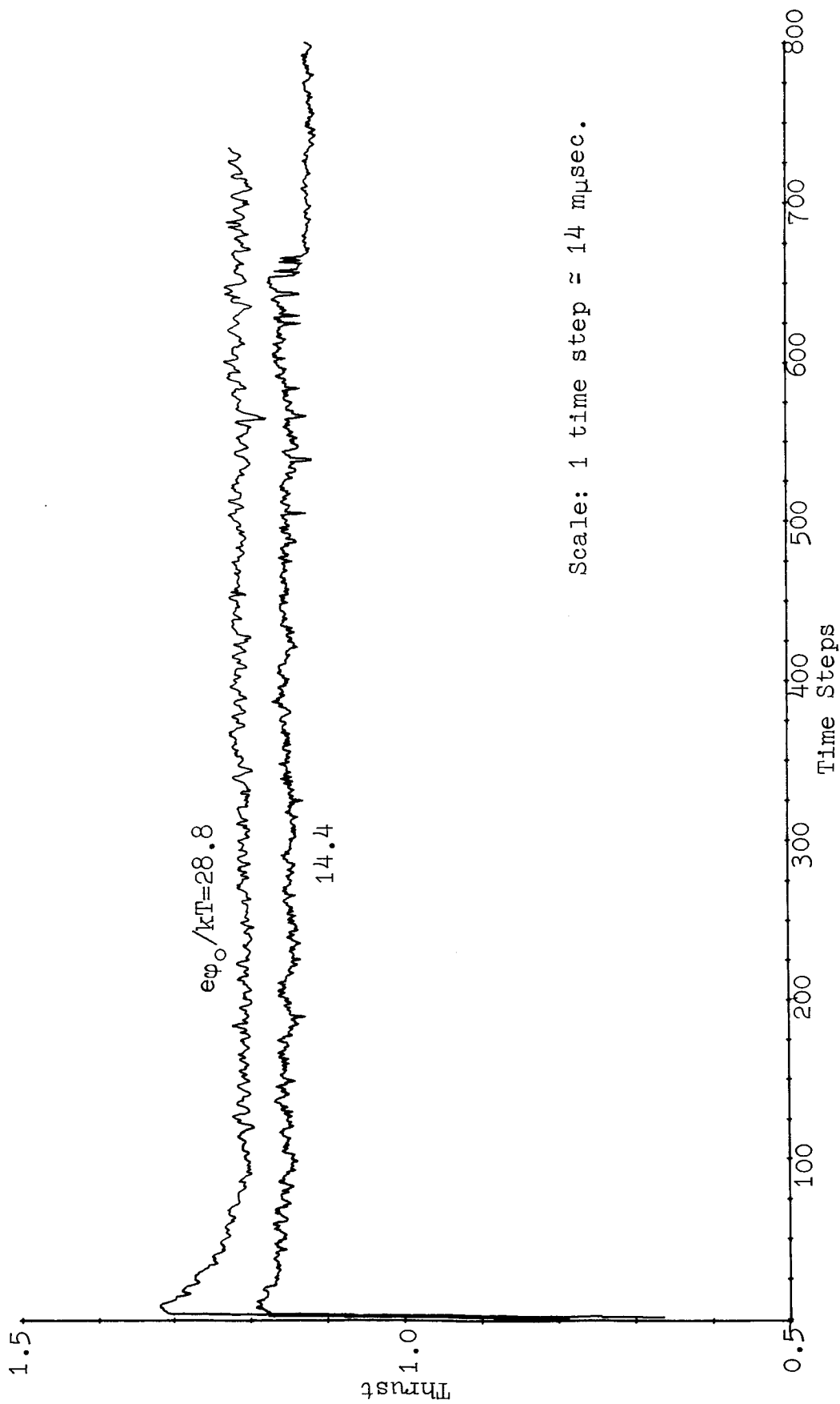
NORMALIZED THRUST VERSUS TIME, $\varphi_1/\varphi_0 = 0.428$

Fig. 4-6

electrons stay in large numbers in the vicinity of the emitter, thereby, depressing the potential in its neighborhood. This eventually reduces the decelerating field for the ions at the accel plane.

4.3.4 Temperature Calculations

Figure 4-7 shows the ion and electron normalized temperatures plotted for various time steps as a function of x for the run where $e\varphi_0/kT=14.4$ while the corresponding temperatures for the run where $e\varphi_0/kT=28.8$ are plotted in Fig. 4-8. When the thermal energy is reduced, i.e., when $e\varphi_0/kT=28.8$, the ion and electron temperatures are nearly two times as great as in the case where $e\varphi_0/kT=14.4$.

In deriving this ratio of 2, it is necessary to consider that the plots are made for the normalized temperatures and that for the plots shown in Fig. 4-8, normalization is with respect to a temperature half that used in plots shown in Fig. 4-7. When the electron emitter temperature is reduced, very few electrons can overcome the potential barrier existing under space-charge free conditions. The potential in this region tends to become positive because of the ions, and this accelerates the electrons away from the emitter. The electrons overshoot and are reflected back, causing thereby more random motion. This is reflected in larger values of electron temperature and hence larger values of ion temperature. The cooling of electrons and ions is noticed along the distance traversed by the beam, indicating the tendency of good mixing of electrons and ions.

4.3.5 Fractional Excess Charge

The fractional excess charge is shown in Fig. 4-9 as a function of time for the two cases of potential distribution, initial and modified, as explained in Section 4.3.1, for the
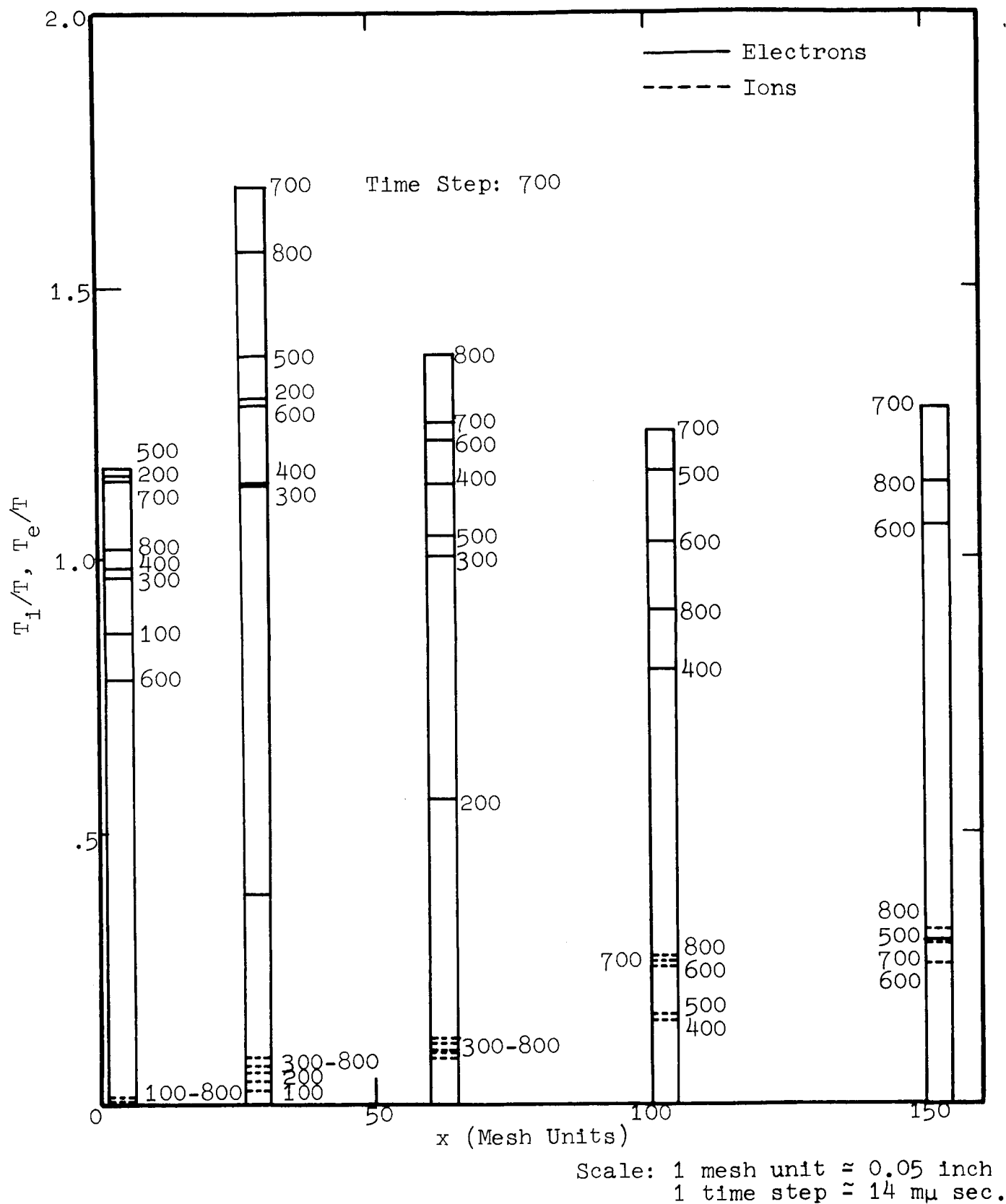
NORMALIZED TEMPERATURE VERSUS x, M/m=144, $e\varphi_O/kT$=14.4
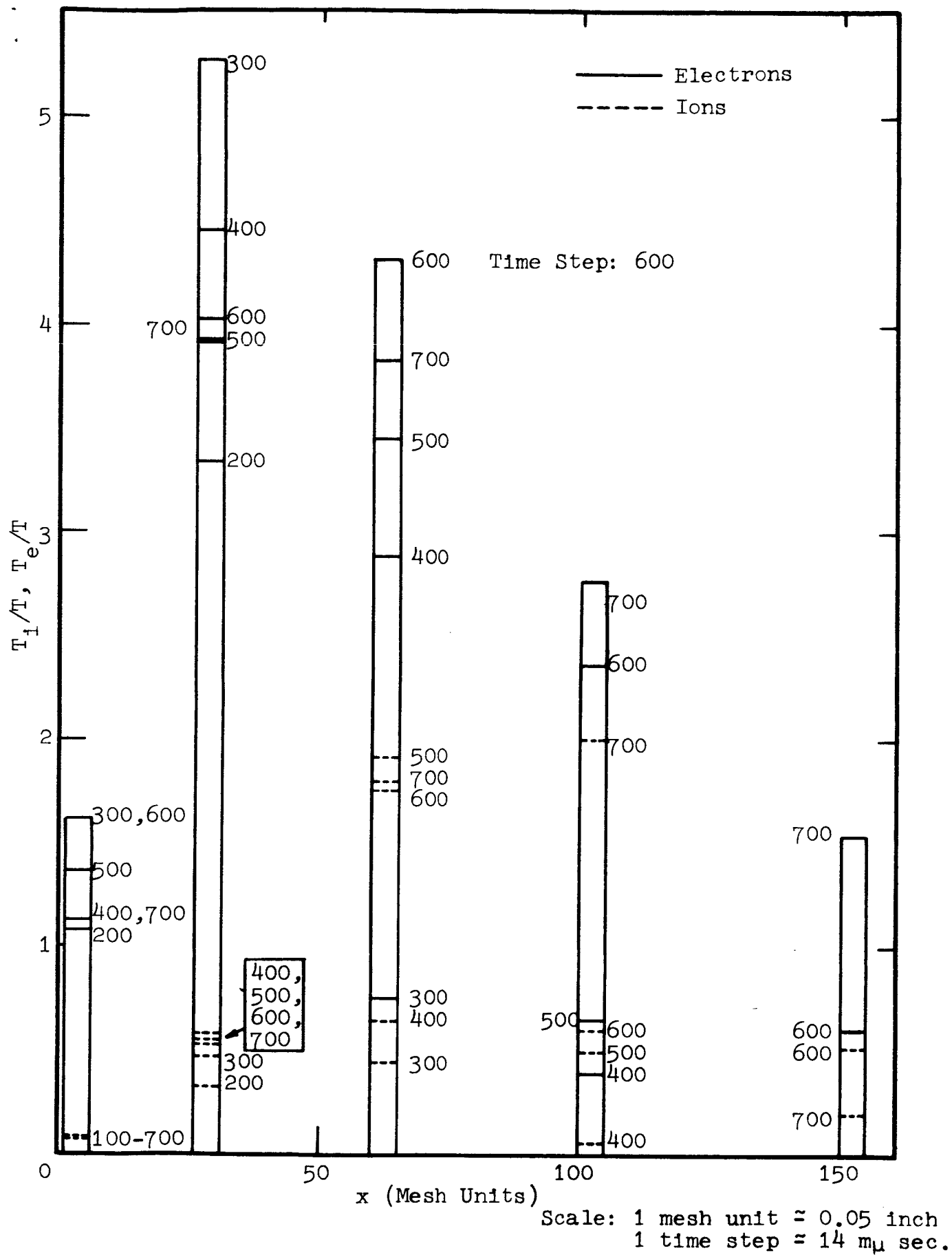
Fig. 4-7

98

NORMALIZED TEMPERATURE VERSUS x, M/m=144, $e\varphi_o/kT$=28.8

Fig. 4-8

99

FRACTIONAL EXCESS CHARGE VERSUS TIME $e\varphi_o/kT=28.8$

Scale: 1 time step $\approx$ 14 mμ sec.

Fig. 4-9

100

case of $e\varphi_O/kT=28.8$; general results for the case of the modified potential distribution are discussed later. The plot for the case of $e\varphi_O/kT=14.4$ (for the case of the initial voltage distribution) was similar to that for the case of $e\varphi_O/kT=28.8$ except that the electrons deficiency was not as high as in the latter case.

It may be noticed that the charge equilibrium is achieved within a short time; however for the case of modified potential distribution, a close charge neutrality is obtained. Because of smaller negative voltages existing in space (in the space-charge-free case) for the case of modified potential distribution electron deficiency is not as high as in the other case at any time. Of course, once the plasma is formed the initial (space-charge free) potential distribution is of very little significance. Furthermore, whether the charge neutrality is obtained earlier or la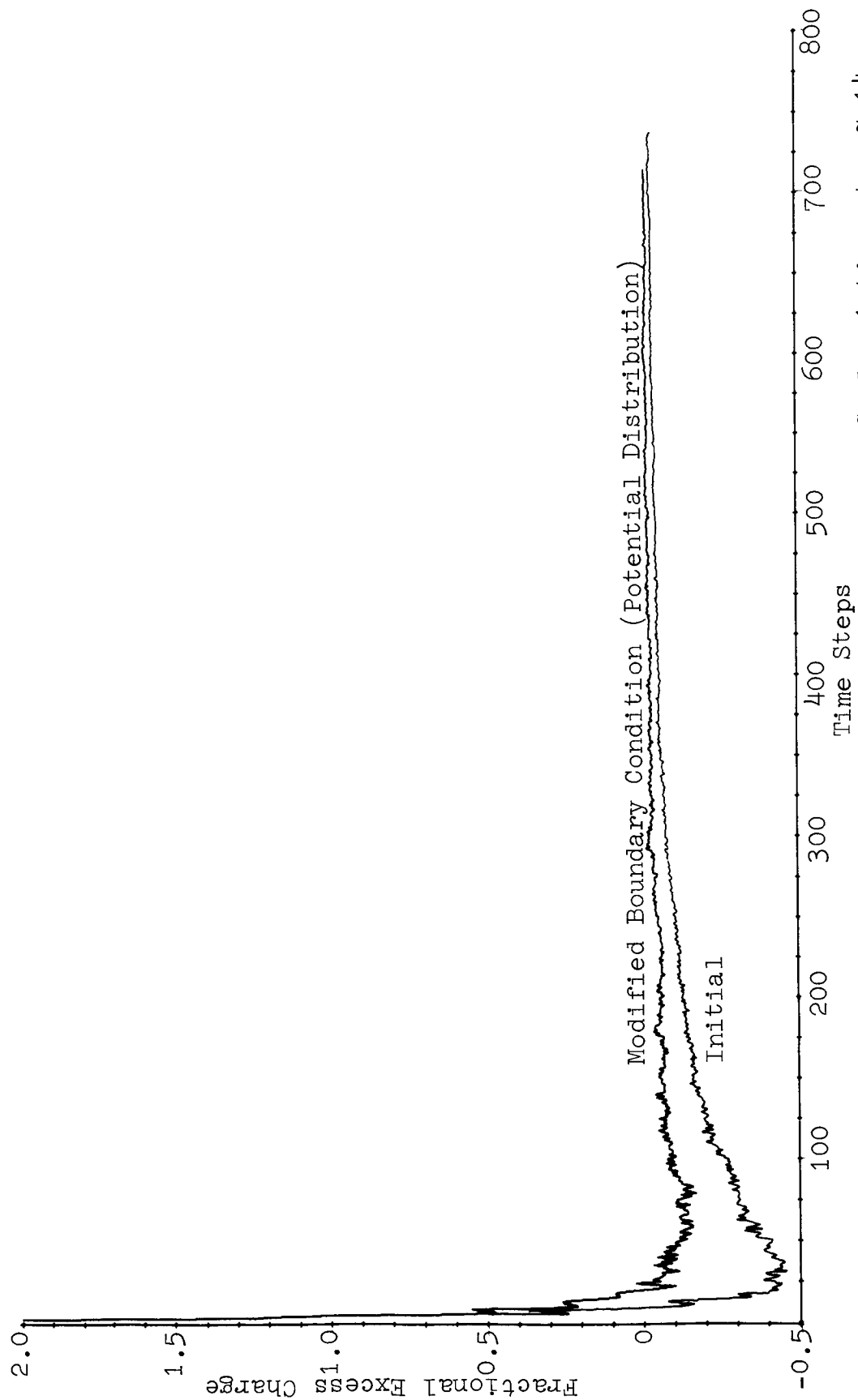ter, and whether there is any deficiency of electrons during the transient stage depend very much upon the primary electrons available from the emitter and the space-charge-free distribution. The plots in Fig. 4-9 show a slight excess of ion charge in the equilibrium condition; this is due to the fact that the electrons leaving the exit plane have not been considered in this plot while the fundamental harmonic of this charge is considered in evaluating the potential distribution in space.

4.3.6 Equipotentials

Figure 4-10 shows the space-charge free equipotential plots in the x-y plane for the low voltage ion beam configuration. This plot compares quite closely, in the vicinity of x=0, with the plots shown in Fig. 4-2, in the r-z plane obtained on the axially-symmetric Litton Precision Resistance Network Analogue.
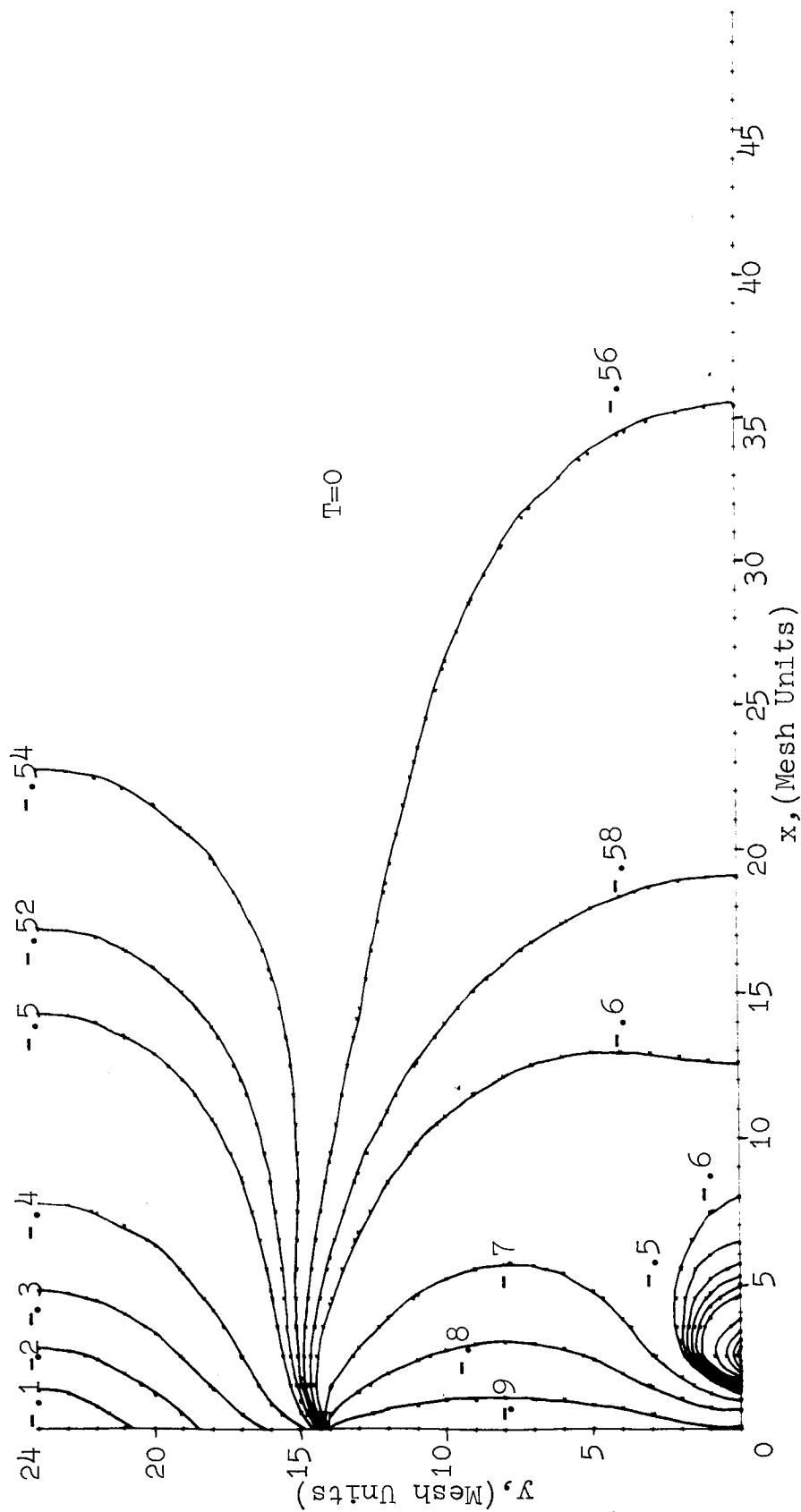
EQUIPOTENTIALS NEAR INJECTION PLANE
(Initial Potential Injection Conditions)

Scale: 1 mesh unit ≈ 0.05 inch
1 norm. volt ≈ 155 volt

Fig. 4-10

102

The equipotential plot at time step 700 for a run made with the low voltage ion beam configuration where $e\varphi_o/kT=14.4$ is presented in Fig. 4-11. The space charge pulls the equipotential lines near the injection plane taut across the beam. The plasma seems to be neutralized at a plateau corresponding to $V_{i,j}=-0.3$ or -0.4. We feel that this occurs because the thermal energy of the electrons is not scaled down in proportion to the reduction made when the voltages are scaled down in the computer model.

As one notices the fluctuations in the plot for the ship potential as a function of time, the plasma potential also varies both as a function of time and space. In order to reduce the amount of the output data, it was considered appropriate to obtain output data periodically - at every 100th time step. Thus, it is necessary to examine the data at several time steps in sequence in order to determine the magnitude of fluctuations in the plasma potential distribution and if possible these fluctuations should be correlated with the ship potential fluctuations. An examination of the data obtained periodically leads to the conclusion that the plasma potential indeed fluctuated although it was difficult to correlate the fluctuations with the ship potential fluctuations because of lack of data at all time steps.

In the initial transient stage the potential in space is negative and only high energy electrons are able to move into this region. Most of the electrons surround the emitter area. Later when the ion beam propagates into this region the potential becomes less and less negative and becomes positive at some locations; this results in drawing more and more electrons into space, resulting eventually in charge neutrality. Once the plasma is formed the potentials in space are not as negative as in the free space-charge case.
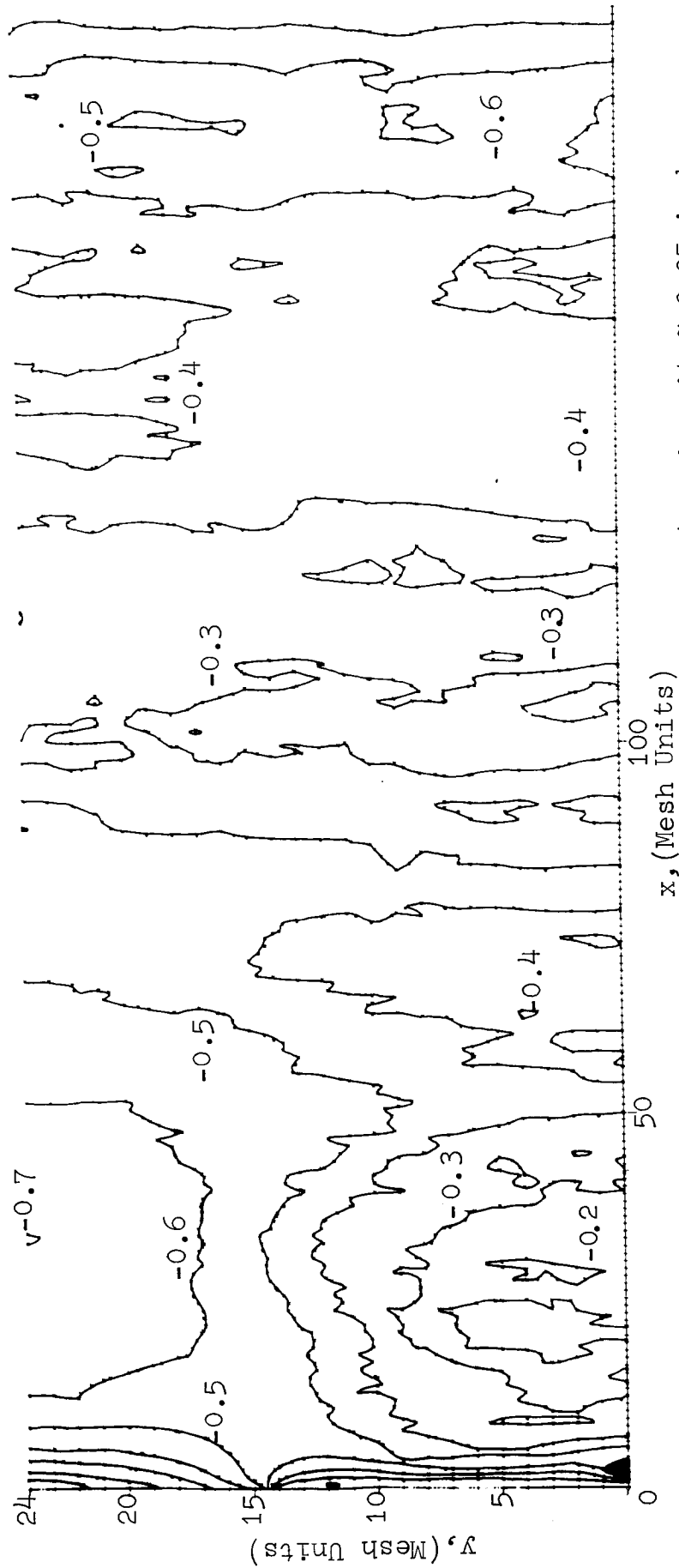
EQUIPOTENTIALS IN ENTIRE REGION, TIME STEP: 700, $e\varphi_o/kT=14.4$
(Initial Potential Injection Condition)

Scale: 1 mesh unit $\simeq$ 0.05 inch
1 norm. volt $\simeq$ 155 volts

Fig. 4-11

104

As mentioned earlier, quite a few electrons leave the exit plane; these electrons are high-energy electrons. In general, the charge beyond the exit plane is not neutralized; thus the potential in this region is always negative with respect to the ship (actually electron emitter). This is one of the reasons why negative potentials are noticed in the equipotential plots, in the vicinity of the exit plane as evidenced in Fig. 4-11, which also shows the bubble or island formation in the plasma, indicating a lack of microscopic neutralization.

Figure 4-12 illustrates the equipotentials at time step 700, resulting from the case where $e\varphi_0/kT=28.8$, i.e., the temperature of the emitter is half the value of the previous run reported. We expected that the level of the potential would rise from $V_{i,j}=-.3$ because not very many electrons would be able to move into space to depress the potential. The average potential lead of the plasma as seen in Fig. 4-12 is higher than that of the previous case, (compared at the same time step) and has increased from negative to positive, but there is no longer a potential plateau. A potential hill is seen just downstream from the electron emitter, which serves as a self-formed anode to pull electrons away from the emitter. Thus a diode is set up between the emitter and the hill.

The results with $N_e/N_i=6$ were very similar to those for the case of $N_e/N_i=4$.

4.4   RESULTS WITH MODIFIED POTENTIAL DISTRIBUTION

4.4.1   Introduction

It has been mentioned earlier that the potential distribution in the x-y plane as obtained by simulating the boundary conditions was not close to that in the r-z configuration; these boundary conditions (potential distribution along the
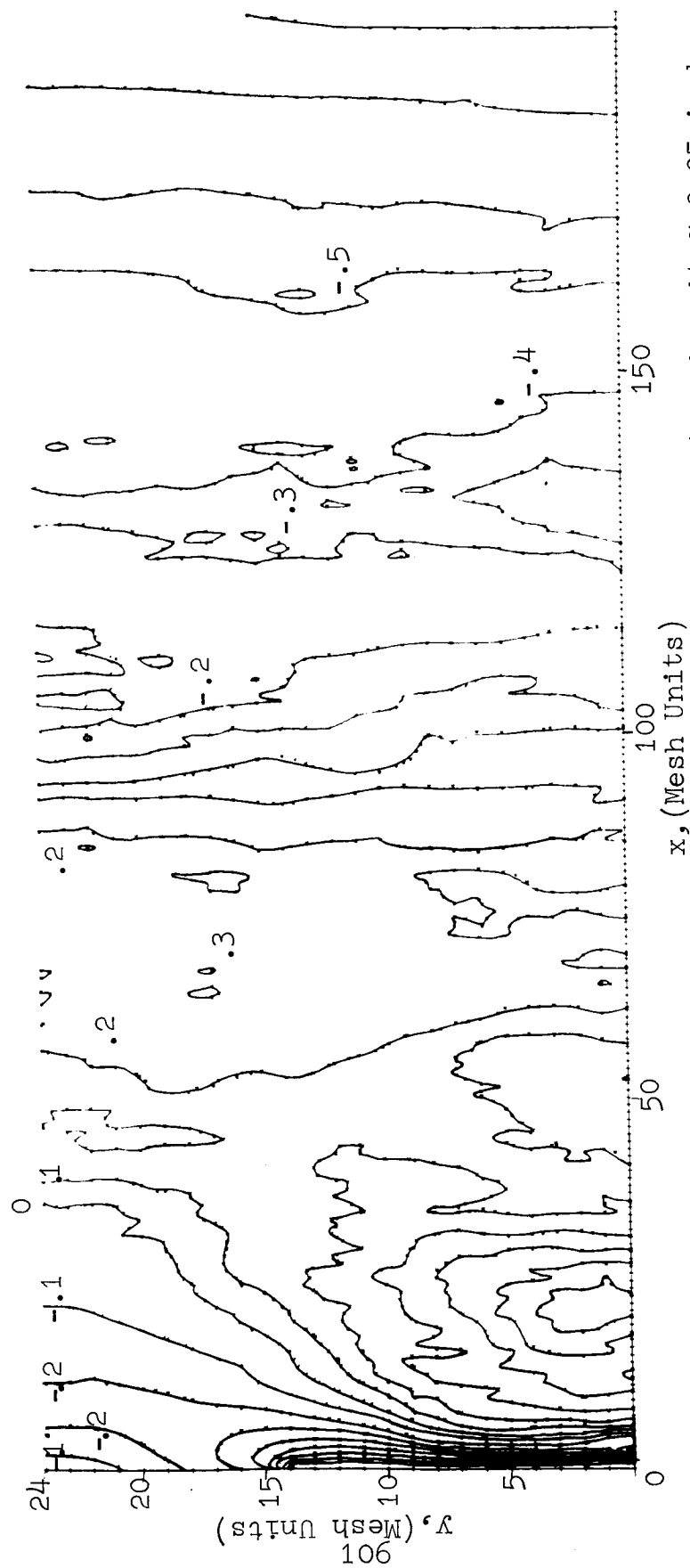
EQUIPOTENTIALS IN ENTIRE REGION, TIME STEP: 700
(Initial Potential Injection Condition)

Scale: 1 mesh unit ≃ 0.05 inch
1 norm. volt ≃ 155 volts

Fig. 4-12

106

injection plane) were obtained from the potential distribution in the r-z configuration. The results from the initial potential distribution yielded good charge neutrality; however, the plasma potential did not stabilize at least within the duration of study and some fluctuations in the plasma potential distribution were noticed. It was then argued that if the boundary conditions are altered slightly so as to give potential distribution in the x-y plane much closer to that in the actual r-z configuration, one might be able to notice uniform (or less varying) plasma potential in addition to the charge neutrality. Figure 4-13 shows this modified potential distribution, which is much closer to that in the actual r-z configuration. A production run was made with this input data and with $e\varphi_o/kT=28.8$. The ion and electron trajectories were more or less similar to those for the earlier case.

4.4.2 Ship Potential and Thrust

Figure 4-14 shows the variation of the normalized ship potential as a function of time for the two cases - two potential distributions. For the case of the modified potential distribution more electrons are able to move into space making the ship potential more positive as compared to that in the initial potential distribution. However, within about 250 time steps the average level of the ship potential begins to drop and compares favorably with that in the other case. In both cases the oscillations in the ship potential are at the electron plasma frequency. In order to compare the plasma potential distribution in the two cases it is necessary to take into account the phases of these oscillations in the two cases. This will become clearer in later discussions. The peak around time step 700 seems to have occurred due to a large shift of electrons away from the emitter thereby making the ship potential highly positive. This is correlated with the thrust variation
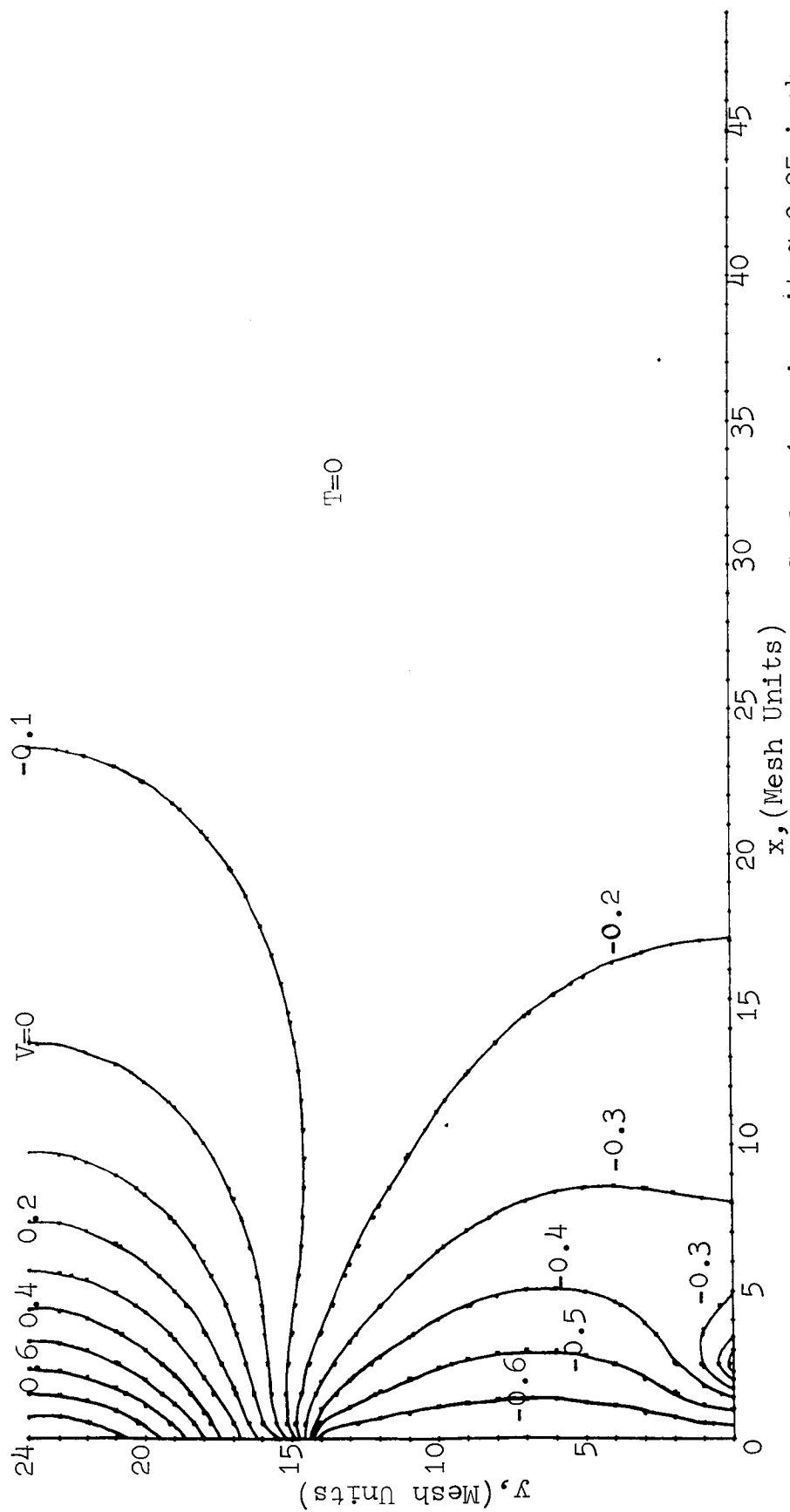
EQUIPOTENTIALS NEAR INJECTION PLANE
(Modified Potential Injection Conditions)
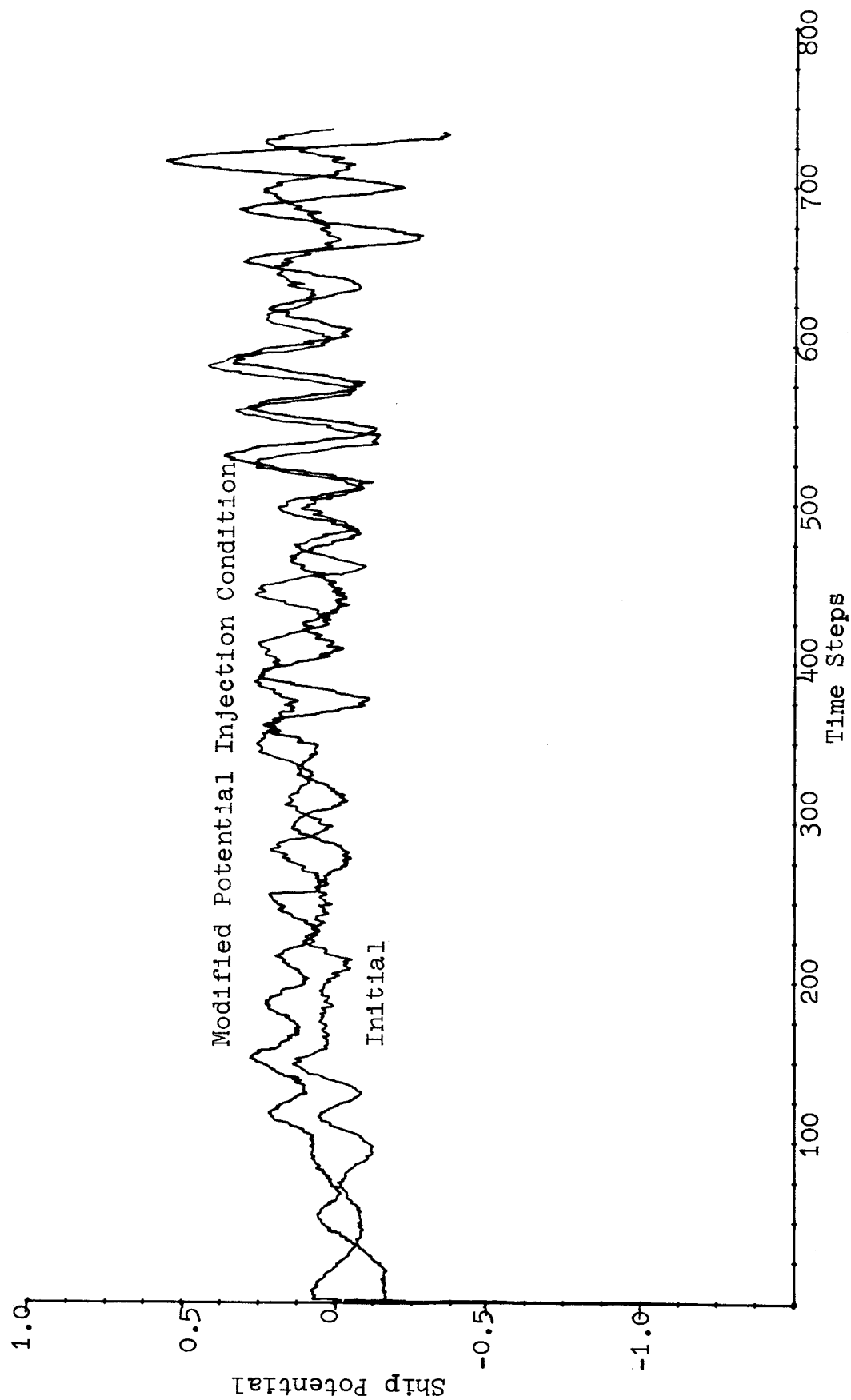
Scale: 1 mesh unit ≅ 0.05 inch
1 norm. volt. ≅ 155 volts

Fig. 4-13

108

NORMALIZED SHIP POTENTIAL VERSUS TIME, $e\varphi_o/kT=28.8$

Scale: 1 time step $\approx$ 14 mμ sec.
1 norm. volt $\approx$ 155 volts

Fig. 14-4

shown in Fig. 4-15, which shows the variation of thrust as a function of time for the two cases. Enough data are not available to further correlate this buildup in ship potential fluctuations; it may be due to the two-beam instability.

It may be noticed that the normalized thrust for the case of the modified potential distribution is reduced by slightly more than 10 percent. This is primarily due to the fact that the potential in the vicinity of the emitter is more positive. This increases the decelerating field for ions at the accel grid, which reduces the thrust value.

4.4.3 Temperature Calculations

Figure 4-16 shows the variation of the normalized temperature for electrons and ions for the case of the modified potential distribution. A comparison of these plots with those shown in Fig. 4-8 indicates that temperatures in the latter case are slightly lower; however, enough data are not available to make any conclusion about the neutralization mechanism, as the difference in temperatures is not large. Again, because of potential peaks developed due to the presence of the ion beams, the electron temperature is increased downstream near the electron emitter and is then reduced as the electrons move along the ion beam, which indicates a good mixing of electrons and ions.

4.4.4 Excess Charge and Potential Distribution

The plot for the fractional excess charge for the case of the modified potential distribution is compared with that of the initial potential distribution in Fig. 4-9. Because of the reduction in the magnitude of the negative voltages in space, more electrons can escape into space; as a result of this the deficiency of electrons is never as high as in the former case. However, this study is only on a relative scale; deficiency or abundance of electrons depends very much upon the potential distribution and the primary electrons available from the emitter.
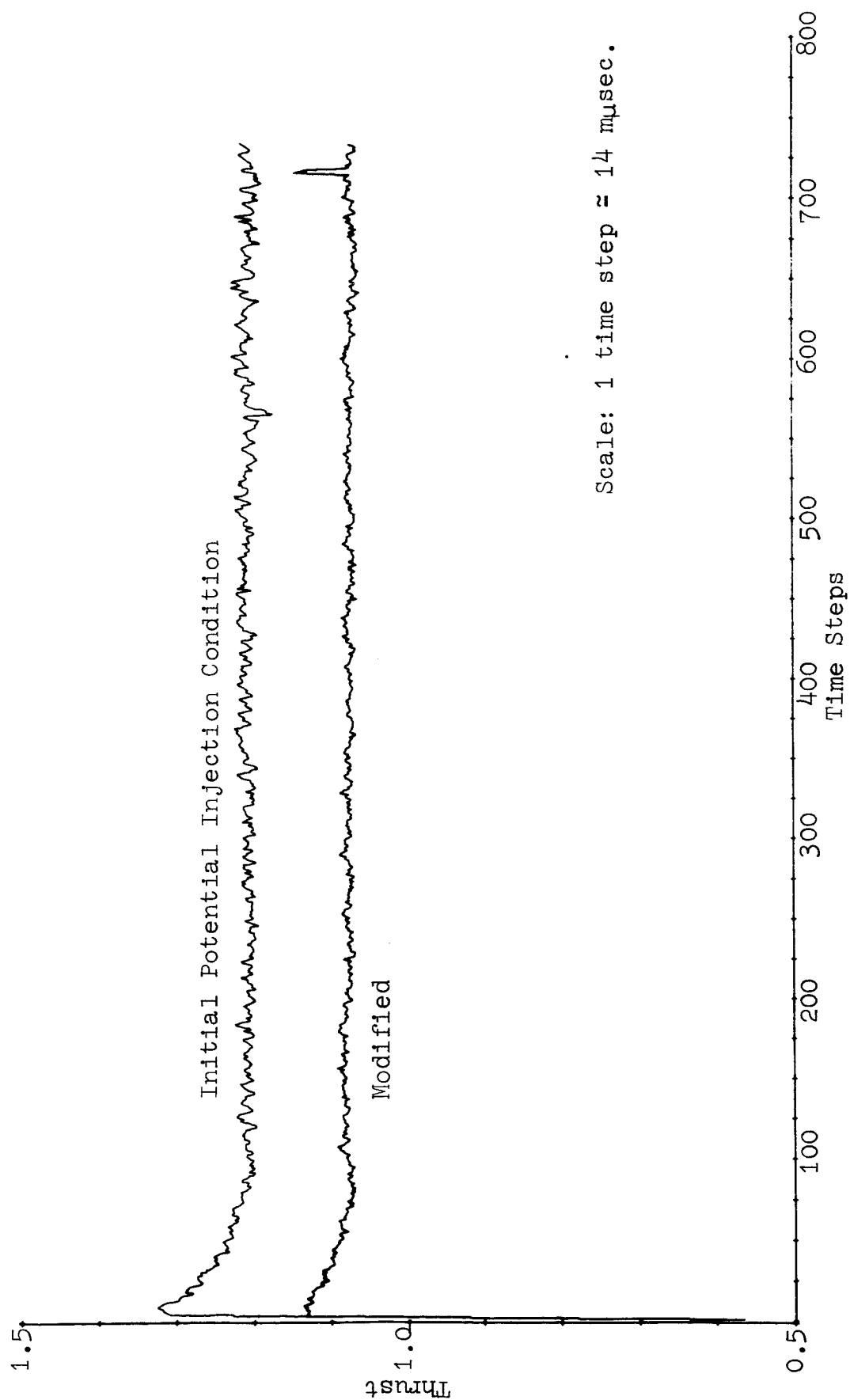
NORMALIZED THRUST VERSUS TIME, $e\varphi_o/kT=28.8$

Fig. 4-15

Scale: 1 time step $\approx$ 14 mμsec.

111
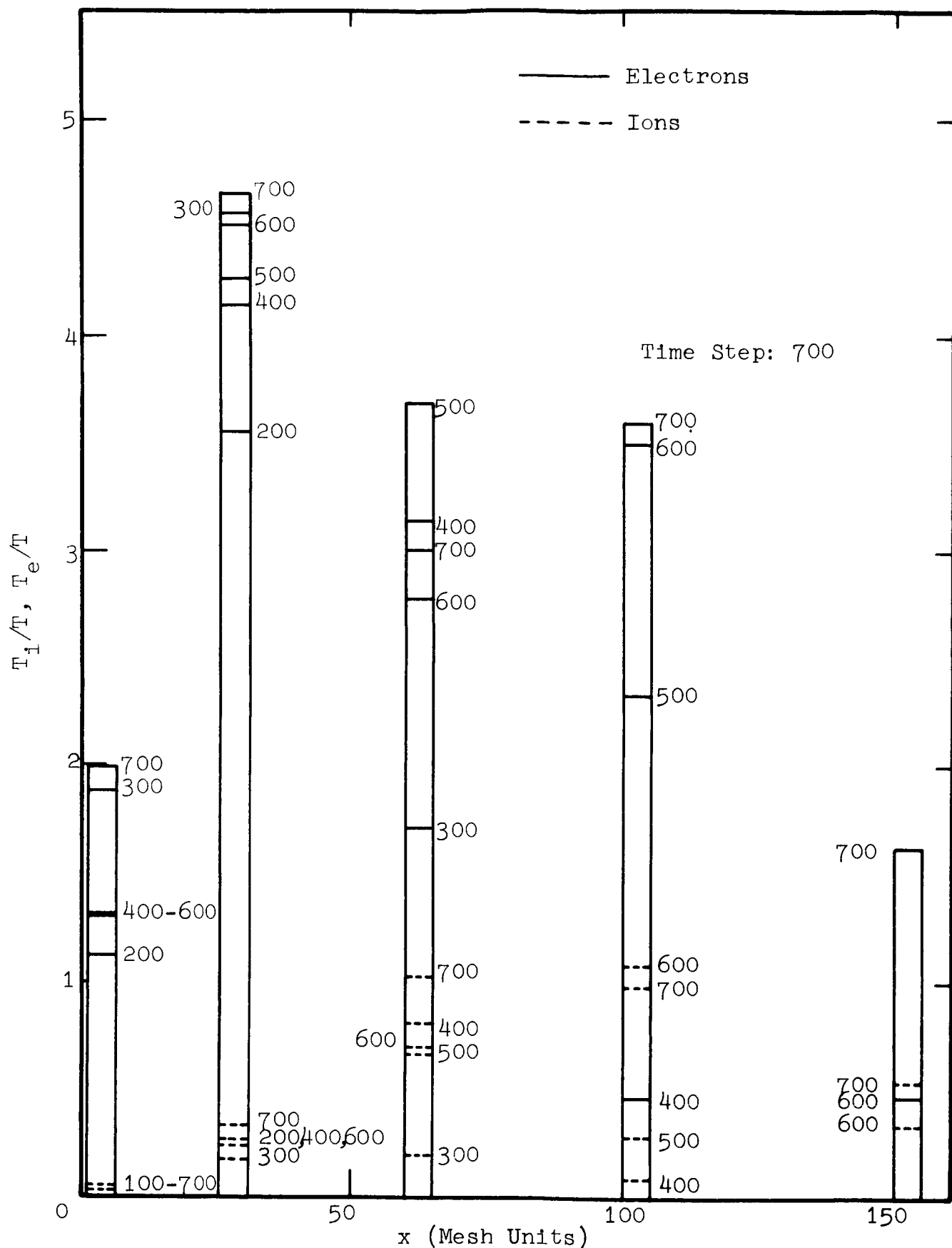
NORMALIZED TEMPERATURE VERSUS x, M/m=144, eφ_o/kT=28.8
(MODIFIED POTENTIAL DISTRIBUTION)

Fig. 4-16

Figure 4-17 shows the equipotential plots in the x-y plane at time step 700. A comparison with the plots shown in Fig. 4-11 indicates that the plasma, in the latter case, adopts in general more positive potential than in the former case. This comparison is somewhat deceiving because one should also compare the phase shift of the fluctuations in plasma in the two cases. As it is noticed from the plots of ship potential in Fig. 4-14, the ship potential fluctuates at the electron plasma frequency and at some time intervals the phases of these oscillations as indicated by these curves are not the same. This is particularly true at time step 700, for which the equipotential plots are shown in Figs. 4-11 and 4-17. A comparison of the data at time steps 500 and 600 did reveal closer potential distributions in the two cases; at these time steps the ship potentials for the two cases are in the same phase. The potential distribution at time step 300 is shown in Fig. 4-18 to illustrate the fluctuations in plasma potential with time and in space.

4.5 CONCLUSIONS

The low-voltage ion beam configuration has been studied for ion-beam neutralization. One of the objectives of this investigation was to compare the results from the computer simulation with experimental results obtained by Sellen. Broadly speaking, neutralization is obtained (as had been hoped for) when an adequate supply of electrons is made available near the ion beam. Charge neutrality is readily obtained. The formation of the plasma is indicated from the equipotential plots at different time steps. However, the plasma does not seem to have stabilized during the time duration for which the movement of the various particles is observed;
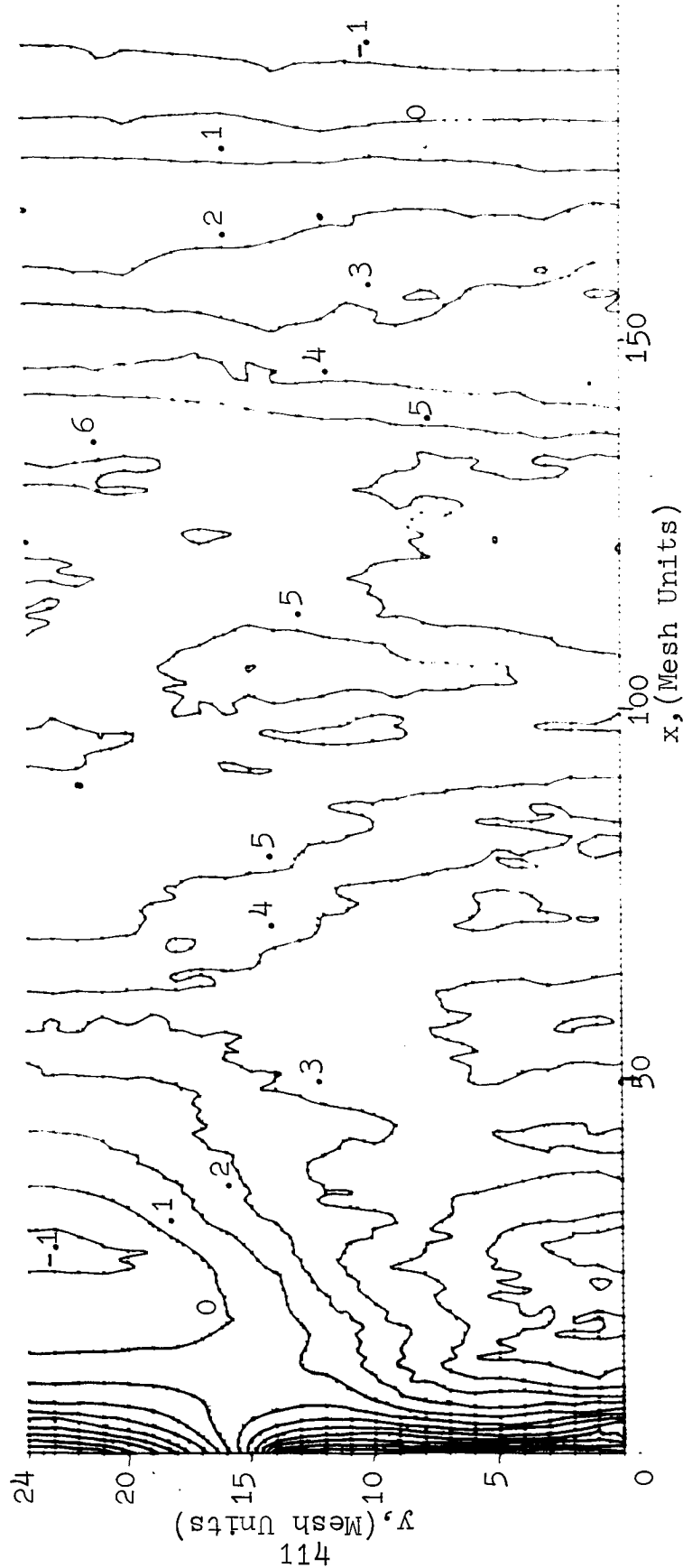
EQUIPOTENTIALS IN ENTIRE REGION, TIME STEP: 700 $e\varphi_o/kT=28.8$

Fig. 4-17

Scale: 1 mesh unit $\simeq$ 0.05 inch
        1 norm. volt $\simeq$ 155 volt

114
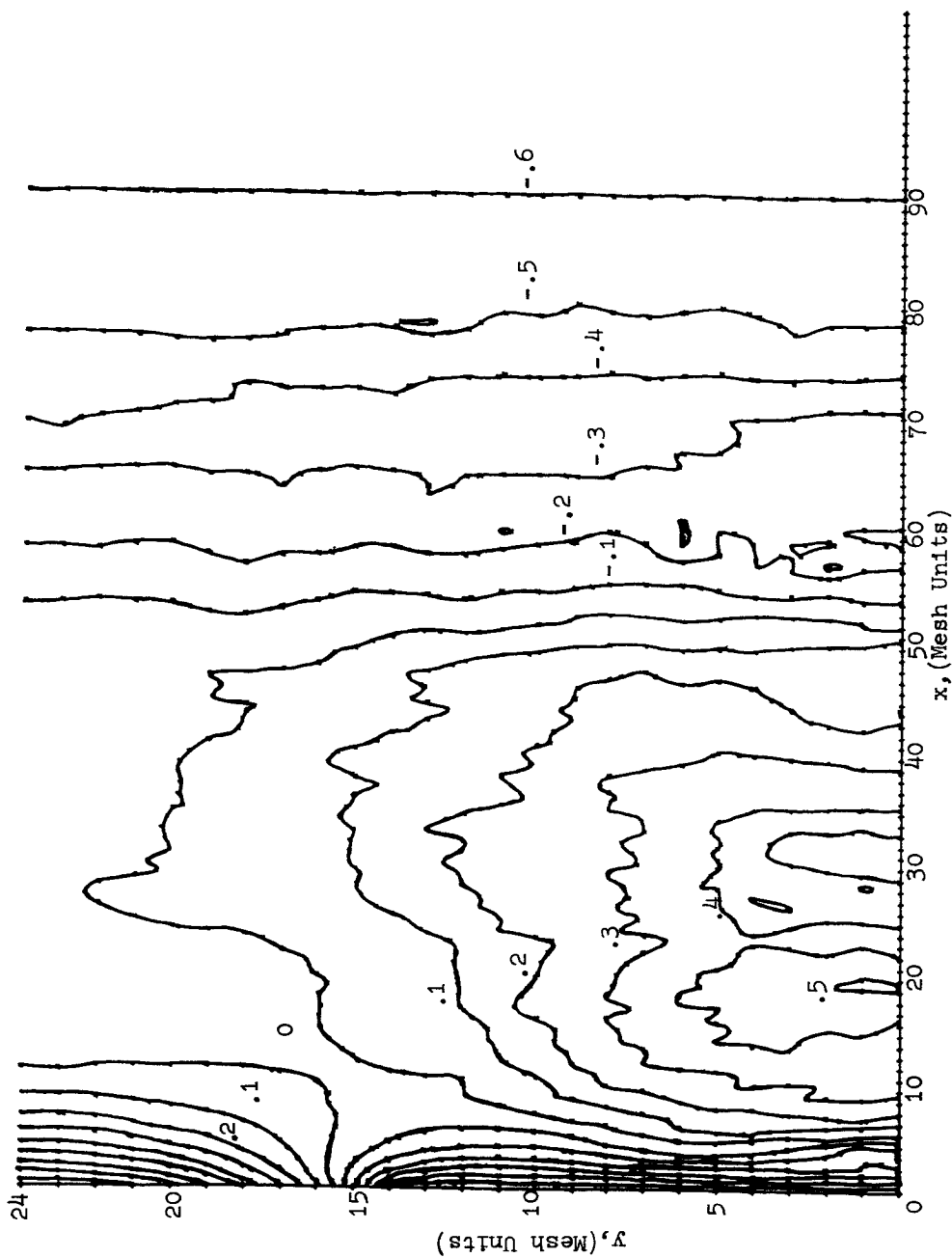
EQUIPOTENTIALS IN ENTIRE REGION, TIME STEP: 300, $e\varphi_O/kT=28.8$
(Modified Boundary Condition)

Scale: 1 mesh unit $\simeq$ 0.05 inch
1 norm. volt $\simeq$ 155 volts

Fig. 4-18

115

there is also some variation in the plasma potential in space. However, the formation of the potential plateaus does seem to indicate a lack of influence by the surrounding boundaries, as noticed by Sellen. Some of these results are somewhat different from what had been expected. It appears that this difference is due to the fact that the potential distributions for the free space-charge conditions as simulated in the computer for the two cases (discussed above) are quite different from what exists in the actual practical configuration. Of course, once the plasma is formed, the initial potential distribution is of little significance. However, large deviations in the initial potential distribution require more computer time to reach the equilibrium stage. Other restrictions were apparent because of computer limitations; for example, the high-energy electrons which cross the exit plane are not properly accounted for, except that the fundamental harmonic of the charge leaving the exit plane is accounted for in evaluating the potential distribution.

In scaling from high-mass ions to low-mass ions the velocity is kept invarient, but the ion and electron energies are not scaled appropriately. This problem is of more significance particularly for the case of low-voltage-ion beams, because the ion energies, when scaled for low-mass ions, tend to become more comparable to the electrons energies than in the case of high-voltage ion beams. This may be one of the reasons why plasma potential is not stabilized, as mentioned above.

The total length simulated on the computer corresponds roughly to about 25 cm of physical length. This distance is very small as compared to the overall length of the tank. Very little experimental data are available within this short distance from the source to make any generalized conslusions about the comparison between computer and experimental results.

There is definitely a tendency toward a thermodynamic equilibrium between ions and electrons. At a distance (physical) of about 20 cm from the ion source, the normalized electron equivalent temperature is near unity and shows a tendency to drop further along the beam. This would have been more evident if calculations had been carried out farther downstream.

5.0 EXTRAPOLATION OF RESULTS TO THE CASE OF HEAVY IONS

The electron-ion mixing studies discussed in this report have been confined to small values of ion mass. The simulation of low-mass ions was made primarily because of computer limitations. General problems of simulation of low-mass ions are discussed in Section 3.3. Three different values of ion mass were simulated so that extrapolation of these results could be made to predict the results for an actual case. This extrapolation is briefly discussed in this section.

For the case of the high voltage ion beam, both immersed and withdrawn emitters were simulated. For the case of the immersed emitter, only one mass ratio ($M/m=144$) was investigated; while for the case of the withdrawn emitter, three values of mass ratio ($M/m=64$, 144, 256) were investigated. (See Sections 3.4 and 3.5.) In all these cases the ion-beam divergence was more than that noticed in the earlier case* for a strip emitter with no initial transverse velocity for ions. (Comparison is made for the same value of M/m.) The ion-beam divergence was, however, smaller for the case of the immersed emitter, primarily because of better coupling between the ion beam and the electron emitter. Ion-beam divergence is reduced as the value of M/m is increased and the extrapolated ion-beam divergence is negligible for the case of cesium or mercury ions.

The ship potential fluctuations, (as a function of time), the plasma frequency of these fluctuations, and the average dc value of the ship potential are reduced as the value of the ion mass is increased. (See Section 3.4.) Again, one may predict that these fluctuations would be negligible for the

---

*   These results were discussed in the earlier final report[1].

case of actual ions. It is worth mentioning here that the data are not enough to predict this information, precisely, for heavy ions since the simulated values of ion mass are very low. Thus, only qualitative predictions can be made. The thrust for the case of $M/m=256$ was very nearly equal to that for the case of $M/m=144$, while it was lower for the case of $M/m=64$. The thrust value for the case of heavy ions would be almost the same or perhaps higher than that for the case of $M/m=156$; although the thrust is lower than the ideal value because of the initial transverse velocity of the ions at the injection plane.

In all cases there is a slight excess number of electrons and the percentage of excess charge remains fairly constant after a few time steps. This occurs even though the number of electrons emitted varies from four to eight times the number of ions emitted. The excess number of electrons fall back on the electron emitter and are absorbed indicating, thereby, a self-adjustment in demand for the electrons for adequate neutralization. (See Sections 3.4 and 3.5.) This indicates a good charge neutrality. Because of the nearly identical behavior in all the cases, one can safely predict that the charge neutrality will be maintained for the actual case of heavy ions.

The equipotential plots given in the report (Sections 3.4 and 3.5) show the potential distribution in space at several time steps while the ship potential variations mentioned earlier indicate the plasma-potential variations with time. There is a certain amount of correspondence between the two results. From the results of the ship-potential fluctuations, one can predict that the equipotentials will be flatter for the case of heavy ions indicating, perhaps, a better electron-ion mixing mechanism.

For the case of lower values of M/m the electron equivalent temperatures were not as high as those for the case of large values of M/m. (See Sections 3.4 and 3.5.) This is primarily due to the fact that lighter ions are more susceptible to electric field fluctuations; this results in a better mixing of electrons and ions. For the two values of M/m, namely 144 and 256, the computed electron equivalent temperatures were nearly equal. Because of the lack of data it would be difficult to predict this behavior for the case of actual ions, although, one might anticipate a similar behavior for the case of heavy ions as that for the case of M/m=256. It is worth mentioning here that the computed electron equivalent temperatures were lower for the case of the immersed emitter.

The low-voltage ion-beam configuration (Sellen's geometry) was simulated for one value of M/m only. From the results of the high-voltage ion-beam simulation, it is possible to make similar predictions for the case of heavy ions for this configuration discussed in Section 4.

6.0 CONCLUSIONS AND SUGGESTIONS FOR FURTHER WORK

6.1 CONCLUSIONS

The computer studies discussed in this report were made for two types of ion guns - those for high voltage and low voltage ion beams used in ion engines. Special attention was given to the transient neutralization mechanism which involves injection of electrons from a hot electron emitter into the ion beam. The emitter may be withdrawn from or immersed into the ion beam. Trajectory plots for several sampled charged particles were made. Ship potential and thrust were monitored as a function of time. Equivalent temperatures for electrons and ions were computed for several segments in space at different time steps.

For the high voltage ion beam the injection plane was not the same as the accel plane. This was for convenience in simulating the problem for the given ion gun geometry. The voltage difference along the injection plane was kept fixed according to data obtained from the gun design work. The minimum voltage difference between the electron emitter and points along the injection plane for the case of low-mass ions was not enough to prevent electrons crossing the injection plane. This necessitated applying some artifical bias along the injection plane; bias was different for each case of ion mass, so that the extrapolated bias for the actual case would be zero. Both withdrawn and immersed electron emitters were investigated.

The macroscopic charge neutrality is obtained within a few hundred time steps after the engine is started. However, microscopic neutrality is not achieved within the periods for which the particles are traced. This is indicated by the plasma potential variation in space and time. The coupling between the electron emitter and ion beam for the case of the withdrawn

emitter is not as good as that for the case of the immersed emitter. This is indicated by a smaller primary current requirement for the latter case. The equivalent temperatures are also lower for the case of the immersed emitter.

The plasma potential fluctuations are reflected in ship potential fluctuations which occur at the electron-plasma frequency. These fluctuations are reduced as the value of the ion mass is increased. The plasma potential is not stabilized to the electron emitter potential. (In previous calculations[1] and in experiments by Sellen[2] for low-voltage ion beams plasma potential stabilized at the electron emitter potential.) It is felt that this is primarily due to the fact that the particles have not been traced for a long enough time and the system is still in the transient stage.

For the low-voltage ion beam, approximate boundary conditions (voltage distribution along the injection plane) were obtained by the use of the Resistance Network Analogue. The results obtained with these boundary conditions yielded similar charge neutrality in the case of the high-voltage ion beam discussed above, but the plasma potential fluctuated in space and time, i.e., the plasma potential did not stabilize within the period for which the particles were traced. (This is strictly due to computer limitations.) It was argued at that time that the free-space charge potential distribution in this case was not the same as in the actual r-z configuration, even with the same boundary conditions, and that this might have resulted in a delay in reaching the equilibrium stage. The potential distribution along the injection plane was varied slightly in order to obtain the potential distribution in space similar to that in the r-z configuration. The results obtained with this new (modified) potential distribution indicated faster charge neutrality, but again the plasma potential did not stabilize,

122

although there was some evidence of fluctuations of lower magnitude. This also resulted in slightly increased thrust because of reduction of the decelerating field for ions beyond the accel plane. There is definitely a good indication of plasma formation, shown by plateaus in the plasma potential distribution. In this case, it is felt, again, that the particles have not been traced for a sufficient duration to have reached the equilibrium condition.

Temperature calculations in both cases indicate that the electrons warm up first along the beam, indicating large fluctuations. Further downstream the electron equivalent temperatures are decreased; this indicates that electrons are getting "tamed" to go along with the ions. Low temperatures downstream indicate a definite mixing of electrons and ions. Since these particles were not traced beyond the exit plane, it is difficult to predict either the beam behavior under the equilibrium conditions, or the time required to reach this stage.

The change in the potential distribution near the injection plane indicates the great influence of the plasma on the potential distribution in the aperture of the injection plane, which has been fixed in our simulation. In an actual case this influence will change the ion injection conditions, which may eventually affect the plasma formation.

6.2 SUGGESTIONS FOR FUTURE WORK

The results described in this report concerning ion-beam neutralization in an ion engine have revealed very interesting observations. These studies have been made only for the transient period. Because of computer limitations, these studies have not been made for intervals sufficient to ensure equilibrium. The particles leaving the exit plane are written off from the

computer memory and only the fundamental harmonic of the charge leaving the exit plane is considered, (in addition to other charges in the system) in solving Poisson's equation. In general, some of these particles get reflected back into the system; this makes it necessary to incorporate a few minor modifications in the program. These will enable us to increase the duration of the runs, which will eventually yield information concerning the fluctuations in the plasma potential in the steady-state level.

Because of the scaling problem (these studies are made for low-mass ions only), the low-voltage ion beam simulation (Sellen's configuration) presents a more severe problem. Sellen's experimental results - namely, (1) that the plasma adopts the emitter potential and is independent of the surroundings, and (2) that there is an appreciable cooling of electrons - have been very interesting. But because of computer limitations the studies have not been made for long durations to correlate these results with the experimental results. The simulation of Sellen's configuration in a one-dimensional model for the actual (or nearly actual) ions will enable us to correlate the results more closely with the experimental results. However, the beam divergence has to be extrapolated from the results obtained from the two-dimensional model. Some modifications in the program can also be made to compute equivalent temperatures of the charged particles over distances farther from the ion source than those for which computations have been made so far.

The potential distribution along the injection plane has been kept fixed in all the runs, while the results of these studies indicate a definite interplay between potential distribution along the injection plane and the plasma boundary.

The effect of plasma will be then to change the ion trajectories. The present gun designs do not take into account the presence of the neutralizer, and any deviations in the ion trajectories will lead to loss in thrust and engine life* (due to ion impingement on the electrodes). Therefore it becomes necessary to combine the gun region and the neutralizer for studying ion-beam neutralization.

Experiments by Kerrisk and Masek[13] have indicated that ion exit velocities from the ion source correspond roughly to 1-2 volts; the increase (from the thermionic equivalent voltage) is due to the residual fields in plasma (confined in Kaufman engine). A simulation of the Kaufman engine will also lead to very useful information concerning the nature of plasma in the engine. This information will eventually be useful in the gun design.

The immersed emitter configuration gives a better coupling between the emitter and ion beam, as compared to that in a withdrawn emitter configuration. Only two positions of the emitter configurations were investigated. For long-life considerations a compromise between erosion on the emitter and coupling is necessary and this requires study of ion-beam neutralization with different configurations and shapes of the electron emitter.

The transient period has not been investigated for a sufficient long time to ensure the existence or nonexistence of instability. One way of investigating this would be to start with some equilibrium distribution of ions and electrons and

---

* A good description of an ion engine and the various problems in improving its characteristic is given by Brewer[12].

then trace these particles for some time. It is expected
that an instability in the system, if any, will show up in the
calculations. This technique (under various computer limitations
for investigating instabilities seems to be quite simple to
simulate, and will certainly yield some useful information
regarding the ion-engine performance.

It is worth mentioning it here that these studies are
oriented towards a better understanding of the physical phenomena
in ion engines and a correlation between experimental and theoret
cal results will eventually lead to better performance of the ion
engine. Needless to say that the various techniques developed in
these programs will be useful in solving problems in associated
fields.

BIBLIOGRAPHY

1. Wadhwa, R.P. and Kooyers, G., "Analysis of Electron-Ion Mixing in Ion Engines," Final Report, Contract No. NAS3-2503, Research Laboratory, Litton Industries, San Carlos, California; March 1964.

2. Sellen, J.M. Jr., "Investigation of Ion Beam Diagnostics" Section III G, on Observation of Neutralized Ion Thrust Beams in the 80 Feet NASA Testing Chamber, Final Report NASA 8603-6037-50-000, Contract No. NAS8-1560, TRW Space Technology Laboratories, Redondo Beach, California; April 1964.

3. Jones, S., Contract Supervisor, Lewis Research Center, NASA Cleveland, Ohio; Private communication.

4. Wadhwa, R.P. and Brauch, D. F., "Analysis of Electron-Ion Mixing in Ion Engines," Quarterly Report No. 3, Contract No. NAS3-5757, Research Laboratory, Litton Industries, San Carlos, California; February 1965.

5. Wadhwa, R.P. and Brauch, D F., "Analysis of Electron-Ion Mixing in Ion Engines," Quarterly Report No. 1, Contract No. NAS3-5757, Research Laboratory, Litton Industries, San Carlos, California; August 1964.

6. Wadhwa, R.P., "Analysis of Electron-Ion Mixing in Ion Engines," Quarterly Report No. 2, Contract No. NAS3-5757. Research Laboratory, Litton Industries, San Carlos, California; November 1964.

7. Hamza, U., Report to be published.

8. Harman, W.W., Electronic Motion, McGraw Hill Publishing Company, Inc., New York, 1953.

9. Wadhwa, R.P., Buneman, O., and Brauch, D.F., "Two-Dimensional Computer Experiments on Ion-Beam Neutralization," AIAA Journal, Volume 3, No. 6, pp. 1076-1081; June 1965.

10. Wadhwa, R P., "Analysis of Electron-Ion Mixing in Ion Engines," Quarterly Report No. 6, Contract No. NASA3-2503, Research Laboratory, Litton Industries, San Carlos, California; December 1963.

11. Sellen, J.M., Jr., Private communication.

12. Brewer, G.R., "Physical Electronic Phenomena in Ion Propulsion Engines," IEEE-Spectrum, Vol. 2, No. 8, pp. 65-79; August 1965.

13. Kerrisk, D. J., and Masek, T.D., "Plasma Nonuniformity and Grid Erosion in an Electron Bombardment Ion Engine," AIAA Journal, Vol. 3, No. 6, pp. 1060-1066; June 1965.

DISTRIBUTION LIST

Jet Propulsion Laboratory
4800 Oak Grove Drive
Pasadena, California
Attn: Mr. J. J. Paulson   1

Hughes Research Laboratories
3011 Malibu Canyon Road
Malibu, California
Attn: Dr. G. Brewer   1

Electro-Optical Systems, Inc.
125 North Vinedo Avenue
Pasadena, California
Attn: Dr. A. R. Forrester   1

General Electric Company
Flight Propulsion Laboratory
Cincinnati 15, Ohio
Attn: R. N. Edwards   1

Ion Physics Corporation
South Bedford Street
Burlington, Massachusetts
Attn: Dr. S. V. Nablo   1

General Dynamics Corporation
General Atomic Division
P. O. Box 608
San Diego 12, California
Attn: M. N. Rosenbluth   1

NASA-Lewis Research Center
21000 Brookpark Road
Cleveland, Ohio 44135
Attn: Library   2

NASA-Lewis Research Center
21000 Brookpark Road
Cleveland, Ohio 44135
Attn: Reports Control Office   1

NASA-Lewis Research Center
Electromagnetic Propulsion Division
21000 Brookpark Road
Cleveland, Ohio 44135
Attn: H. R. Kaufman   1

TRW Space Technology Laboratories
Thompson Ramo Wooldridge Inc.
8433 Fallbrook
Canoga Park, California
Attn: J. M. Sullen   1

NASA Scientific and Technical Information
          Facility
P. O. Box 33
College Park, Maryland 20740
Attn: NASA Representative RQT 2448   6

AFWL
Kirtland Air Force Base, New Mexico
Attn: Capt. C. F. Ellis/WLPC   1

Aerospace Corporation
P. O. Box 95085
Los Angeles, California 90045
Attn: Library Technical Documents Group   1

Westinghouse Astronuclear Laboratories
Pittsburgh, Pennsylvania 15234
Attn: H. W. Syzmanowski, Mgr.
          Electrical Propulsion Laboratory   1